Design and Simulation of a Rapid High Precision Profilometer

by

Lawrence D. Barrett

B.S. Mechanical Engineering
Pennsylvania State University, 1992

**Submitted to the Department of Mechanical Engineering in Partial
Fulfillment of the Requirements for the degree of**

**Master of Science in Mechanical Engineering
at the
Massachusetts Institute of Technology**

June 1997
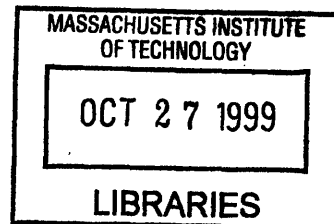
Signature of Author: _____

Department of Mechanical Engineering
May 27, 1997

Certified by: _____

Dr. Kamal Youcef-Toumi
Associate Professor of Mechanical Engineering
Thesis Supervisor

Accepted by: _____

Dr. Ain A. Sonin
Chairman, Department Committee on Graduate Students

Design and Simulation of a Rapid High Precision Profilometer

by

Lawrence D. Barrett

Submitted to the Department of Mechanical Engineering
on May 20, 1997 in the partial fulfillment of the
requirements for the degree of Master of Science in
Mechanical Engineering

ABSTRACT

A high precision profilometry system was developed for the quality assurance inspection of two-sided samples. Based on system specifications and requirements, atomic force microscopy (AFM) was determined to be the most appropriate profilometry technique. The major components of the device include: (1) A commercially available auto-sensing AFM probe, (2) custom designed probe positioning hardware, (3) sample positioning hardware, (4) probe tip calibration and image processing, and (5) scanned image processing and convolution.

The primary focus of this thesis is on the probe positioning hardware design and simulation of the customized profilometer. The design enables the system to simultaneously scan both surfaces of the sample, which increases speed, as well as compensate for distorted samples. The image reconstruction algorithms and system homogeneous transformation matrices (HTMs) are utilized in the simulations of the system.

The simulations examine multiple scanning scenarios to determine the necessary requirements of the device to achieve the specified resolution. The system variables available in the simulations are: (1) probe tip contour, (2) actuator specifications, and (3) sample orientation. Finally, recommended device specifications are determined and documented.

Thesis Supervisor: Dr. Kamal Youcef-Toumi

Title: Associate Professor of Mechanical Engineering

Acknowledgements

This thesis is dedicated to my family and friends who have filled my life with happiness and high expectations.

I would like to acknowledge the support of the following persons in making this project and my graduate studies at MIT an exceptional educational experience.

Sarah Barrett: your patience, kindness and love, made my MIT experience wonderful. I'm glad we had the opportunity to go to graduate school together.

Professor Youcef-Toumi: you gave me a chance to expand my creativity and provided me an academic opportunity that will never be forgotten. Thank you for all of your guidance and advice.

Joachim Ogland: your engineering insight was extremely helpful. Thanks for joining the project. Good luck with McKinsey.

Bernardo Aumond: thank you for your great ideas on this project. I also appreciate all of your help in classes as well. Your innovation and superior engineering skills are well suited for the PhD. Good luck with your profilometer.

Razman Zambri: we've been through thick and thin together. From laser display projects to video conferencing. Good luck at Seagate.

Toolbox Club: consisting of **Steve, Karl, Bernardo**, and **Razman**. Your ability to "tool" your way through our classes added a great deal of fun to the course work. The majority of the academic material I take away from MIT has come from you four.

Jacob Einhorn: the first Mechanical Engineering student I met. From our first class, Dynamics, to our Career Search, we've kept tabs on each other. Thanks for being a good friend and confidante.

Dr. Eric Liu: your experience and knowledge help set the foundation for the project.

Fellow lab mates **Doug, Mitchell, Tetsuya, Masaki,** and **Yong** thanks for making my MIT experience enriching.

Finally, **Leslie Regan** has made my experience at MIT less stressful by assisting me with all the administrative trials and tribulations.

Table of Contents

List of Tables and Figures

List of Tables

List of Figures

11

1. Introduction

1.1   Purpose

The purpose of this project is to design an instrument that can reliably and accurately measure the geometric profile of the tip region of a two-sided sample with nanoscale precision and assembly line speed.

1.2   Design Applications

The device is to be developed for usage in the quality assurance portion of an industrial assembly line. The sponsor requires nanometer resolution of the surface in order to ensure the product's critical dimensions meet their predetermined specifications. Since this is an industrial application, the quantity and speed of the scans per sample must be maximized and the system needs to be robust in order to reliably produce these high resolution scans. The interface must also be user friendly so that pertinent information can be easily and quickly extracted by the operator. The required specifications of the probe are highlighted in Table 1.1. The nominal critical sample dimensions are shown in Figure 1.1.

Range:		
	Three Dimensional	$1\mu m^3$
Resolution:		
	Vertical	$\leq 0.005\mu m$ (5nm)
	Lateral	$\leq 0.020\mu m$ (20nm)
Speed:		
	Scan Frequency	$\geq 10Hz$
	Sample Frequency:	$\geq 1\ Hz$
	Scans per Sample	10

Table 1.1 Probe system minimum specifications.

Normalized profile of typical sample
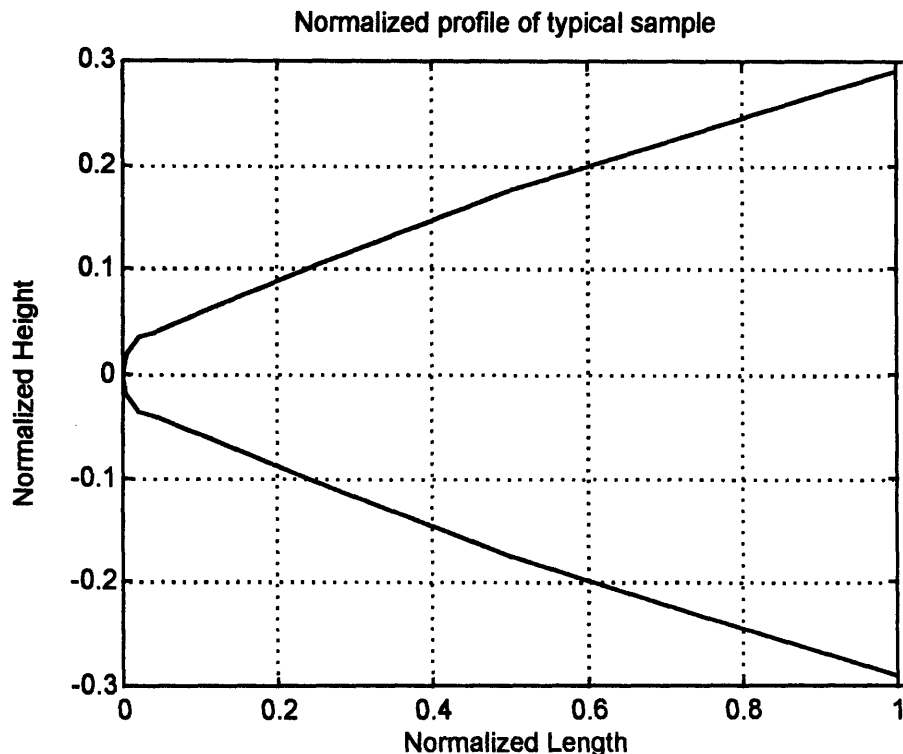
Figure 1.1 Normalized profile of typical sample.

1.3   Thesis Contents

The document is organized as follows: Chapter 2 reviews many of the techniques available for precision profilometry. Some of the techniques examined include scanning electron microscopes, optical methods, mechanical stylus method, scanning tunneling microscopy, atomic force microscopy, and near-field optical methods.

Chapter 3 thoroughly discusses several of the design alternatives. These design were analyzed and judged on many different characteristics including speed, resolution, repeatability, accuracy, and cost. The final design selection justification is also reviewed.

Chapter 4 reveals detail about the system design including both hardware and software. The hardware focuses on the probe mechanism, the positioning system, the sample fixture, the calibration piece, and the system frame. The software focuses on the convolution of the probe and scanned images to obtain the sample surface.

Chapter 5 discusses and illustrates the implementation of system simulations. The simulations allow for the evaluation of different scanning scenarios. These will include the ability to utilize various actuators, different sample orientations, and multiple probe contours. After simulating multiple scenarios, system capabilities, identification of the actuator specifications, and system optimization will all be documented.

Finally, Chapter 6 documents the conclusions and makes recommendations about the final results of the system. The highlights of innovation and strengths of design are carefully reviewed as well as possible system enhancements.

2. Review Methods of Profilometry

2.1　Introduction

In this chapter, profilometry methods and techniques are reviewed and explored. From this examination, a selection is made for the most appropriate technique to be used in this specific application.

2.2　General Discussion about Profilometry

We examined different types of profilometry methods that were capable of measuring the geometric profile of the samples with nanometer precision. In order to put some perspective on the size of a nanometer, consider the logarithmic scale bar shown in Figure 2.1. This shows the relative size of several familiar and unfamiliar systems. Objects visible by the human eye are usually on the order of tens of micrometers, hence the need for instruments to measure motions and dimensions with resolution in the sub-micrometer range. In most profilometry applications, the highest resolution is desired in the vertical direction or the direction which is normal to the sample surface. The lateral resolution, which is in the direction of the scan and in the same plane as the sample surface, usually tends to be more difficult to resolve than the vertical resolution. This is usually not a problem because the lateral resolution is typically not the critical measurement desired. The reason for the discrepancy between the vertical and lateral resolution is that the lateral resolution has been limited by the technology of the scanning systems. In our application, both vertical and lateral resolution are crucial, however the vertical resolution requirement is higher than the lateral resolution. Currently, there are over a dozen techniques which are commonly used for precision profilometry, and each year current methods are improved and new technologies and research open the door for even more techniques. A survey of some of the techniques, which were considered for our application, is documented in the next subsection.
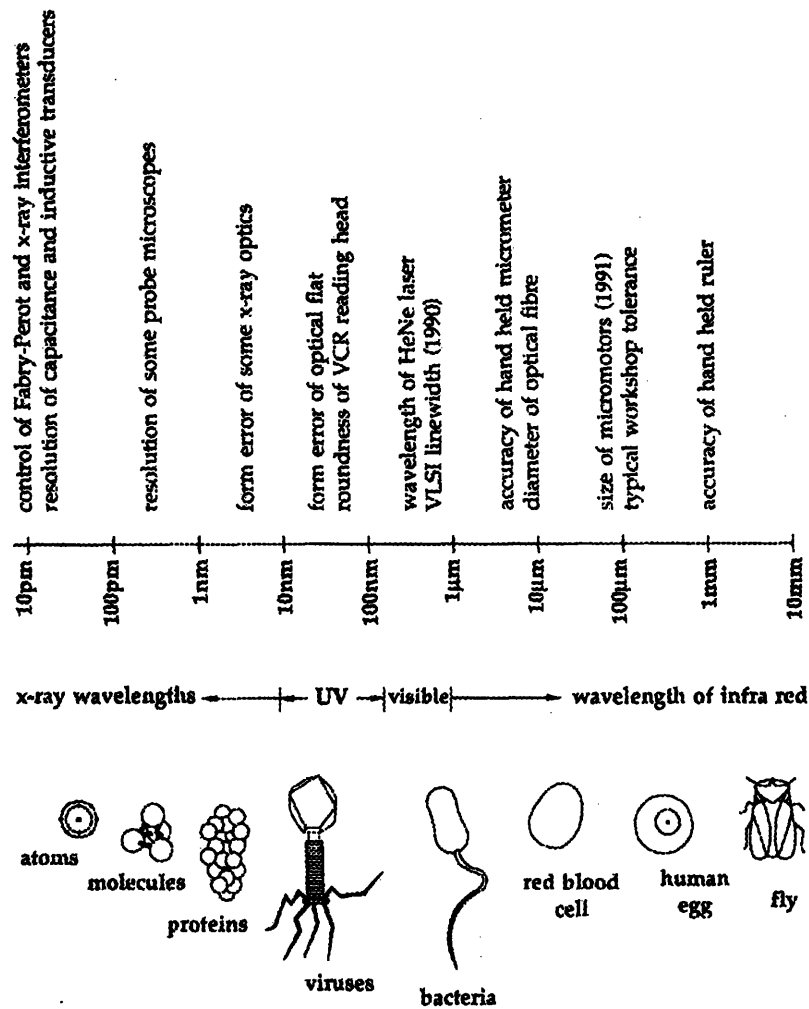
Figure 2.1 Scale bar comparing relative sizes of common objects.[A1]

2.3   Considered Profilometry Methods

Considered profilometry techniques include scanning electron microscopes, optical methods, mechanical stylus measuring system, and scanning probe microscopes which encompasses the scanning tunneling microscope, atomic force microscope, scanning near-field optics microscope, scanning thermal microscope, scanning capacitance microscope, and magnetic and electrostatic microscopes. A historical progress of microscope spatial resolution is shown in Figure 2.2. The following subsections describe the operating principle and strengths and limitations of each technique.
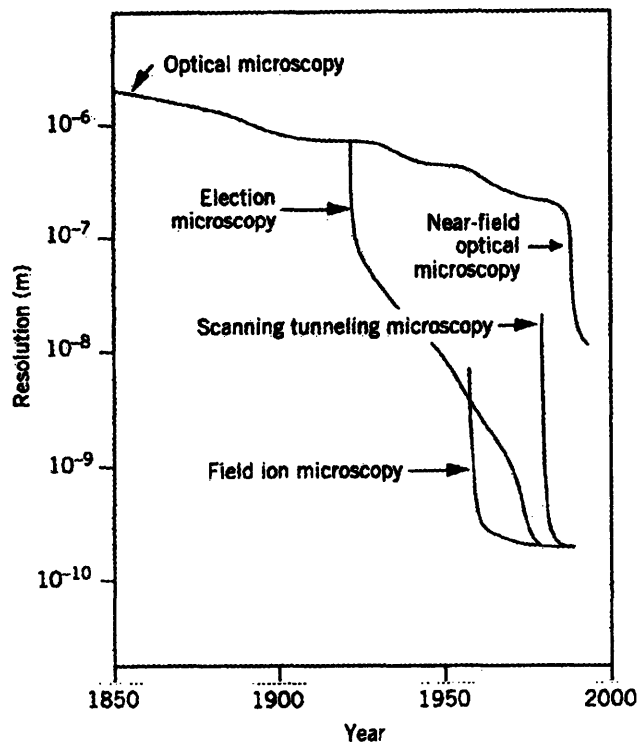
Figure 2.2 Historical progress of microscope spatial resolution.[A2]

2.4   Scanning Electron Microscope

One of the original instruments used to determine precision surface profilometry is the Scanning Electron Microscope (SEM). In an SEM, electrons are accelerated by a voltage source (1 to 30 kV) and directed down an electron optical column toward the sample. The electron beam bombards a sample surface resulting in secondary surface electron emissions. These emissions are then collected to form the data image. SEM's are a powerful metrology instruments, capable of resolutions as high as 0.4 nm [A3] and a linewidth measurement linearity of 1%[A4]. Since SEM generate contrast that does not reveal height, the sample cross-section must be imaged in order to obtain that information[A5]. In order to obtain access to the cross-section at multiple points along the sample, the sample must be destructively modified which is not an option for our application. Figure 2.3 shows a block diagram of an SEM.

ELECTRON
GUN

GUN
SUPPLY

CONDENSER
LENS

STIGMATER

OBJECTIVE
LENS

LENS
SUPPLY

MAGNIFICATION
UNIT

SCANNING
CIRCUIT

SCANNING
COIL

SPECIMEN

DETECTOR

AMPLIFIER

DISPLAY UNIT

VACUUM
SYSTEM
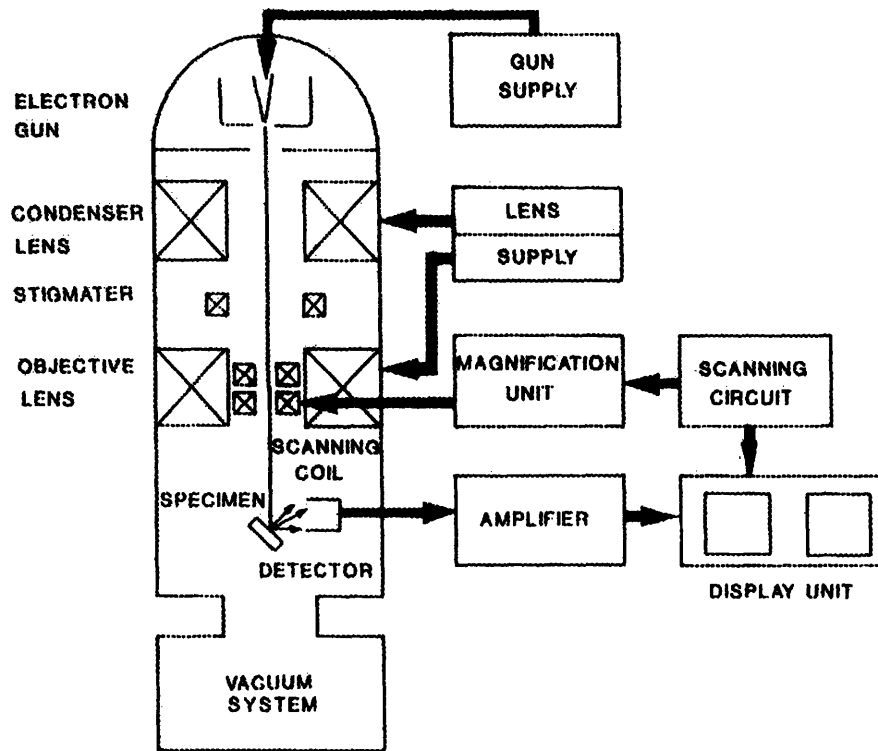
Figure 2.3 SEM block diagram.[A6]

2.5   Optical Methods

With the growing need for non-contact systems, optical measuring systems allow nanometer resolution without interfering with the surface being measured.   In optical profilometry, the most commonly used technique is based on phase-measuring interferometry, where a light beam reflecting off the sample surface is interfered with a phase-varied reference shown in Figure 2.4. The surface profile is determined from the resulting fringe patterns. With a collimated light beam and a large array of photodetectors, a large portion of the surface can be profiled simultaneously. The resolution is dependent on the stability of the medium it travels through, e.g. the refraction index of air.   With corrective measures implemented, typical vertical resolution is 0.3 nm, however the lateral resolution, which is limited by the diffraction limit of the visible light used, is approximately 1.5 μm[A3].   The lateral resolution of this method is not high enough for our application.
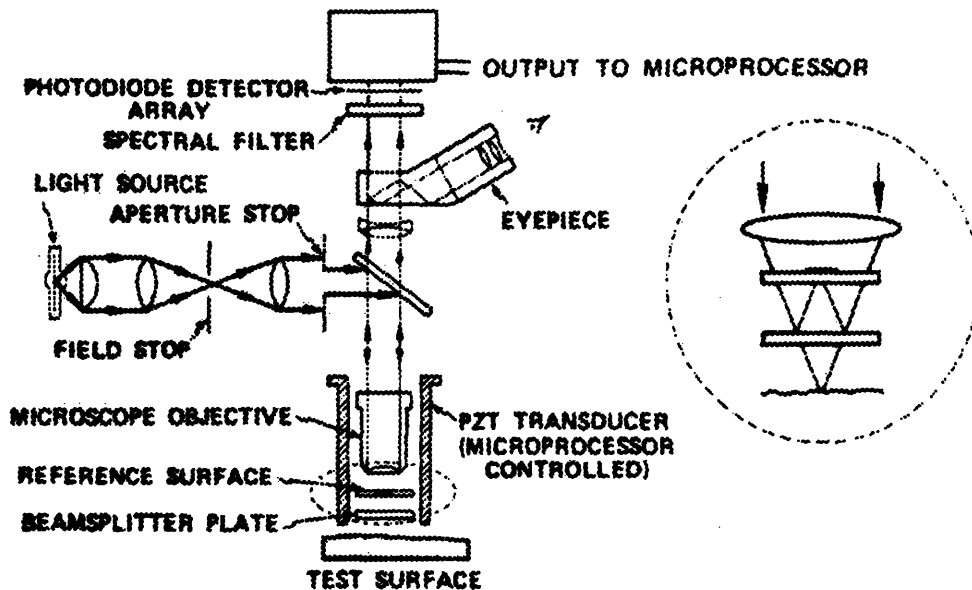
Figure 2.4 Laser interferometer.[A7]

2.6   Mechanical Stylus

A mechanical measuring system typically consists of a stylus with a sharp tip which is dragged along a surface. This is shown in Figure 2.5. The resulting mechanical displacement is converted to an electrical signal and recorded as the surface profile. The major draw back of this system is the fact that the stylus tip radius and the lateral resolution are generally about 0.1 µm. In order to obtain vertical resolution of $\leq$ 10 nm, the feedspeed must be between 2-100 µm s^{-1} and probe-to-surface contact forces range from 10^{-5} to 10^{-3} N [A3].
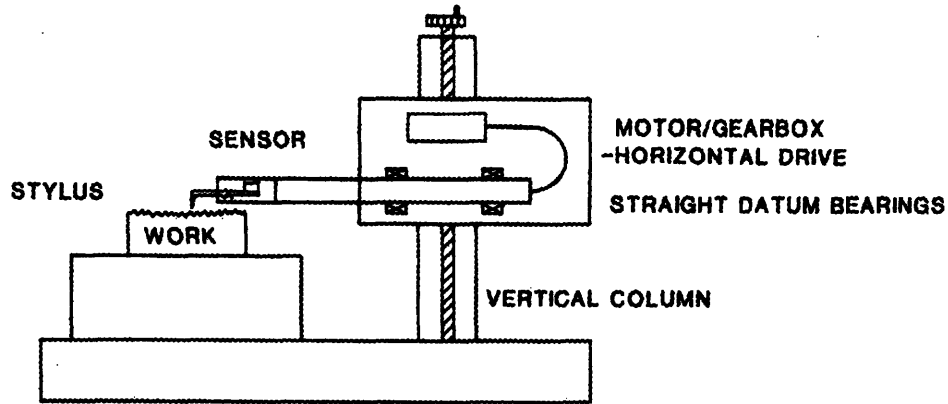
Figure 2.5 Mechanical Stylus System.[A6]

One particular mechanical stylus method utilizes a linear variable differential transform (LVDT) to record the surface topography by displacing a LVDT, Figure 2.6. One particular instrument was specially designed to diminish the effects of thermal drift. This device had contact forces ranging from 10^{-5} to 10^{-6} N, a lateral resolution, which is dependent on the width of the stylus tip, of 50 nm, and a vertical resolution of approximately 0.1 nm . In order to obtain this precision, the feedspeed was approximately 0.025 Hz or 10 μm s^{-1} [A8]. Not only are the feedspeeds are too slow for our application, but the lateral resolution also does not meet our specifications.
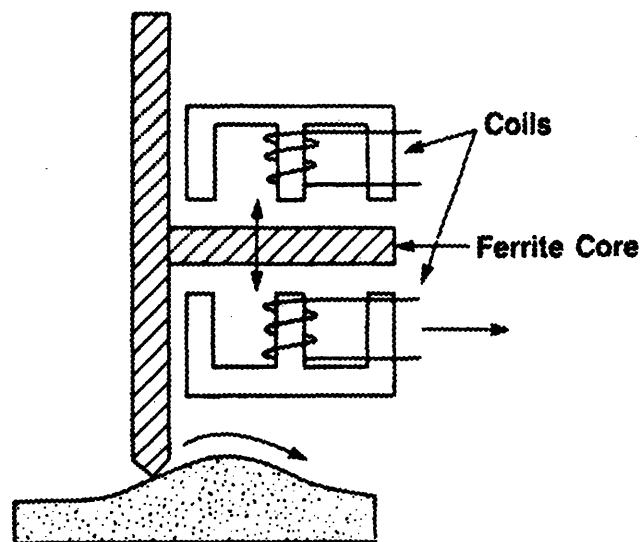
Figure 2.6 Schematic of LVDT stylus.[A7]

2.7 Scanning Probe Microscope

Based upon the lateral resolution requirement (less than 0.02 μm), most of the conventional methods mentioned above are not suitable high resolution profile solutions. From Figure 2.7, the scanning probe microscopes (SPM), such as the atomic force microscope and scanning tunneling microscope, have the ability to meet our vertical and lateral resolution requirements. SPMs utilize a probe which is moved over the sample surface with a piezoelectric positioner. SPM probes vary greatly which is why so many instruments fall under this category. First, the Scanning Tunneling Microscope (STM) detects the changing tunneling current between the sample surface and the probe tip. Next is the Atomic Force Microscope (AFM) which utilizes a contact method with probe tips made of diamond, silicon, and silicon-nitride. Also being utilized is the Scanning Near-field Optical Microscope (SNOM) which utilizes optics in the near-field of the sample surface. Finally several less conventional methods discussed are scanning capacitance microscope, scanning thermal microscope, magnetic force microscope, eletrostatic force microscope, and non-contact atomic force microscope.
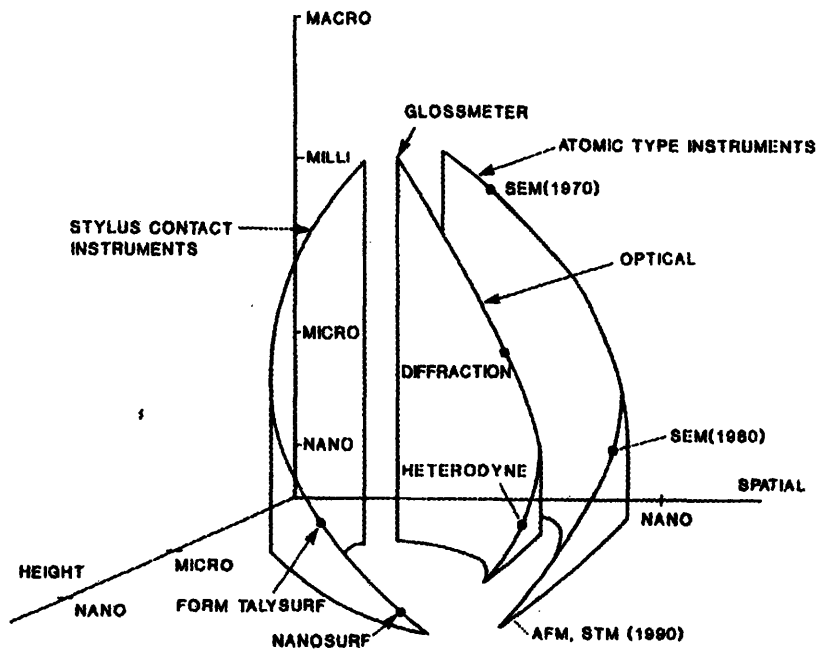
Figure 2.7 Trends in Resolution or Probe Microscope vs. Stylus.[A6]

25

2.7.1 Scanning Tunneling Microscope

The concept of a Scanning Tunneling Microscope (STM) was first developed in 1972 by Young, *et al*[A9]. The STM works by suspending the probe tip nanometers away from the sample surface and applying a voltage potential between the sample surface and probe tip. The resulting tunneling current is then monitored. The microscope then uses piezoactuators to scan the surface by moving the probe, and the "Z" actuator maintains a constant tunneling current which corresponds to a constant spacing between the tip and sample surfaces, see Figure 2.8. The STM is attractive because it is a non-contact device, which results in no surface damage and a potential for high speed profiling. Typical vertical resolution of the STM is ≤0.1 nm and lateral resolution is ≤1 nm [A6]. Figure 2.9 clearly shows the strengths of the STM compared to some of the more conventional methods discussed earlier. The primary limitation of the STM is that it can only be operated using electrically conductive surfaces. In our application, the sample surface can be electrically nonconductive. As a result, the powerful STM technique is not a viable option for our application.
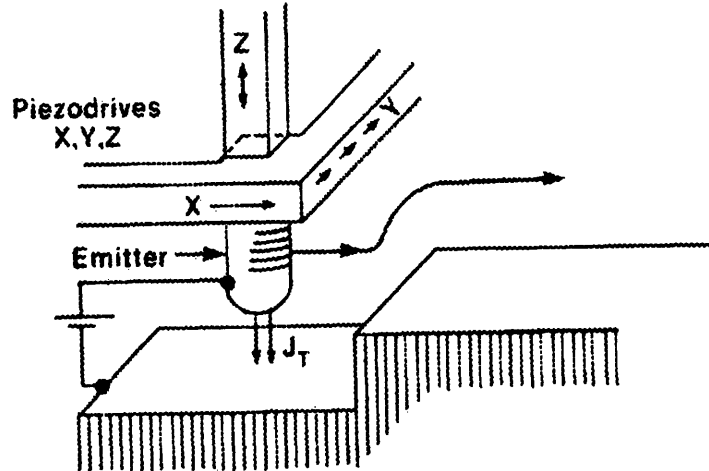
Figure 2.8 STM performing a scan.[A7]
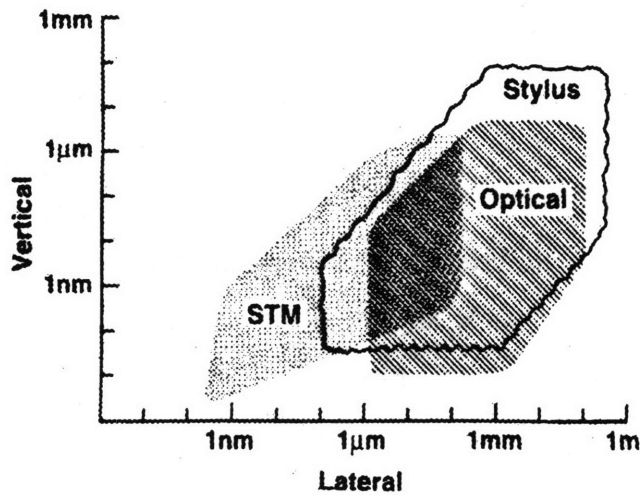
Figure 2.9 STM compared with optical and stylus methods.[A7]

2.7.2 Atomic Force Microscope

The atomic force microscope (AFM), developed by Binnig, *et al*[A10] in 1981, is able to obtain very high vertical and lateral resolution on both conducting and nonconducting surfaces[A11]. A contact mode AFM performs a scan by moving a tip, mounted on a cantilever beam, relative to a sample surface using precision actuators, Figure 2.10. The cantilever deflection directly measures the topography of the sample surface. With a probe tip radius of approximately 20 nm, the AFM offers high lateral resolution ≤ 20 nm and vertical resolution ≤ 1 nm [A12] and probe-to-surface contact forces range from 10^{-8} to 10^{-11} N [A7].
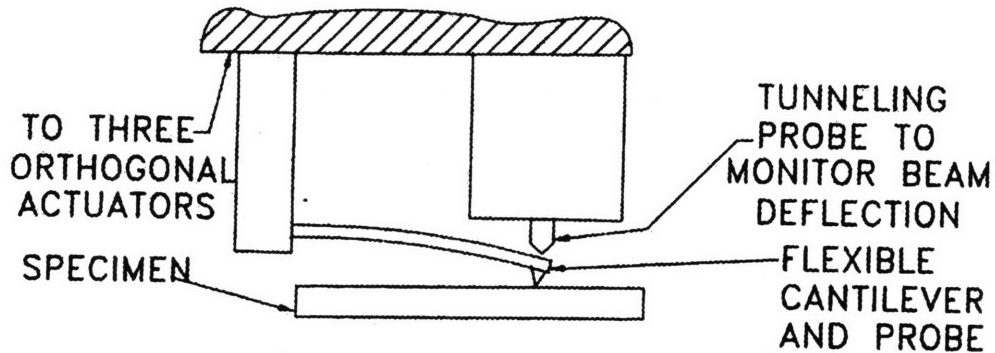
Figure 2.10 AFM with STM cantilever beam position sensor.[A6]

The contact AFM uses different techniques for detecting the cantilever beam deflection. Figure 2.10 shows the use of an STM to detect the cantilever position while Figure 2.11 demonstrates the more commonly used optical lever. The optical laser A little less common is the use of piezoelectric and piezoresistive cantilevers which have the cantilever detection mechanism embedded into the cantilever itself [A11]. Figure 2.12 shows the piezoresistive cantilever without a tip. All of these systems are able to provide sub-nanometer resolution. However, the optical lever and STM both require some type of alignment and also add the complexity and size of another system to the design. Since our application needs to be as physically small as possible in order to meet the speed requirement, the piezoresistive cantilever is most attractive.
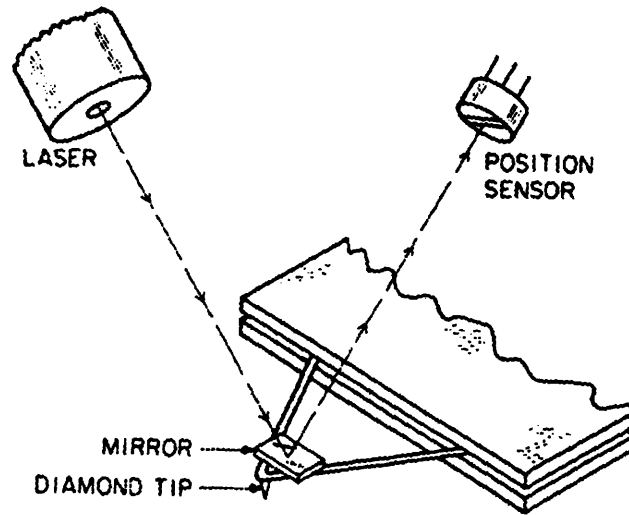
Figure 2.11 AFM with optical lever sensor.[A12]

$$V_1 \cdot V_2 = -V \frac{\Delta R}{4R}$$
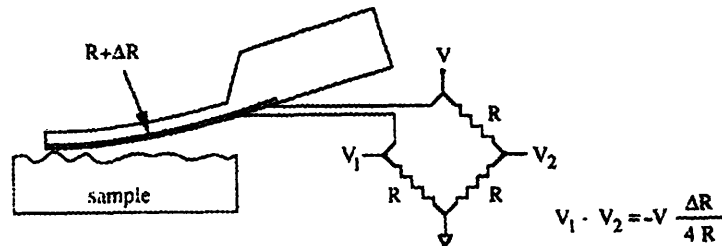
Figure 2.12 Piezoresistive cantilever (no tip).[A11]

2.7.3 Scanning Near-Field Optical Microscope

In a scanning near-field optical microscope (SNOM) the sensing probe utilizes a small hollow tapered tip with an apex radius of curvature on the order of 10 nm. The tip is often a specifically manufactured fiber optic. The probe is brought within the near field of the surface, approximately 10 nm, and the sample surface is exposed to light from the probe. The resulting transmitted or reflected light is then collected to determine the image of the surface. Figure 2.13 shows a schematic of the many components of an SNOM. Figure 2.14 provides a detailed close-up of the probe portion of the SNOM. SNOM technology is still currently being researched with lateral and vertical resolution down to 10 nm [A13]. However, the major limitation of this method are the long scan times which are approximately 1 μm s^{-1}, caused by maintaining the tip to sample spacing on the scale of nanometers [A2]. For our application, the near-field optical microscopes do not meet our vertical resolution or speed requirement.
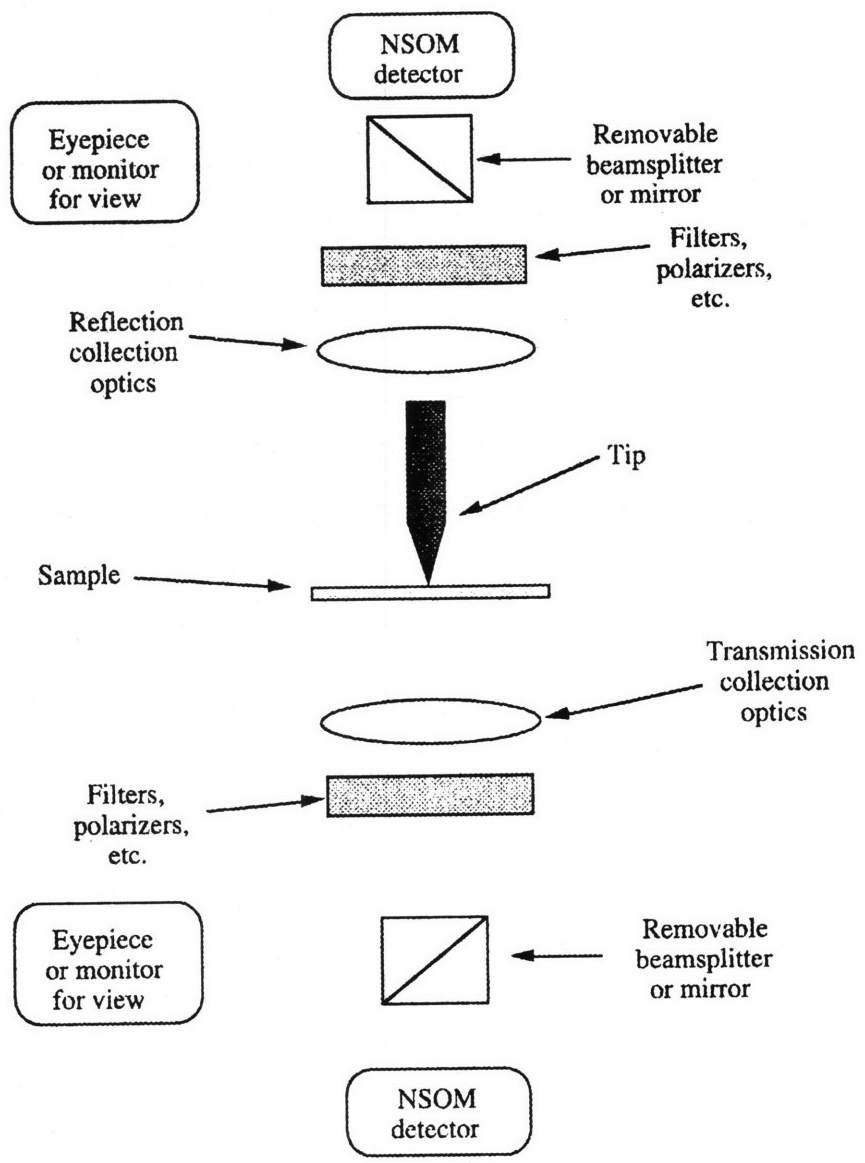
Figure 2.13 SNOM schematic.[A13]
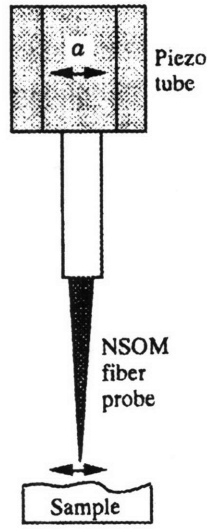
Figure 2.14 SNOM probe.[A13]

2.7.4 Non-contact AFM

In the non-contact AFM, van der Waals Forces are measured by vibrating the cantilever, with stylus tip, near its resonance frequency, and detecting the change in the vibrational amplitude of the beam due to a change in the force gradient. The force gradient is proportional to the surface profile [A14]. The reason for the van der Waals interactions can be seen in Figure 0.1. Figure 0.2 provides a detailed look at a non-contact AFM probe. Notice that the piezoactuator oscillates at a specified frequency in order to control the vibration amplitude of the cantilever. The non-contact AFM is more susceptible to noise because van der Waals forces are difficult to measure. Also, since the tip is suspended above the surface, the achievable lateral resolution, approximately 30 nm, is decreased as well [A9]. As a result, the contact AFM would be preferred to the non-contact AFM.
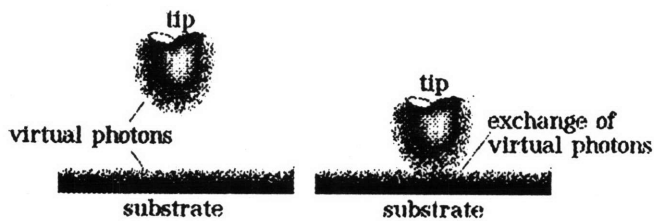
Figure 2.15 Virtual photon exchange give rise to van der Waals interactions.[A16]

AFM cantilever & tip

a

$A = aQ$

Piezo
actuator

Sample
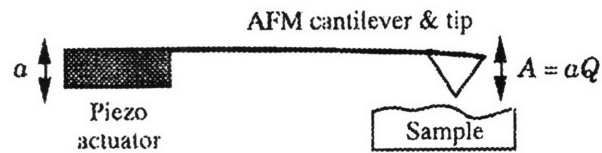
Figure 2.16 Non-contact AFM probe.[A2]

2.7.5 Scanning Thermal Microscope

The scanning thermal microscope measures the temperature of an electrically heated probe tip. Figure 0.3 shows a detailed schematic of the thermal probe. As the tip comes into close proximity of the sample, a thermal coupling between the tip and sample results in heat transfer. The thermal coupling and heat transfer vary as a result of gap spacing between the probe and sample surface changes. As the heat transfer rate varies, the probe tip temperature changes, hence the surface topography can be obtained from measuring the temperature of the probe tip. This temperature change is detected by a very small thermal probe and this information is fedback to the piezoacuators which move accordingly. The primary limitation is rather large lateral resolution which is approximately 100 nm, which is caused by the size of the thermal probe because of the thermal interaction between the probe and the surface features, however the vertical resolution has been measured to be 3 nm [A17]. This method is not viable for our application because the lateral resolution capabilities do not meet our requirements .
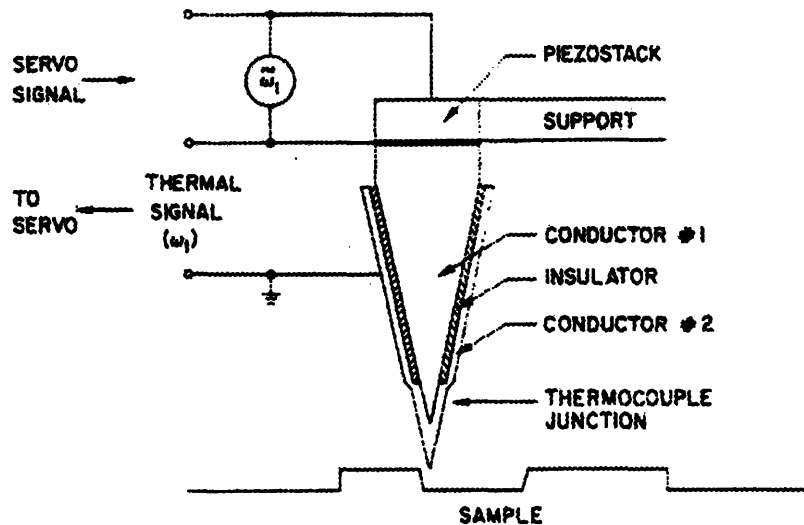
Figure 2.17 Scanning thermal microscope probe.[A17]

2.7.6 Magnetic and Electrostatic Force Microscopy

The magnetic and electrostatic force microscopes measure the force due to a magnetic and eletrostatic potential field, respectively. The magnetic force microscope has a vertical resolution of ≤10 nm, which is limited by probe tip size and its interactions with the surface features [A18]. The electrostatic force microscope measures the force between the tip and sample caused by an applied AC voltage. The primary limitation with these methods is that both sample and tip need to be conductive which is not the case in our application [A19].

2.7.7 Scanning Capacitance Microscopy

The scanning capacitance microscope measures the capacitance between the probe tip and sample. Figure 0.4 provides an electrical schematic of the scanning capacitance microscope. Although vertical and lateral resolution of 25nm have been achieved, vertical and lateral resolution of 10 nm is predicted [A20]. The limiting factor of this resolution is the probe tip size and its interaction with the surface features. Even though this method does meet the lateral resolution requirements, the desired vertical resolution cannot be achieved.

33
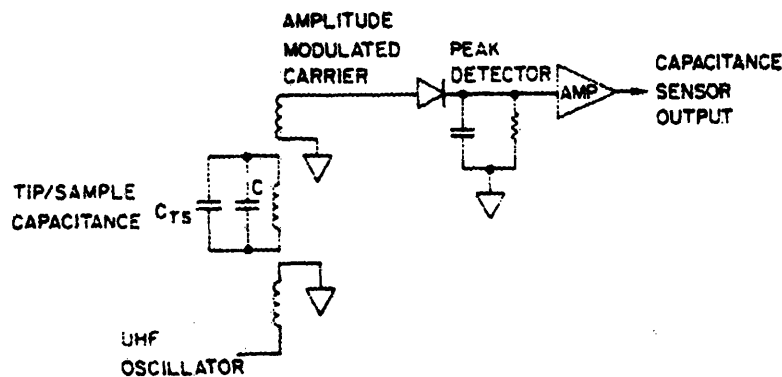
Figure 2.18 Scanning Capacitance Microscope schematic.[A20]

2.8   Selection of Profilometry Method

Having reviewed several of the more conventional profilometry techniques, the most appropriate method for our particular application will be selected. Since a thin nonconductive film covers the entire scanning region, some of the above techniques are not feasible for our application. Also, the non-contact methods were not designed to measure topography directly, because they are a function of both surface topography and other properties such as local dielectric constants, van der Waals forces, etc. This often reduces lateral resolution significantly. Furthermore, the samples are not to be destructively tested which further limits our choice of available profilometry methods. The effect of these application specific requirements on the selection of a profilometry technique is discussed below.

First, some of the physical characteristics of our sample immediately eliminate several techniques. Since our sample surface is encased with a thin film of insulated material, the STM, magnetic force microscope, and electrostatic force microscope cannot be utilized. These methods require the establishment of a potential between the sample and probe surfaces and the insulating material prevents this from occurring.

Secondly, the requirements placed on the performance of our device exclude several more techniques. Since the vertical resolution needs to be less than 5 nm, the scanning capacitance microscope is not able to meet those specifications. Since the lateral resolution is required to be

less than 20 nm, the optical methods, mechanical stylus methods, scanning near-field optical microscope, non-contact AFM, and scanning thermal microscope are also not viable solutions. The speed of the scan is also a requirement which several of the aforementioned methods cannot achieve.

Finally, the condition of the sample, after the scan, must be unmodified. In other words, the act of scanning the sample is not to disturb or damage the sample surface in any manner. As a result, the SEM is a technique which cannot be utilized.

Hence, the contact AFM is the most appropriate choice for profilometry method. With the contact AFM, the necessary resolution is met and the scans can be performed without damaging the sample surfaces. In order to maintain the speed requirement, the peizoresistive cantilever will be utilized to reduce weight and system complexity.

2.9 Summary

In this chapter, the above examination documents the strengths and limitations of many profilometry techniques. The technique chosen to be the most appropriate for this particular application is scanning probe microscopy. In particular, a contact AFM with a piezoresistive probe will be implemented in our device to perform the profilometry of our sample.

3. Design Alternatives

3.1 Introduction

After determining that the contact AFM method is the most appropriate technique for this particular application, several design alternatives were developed and evaluated. In the previous chapter, the best type of AFM cantilever beam detection device for our application is a piezoresistive cantilever. Since the only commercially available piezoresistive cantilever is the Park Instruments Piezolever[B1], all of the conceived designs specifically consider this piece of hardware. The design information of the Piezolever will be discussed in section 4.2 System Hardware. Multiple designs were considered and some designs were immediately discarded due to specific limitations of actuator technologies and other application specific concerns. The four most promising designs were considered for further examination and were compared with one another for a final selection.

3.2 Design Alternatives with Atomic Force Microscopy probes

After reviewing several methods of contact AFM scanning, two different classes of devices were examined. One category of devices maintains the probe's tip position normal to the surface and the other category uses software to process the scanned image with the tip contour to determine the sample surface. In both cases, the Piezolever approaches the sample, and as the tip contacts the surface, the cantilever beam begins to deflect. This deflection is detected by the piezoresitive material in the Piezolever. The actuators continue to move until a predetermined deflection is reached and then the scan begins. During the scan, the predetermined deflection is maintained by feeding back the Piezolever signal to control the actuators' motion. The voltage or current quantities are recorded to determine the scanned image of the surface, Figure 3.1.
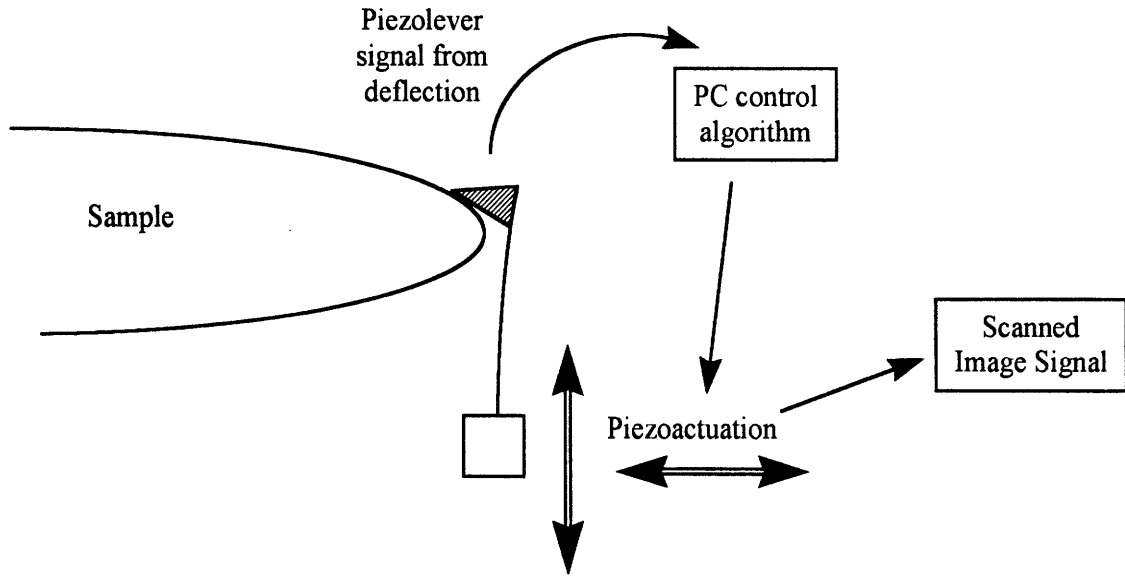
Figure 3.1. Scanning with a Piezolever.

3.3 *Designs that Maintain the Probe Tip Normal to the Surface*

This class of designs maintains the probe tip perpendicular to the sample surface as shown in Figure 3.2(a). This not only avoids additional computer image processing, which could delay our scans, but also significantly reduces many errors associated with a skewed tip's interaction with the surface Figure 3.2(b). The following designs and their hybrids were considered.
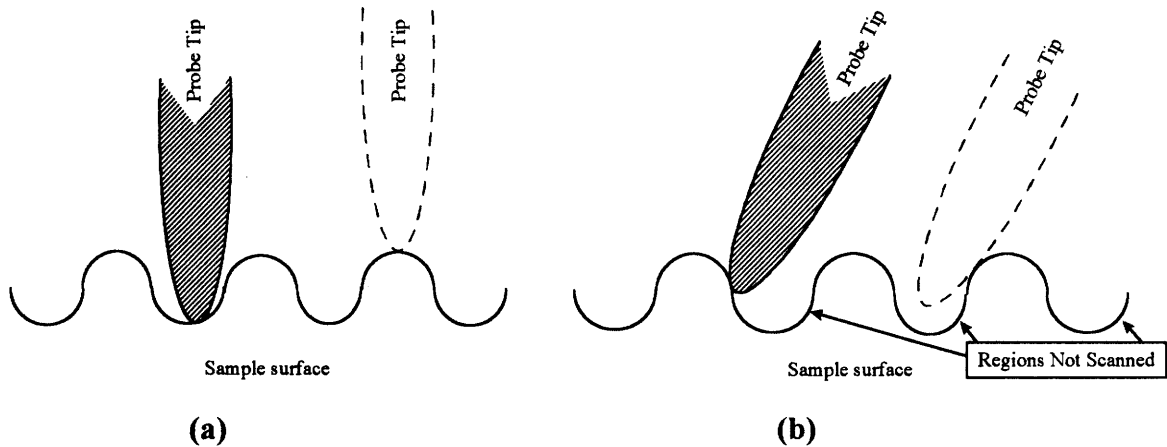
Figure 3.2 Tip's interaction with the sample surface.

3.3.1 Skid Design

The Skid Design employs a passive mechanism to maintain the orientation of the probe tip perpendicular to the sample surface. A skid, which has a larger contact surface area than the

probe tip, is used to maintain local perpendicularity to the sample surface, Figure 3.3. In order for this design to be effective, the skid needs to be located as close as possible to the probe tip. This physical separation might result in the probe's tip orientation containing a significant amount of error, especially when the skid encountered the sample tip surface. Close to the sample tip the orientation changes approximately 80° in less than 50 nm. As a result of the errors close to the sample tip, this design will not be considered for further examination, Figure 3.4.
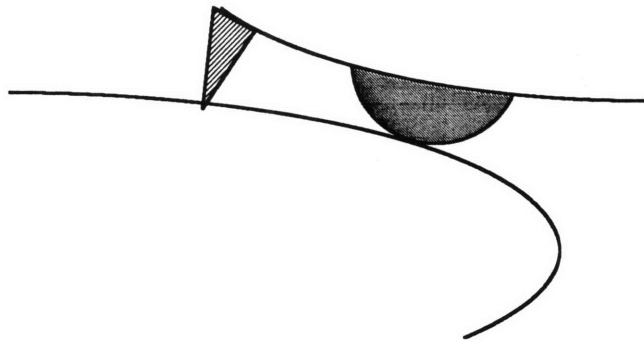
Figure 3.3 Skid Design.
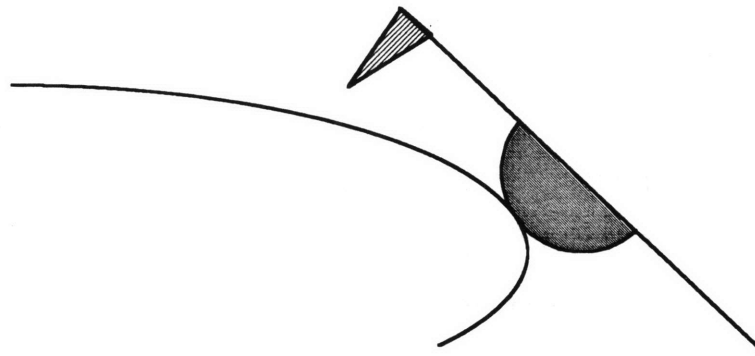
Figure 3.4 Skid Design encountering the sample tip.

3.3.2 Follower Design

The Follower Design adds an additional probe to the design, so now there are two probes. The first probe scans the surface to obtain the localized slope of the sample. Then the second probe uses the information gained from the first probe scan, specifically the slope of the surface profile, and actively orients itself to ensure it is continuously normal to the sample surface, Figure 3.5. This technique is the foundation of all the active orientation designs discussed in the following subsections. After reviewing this method, it was determined that one probe could properly

maintain the probe tip orientation normal to the surface by utilizing the information from the sensors to obtain the local slope of the sample. As a result, this particular design is not considered for further examination but several of its descendents will be.
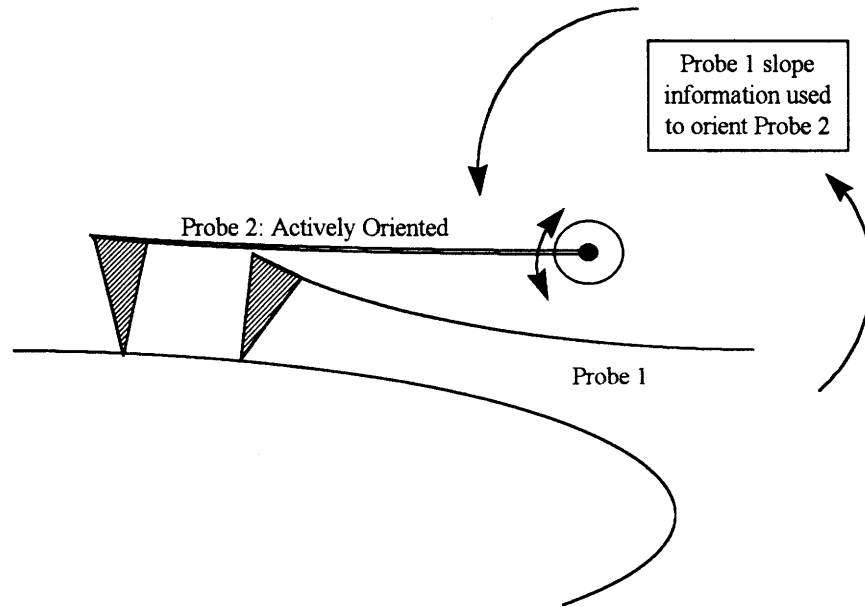
Figure 3.5 Follower Design

3.3.3 Parallelogram Device

The Parallelogram, Figure 3.6(a), uses two linear actuators to actively control the y position and orientation of the probe tip. There is also a coupling of the x and y positions with the rotation of the tip. The third linear actuator controls the x position of the probe tip. In order for this design to function, the hinge stiffness needs to be maintained with respect to one another. Hinge 1 must have a lower stiffness than Hinge 2 and Hinge 3. Hinge 2 and Hinge 3 must have different stiffnesses, and it does not matter which is more stiff as long as the quantities are known. Knowledge of the hinges' stiffness is necessary in order to accurately predict the behavior of the device. As advanced materials become more readily available, the stiffness of materials will become more easily controllable. At this point in time, stiffness control is still in the research and development phases[B2]. A hybrid device, called the Sliding Parallelogram, is shown in Figure 3.6(b). Both of these designs, will actively determine the orientation and position of the probe tip by moving the probe in small steps in the x or y direction and then compensating to reapply the desired preload to the piezolever. From this information, the local slope of the sample surface can

be calculated, hence the use of a second probe, as in previous designs, is not necessary . Using piezostacks to provide the precision actuation, the device is capable of meeting our requirements so it will be further examined in the final section of this chapter.

(a)

Parallelogram

(b)

Sliding Parallelogram
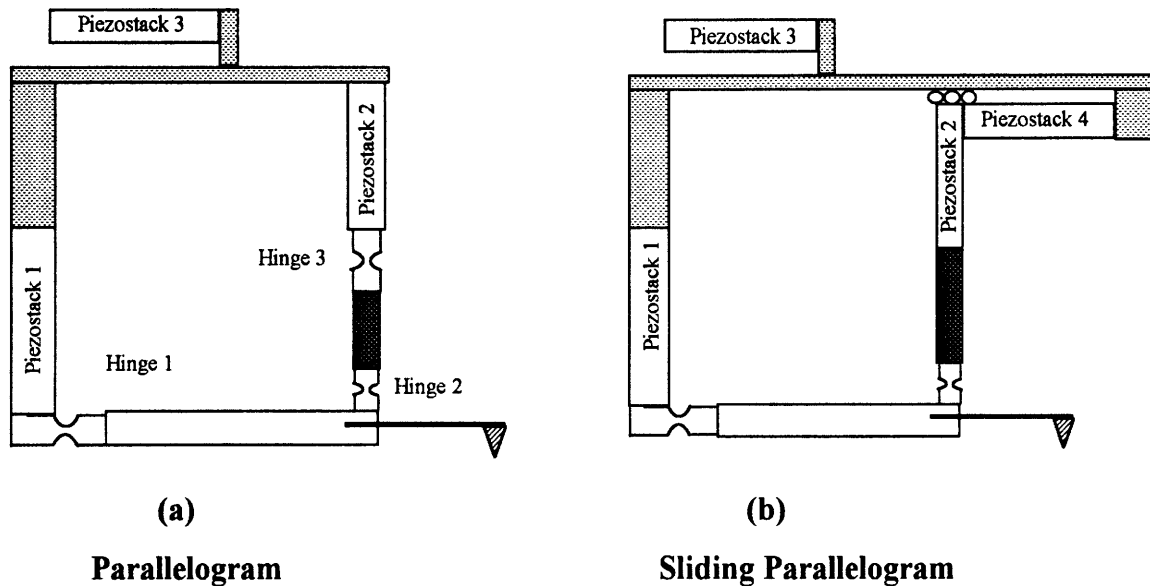
Figure 3.6 Parallelogram Designs.

3.3.4 Motor Driven Radial Rotation Design

The Motor Driven Radial Rotation Design uses two linear actuators and a rotary actuator, Figure 3.7. This device allows the probe tip to remain normal to the sample surface during the entire scan. In order to maintain high speeds, the rotary actuator must be physically as small as possible as well as light weight. This device concept proved difficult to design because the rotation of the actuator caused significant disturbances in the x and y position of tip. Since the distance from the point of rotation to the contact point on the tip of the probe is approximately 3.5 mm, piezostack P1 would have to move $3.5cos\theta$ mm and P2 needs to move $3.5sin\theta$ mm to compensate for the disturbance, see Figure 3.8. If θ rotates from zero to 45 degrees, the required compensatory motions of P1 and P2 would be 1.03 mm and 2.47 mm respectively. Piezostacks with this range of motion have resolution greater than 1 μm [B3]. As a result, we did not pursue this particular design any further, however it was the foundation for the next design alternative.
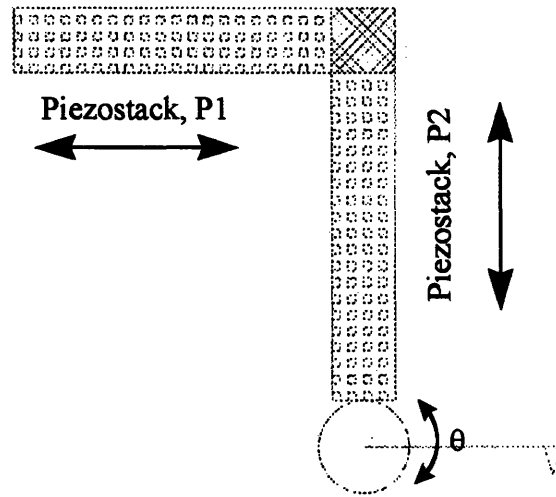
Figure 3.7: Motor Driven Radial Rotation Device.
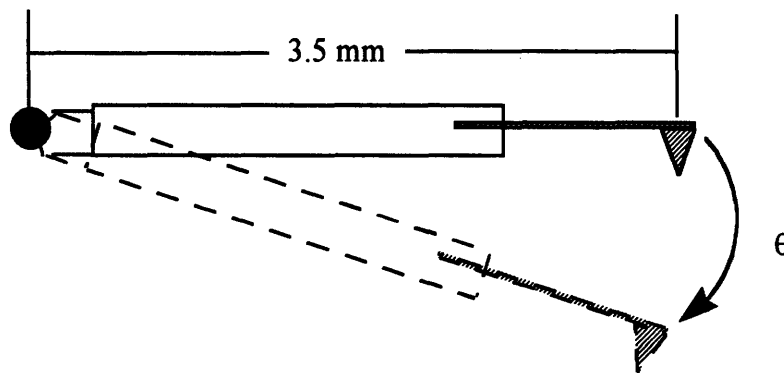
Figure 3.8 Rotation of Probe.

3.3.5 Motor Driven Axial Rotation Design

The Motor Driven Axial Rotation Design utilizes the premise of the previous Radial Rotation Design and simply changes the orientation of the position of the probe Figure 3.9(a) and (b). By changing the position of the probe, this design removes the large range requirement of the actuators. With a small motor, this system could maintain perpendicularity of the probe tip. The smallest commercially available motor which meets our mass and precision requirements is available from Precision Motion Controls[B4]. Their smallest motor is 10mm x 10mm x 30mm and has a mass of 50g with resolution to $9°$[B4]. The range of both linear actuators or piezostacks needs to be more than 5 μm in order to ensure that the probe tip does not collide with the sample when positioning. Physik Instrumente makes piezostacks with this range and resolution to 20 nm[B3]. The main concern with this design is that most commercially available

probes are scanned in the longitudinal direction, not the lateral direction, Figure 3.10(a) and (b). After discussing this unconventional use of the Piezolever with Marco Tortonese, the designer and developer of the Park Scientific Instruments' Piezolever, he mentioned that extensive finite element analysis and system testing and evaluation would be required to determine the predictability of such a change[B5]. This design meets all of our requirements and will be examined with other designs in the final selection process.

(a) Front View   (b) Side View
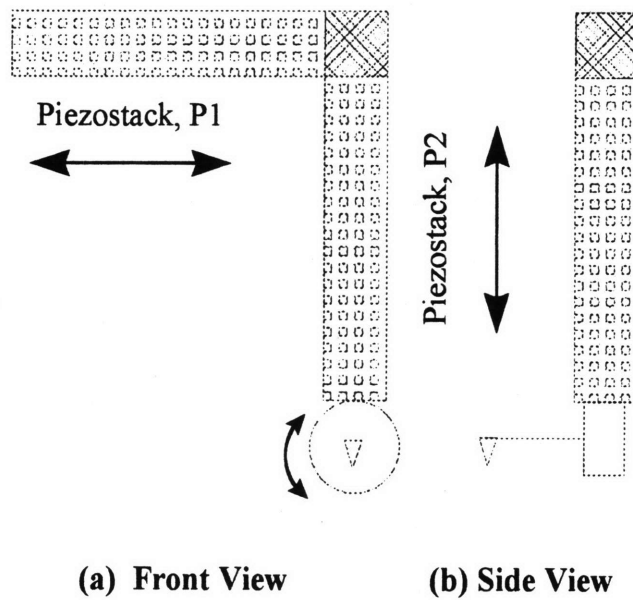
Figure 3.9 Motor Driven Axial Rotation Device.

(a) **Longitudinal Scan**   (b) **Scanning Laterally**
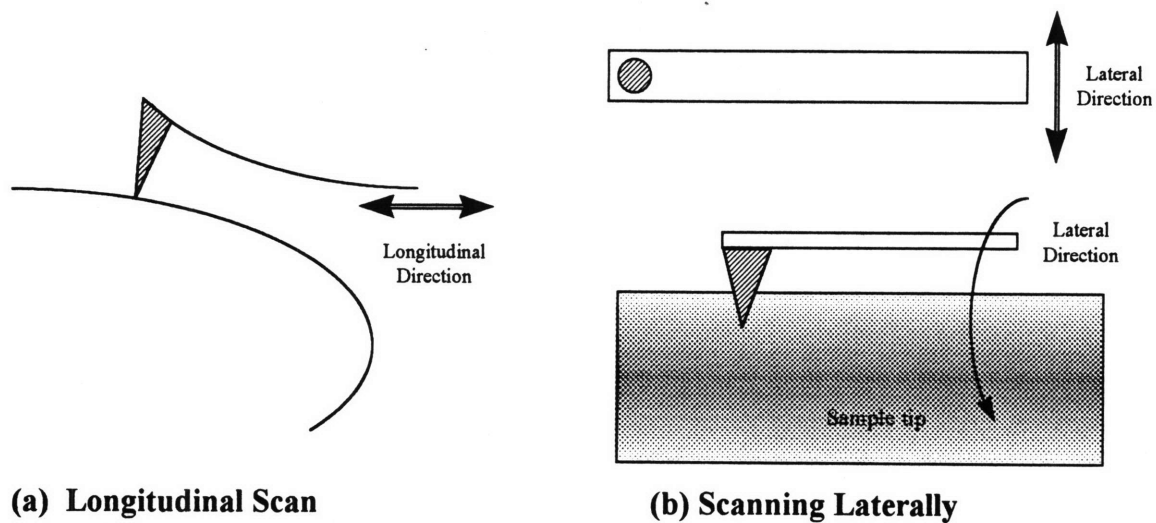
Figure 3.10 Cantilever Scanning Methods.

3.4 Designs that Require Software to Process the Image

This class of design initially performs the scan on a calibration piece in order to obtain the contour of the piezolever tip. Next, the sample is scanned and an algorithm takes this scanned sample image and the image from the tip scan and processes the information to reconstruct the actual surface of the sample as seen in Figure 3.11. The image resolution is still dependent on the contact angle of the tip to the surface, so maintaining the tip as close to perpendicular as possible is desired. If this class of design is selected, a more thorough exploration of the topic will be discussed in Chapter 4. The following four designs were considered.
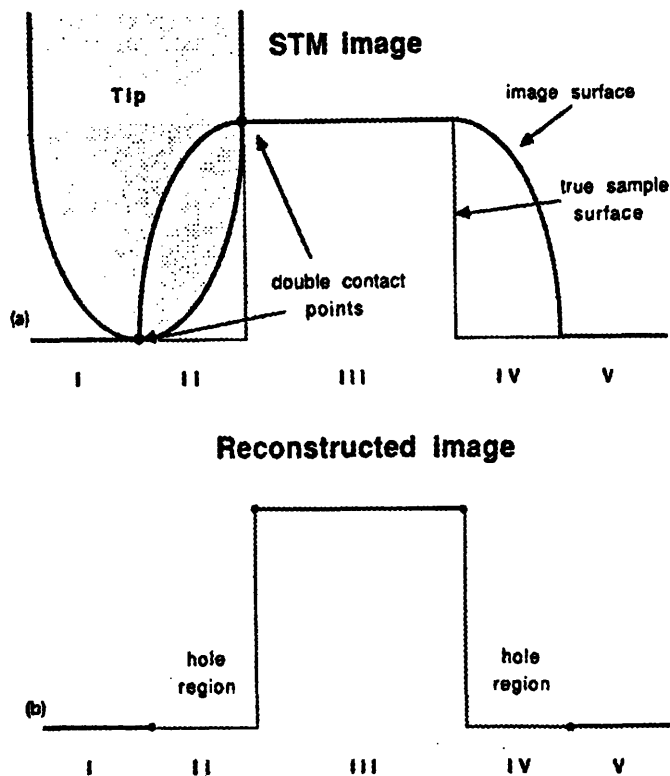
Figure 3.11 Reconstruction of image.[B6]

3.4.1 Single Pass Design

The Single Pass Design is the most simple of any of the designs reviewed. Since the tip length if the piezolever is 3 μm[B7], there is only a need for two linear actuators, Figure 3.12. P1 needs to be a high resolution actuator, however P2 only needs to have resolution on the order of 500 nm. The deflection of the cantilever and the image convolution will obtain the desired surface image.

The strength of this design is the fact that the resolution close to the tip of the sample is very high, however, since the probe is almost parallel to the slope of the sample toward the base of the sample, the image resolution is not as high in that region. This design is attractive because of its resolution at the tip, the need for only two actuators (only one of which needs nanometer resolution), and its simplicity. This design will be considered for further evaluation in the design selection of this chapter.
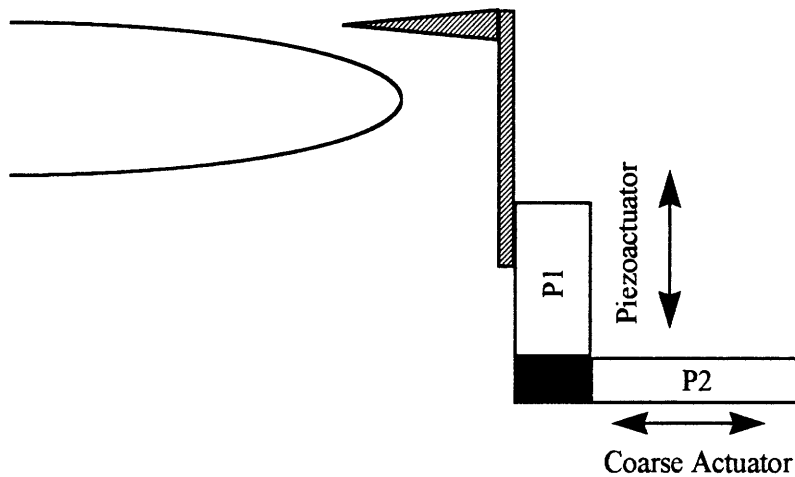
Figure 3.12 Single Pass Design.

3.4.2 Sheath Design

The Sheath Design incorporates the design of the Single Pass Design and introduces the use of a datum as a reference in the performance of the scan, Figure 3.13. The sheath itself is the datum and its dimensions are used in conjunction with the scanned information to determine an image of the surface. This method attempts to maintain the probe normal to the surface for the majority of the scan. This design requires two actuators: one to adjust the vertical position of the probe tip and the other to drive the device along the contour of the sheath. Both of the actuators must be high resolution. The major disadvantage of this design is the mechanism used to drive the probe about the sample. The cart and sliding mechanisms able to perform the type of motion with the resolution and speed this design requires is not feasible. As a result, this design is not considered for further study.
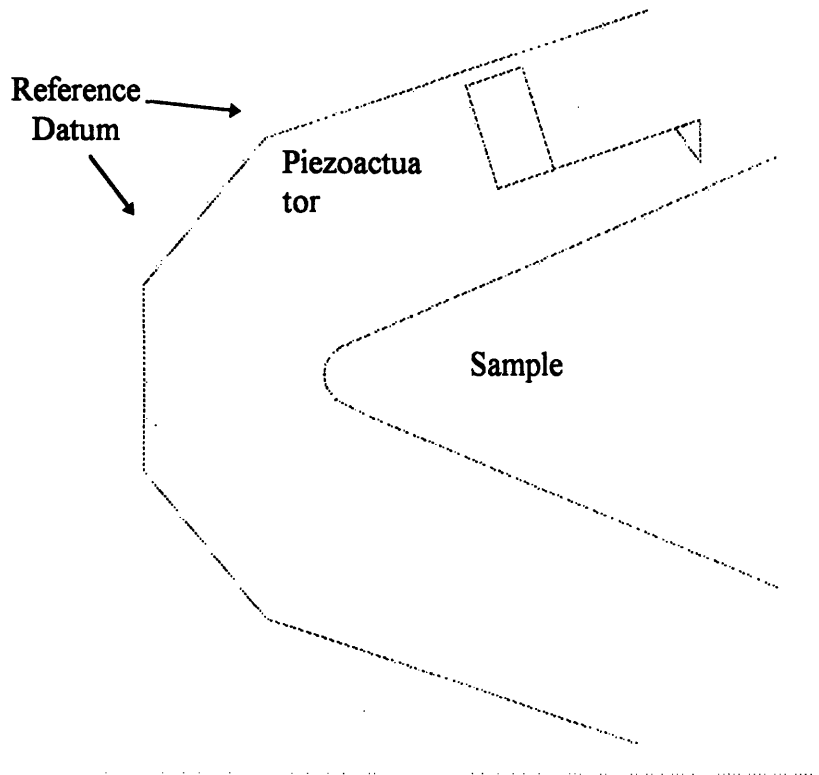
Figure 3.13 Sheath Design.

3.4.3 Lock and Pull Design

The Lock and Pull Design utilizes the principles of the Single Pass Design and applies it to a dual probe approach. The two probes are fixed to a coarse actuator, P1, as show in Figure 3.14, and are brought together and locked prior to the scan. Both probes are heavily loaded in the beginning of the scan and as the second actuator, P2, pulls the two probes down the sample surface, the piezolever records the necessary information. The major advantage of this design is that it provides faster scan times because both sides of the surface are being scanned simultaneously. This design also only needs two actuators, one with high resolution, P2, and the other actuator, P1, does not require high resolution motion and could even be a ball screw mechanism. There are two major concerns with this design. First, the scan resolution close to the tip of the sample is poorer, because the probe tip is almost parallel to the surface. Second, the samples are not always symmetric about the centerline, Figure 3.15. This can cause increased loads on the piezolevers and its unpredictability leads to the need to independently control the

46

position of the probes. As a result of these disadvantages, this design does not receive additional consideration however it is the foundation for the next design concept.
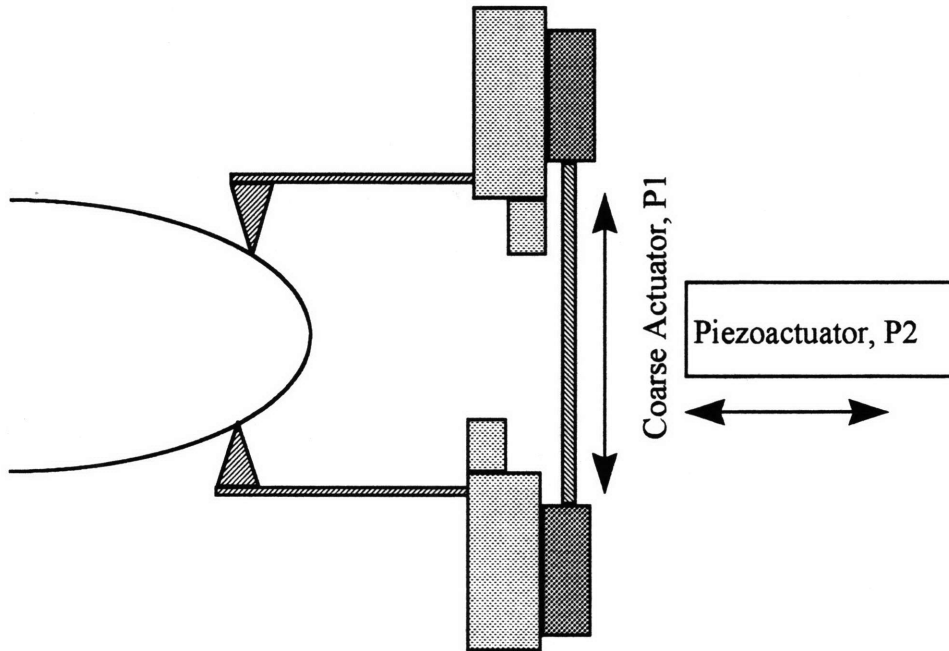
Figure 3.14 Lock and Pull Design.
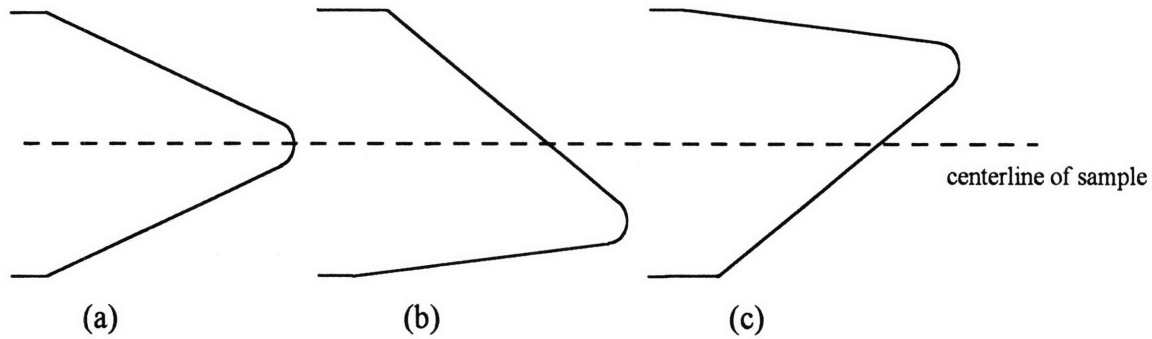
Figure 3.15 Sample shape uncertainty.

3.4.4 Scissors Design

The Scissors Design utilizes the dual probe approach mentioned in the Lock and Pull Design, but adds independence to the control and positioning of both of the probes. In this slightly more complex design, the scan is still performed on both sides of the sample simultaneously, however the independence of each probe allows for the scanning of any unbalanced samples. As in the

Lock and Pull Design, neither probe tip will be continuously normal to the sample surface, but this discrepancy will be minimized by optimizing the position of the probe with respect to the hinge mechanism [B8]. Figure 3.16 shows the Scissors Design. Piezostacks P1 and P2 independently push on Arm 1 and Arm 2 respectively. The arms have the same axis of rotation at the hinge. The "preloads" specified in the drawing are to make certain that the axis of rotation for each arm remains constant. On the end of Arm 1 closest to the sample is Probe 1, which is a piezolever. Arm 2 has Probe 2 attached to it. The hinge and all piezostacks are attached to the housing. The system requires three high resolution linear actuators, which would probably be piezostacks. Piezostack P3 drives the scissors apparatus along the required scan length of the surface with the necessary resolution, while piezostacks, P1 and P2, independently control the position of the two respecitve probes. This design will also be considered against the best designs in the design selection portion of this chapter.
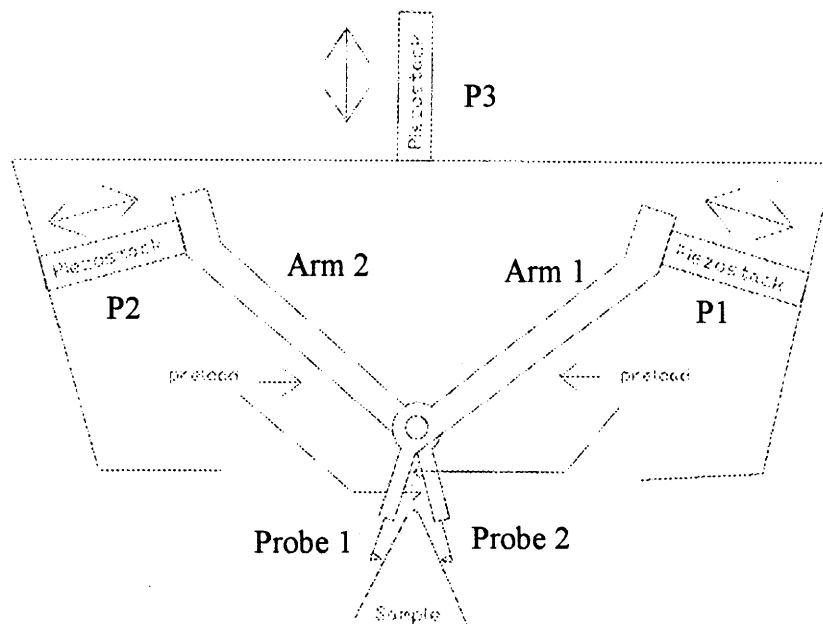
Figure 3.16 Scissors Design

3.5   *Design Selection*

Having discussed several designs in the previous sections, the top four designs are being more carefully reviewed and compared to one another in order to determine the best design to implement. The four designs that meet our functional requirements: (1) Motor Driven Axial

Rotation Device, (2) Parallelogram, (3) Scissors, and (4) Single Pass are all examined in Table 3.1. The criteria used to judge the designs are Range, Resolution, Accuracy, Repeatability, Cost, Speed, Wear, and Maintenance. Range considers the ability for the probe(s) to travel the required distance. Resolution is the largest of the smallest motion the probe tip can make. Accuracy is the ability to tell the truth or the correctness between the sample surface and the measured sample surface and includes error susceptibility which considers: (1) stiffness of the design, (2) heat dissipation, and (3) how well the design attenuates errors, such as cantilever effects, ambient resonances, etc. Repeatability is the act of reliably and repeatedly obtaining the same piece data[Slocum]. Cost considers the amount of resources needed to design and develop the device. Analysis time, number of actuators, manufacturing expenses, and material expenses are all examples of items considered under Cost. Speed considers the time it takes the device to produce one scan. Since this is an assembly line application, the faster devices receive higher grades. Wear considers how often parts and actuators become damaged such as hinges, piezostacks, probe tips, etc. Finally, Maintenance considers the ease, time, and cost of replacing worn or damaged parts. Of the eight criteria examined, the areas most heavily valued are Resolution, Accuracy, Speed, Range, and Repeatability. Cost, Wear, and Maintenance are important, however the device can still accomplish its tasks even if these three areas are receive low grades.

The grading system, * - Excellent, + - Good, o - Fair, and x - Poor, is defined by using engineering judgment to compare the four selected designs with one and other. It is easiest to explain by example, so Cost will be examined. The main characteristics that influence Cost are the number of actuators and the design complexity. Axial Rotation design received a "Poor" grade for Cost because a significant amount of time and analysis is required to examine the performance of the piezolever being loaded in the lateral direction. Also that design requires three actuators which adds to the cost. The Single Pass design received an "Excellent" grade, because only two actuators are needed of which only one is high precision. This design is also simple and the convolution algorithm requires a minimal amount of analysis. The Parallelogram received a "Fair" grade because the system has three actuators and calibration of the hinges will be time consuming. The Scissor Design, which received a "Good" grade also requires three actuators and most of the additional analysis is in the software portion of the system, such as the convolution

49

algorithm and controller schemes. Hence, for Cost, the "average" design has three actuators and requires a moderate amount of system analysis.

Design Criteria	Parallelogram	Single Pass	Axial Rotation	Scissors
Resolution	o	x	*	*
Accuracy	o	+	+	*
Speed	o	*	*	*
Range	o	*	*	*
Repeatability	o	*	*	*
Cost	o	*	x	+
Wear	o	*	+	+
Maintenance	x	*	+	o

* - Excellent + - Good o - Fair x - Poor

Table 3.1 Comparison of top ranked designs.

3.5.1 Parallelogram

Table 3.1 shows that the Parallelogram is one of the weakest designs compared to the other finalist designs. The Parallelogram's size and hinge complexity make its response difficult to predict. The "Fair" grade in Range, Resolution, Accuracy and Repeatability is because the piezostacks will have to travel a significant amount distance in order to perform the desired scan. Also, the long arms and hinges, introduce a significant amount of uncertainty into this design and predictability is a major concern. Speed is another area in question, because the system will undoubtedly have several resonances with three hinges that need to settle. Also the large ranges required by the piezostacks will take a longer time to traverse. The required analysis and calibration time also add to the unfavorable grades in Cost and Maintenance. Wear is also a possible problem area because the hinges may wear at different rates and make the response unpredictable.

After running some simulations [Appendix A], with this design criteria and the characteristic equations of motion, the Parallelogram design would be able to maintain the desired position normal to the surface. However it would be difficult to obtain the required resolution because the arms of the device need to be quite long and the stiffness of each hinge would need to be carefully constructed. For instance, the length of the bar between Hinge 2 and Hinge 3 becomes several micrometers long in order for the probe tip to rotate 160°, which is required for this particular approach. Adding an additional probe so that the rotation of each probe is 80°, helps the situation, but again the arm length is still on the order of a micrometer. Furthermore, the ability to manufacture these pieces would also become difficult and extensive calibration time would be required in order to ensure predictability and repeatability. The long appendages would also be prone to cantilever error and ambient resonances including wind currents. Operating this system in a vacuum would prevent some disturbances, but it also adds another system to our device. The hybrid design has the similar disabilities found with the Parallelogram. The Parallelogram has too many engineering uncertainty problems to overcome compared to the other designs. As a result, the Parallelogram will not be the design with which we will implement our probe.

3.5.2 Single Pass

The Single Pass design is one of the simplest designs considered. It is one of the most cost effect techniques examined and Table 3.1 clearly demonstrates this. The Single Pass received "Excellent" marks in Range, Repeatability, Cost, Speed, Wear, and Maintenance. This design only consists of two actuators, only one of which was high resolution, and the Piezolever. Maintenance would be extremely inexpensive compared to the other designs. The wear on system components is insignificant compared to the other designs. Cost would also be lowest of any of the final four designs. Range would be limited only by the piezostack actuators which are the same for all of these designs, and Repeatability for this design received high marks as well because the simple system is reliable and easily controlled. The speed of the scans is limited only by the performance of the actuators, but a convolution software algorithm would be needed to enhance the resolution. The reason for the "Poor" grade in Resolution is because the vertical resolution toward the base of the sample is lower than the other designs, Figure 3.17. The atomic surface roughness, in that region, will be difficult to accurately resolve. Anomalies in the sample or tip

surface would cause significant errors in the scanning image. Cantilever errors are also a concern for this design as well. Hence, Accuracy received a "Good" grade because of these errors and the fact that the accurate placement of the Piezolever tip along the sample at the beginning of each scan might be difficult with this technique. The Single Pass design is a simple, economical method with high resolution at the region of the sample tip. However, the poor vertical resolution toward the base of the sample and the concern about cantilever errors leads to exclusion of this design from our application.
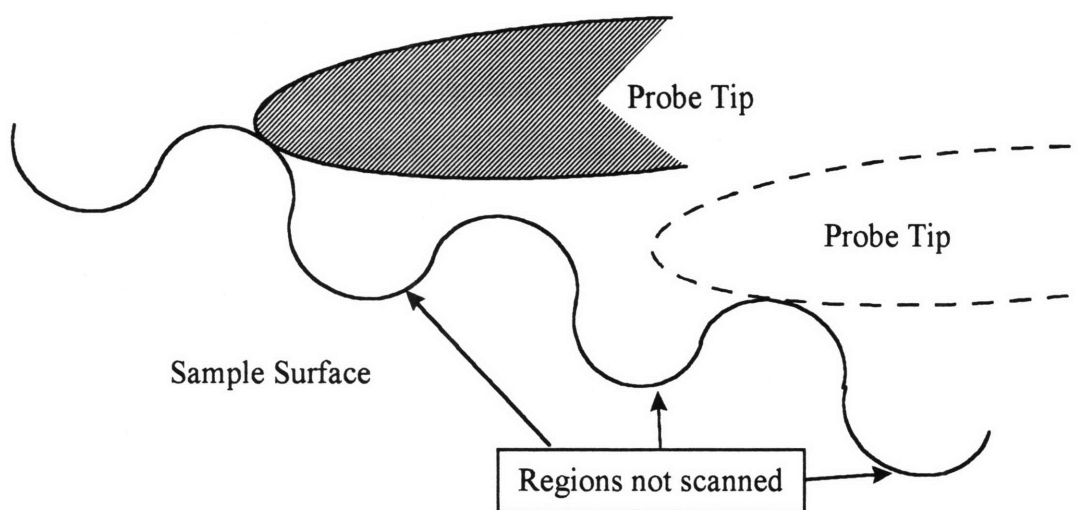
Figure 3.17 Single Pass resolution toward the base of the sample.

3.5.3 Axial Rotation

The Axial Rotation design compares quite well with the other designs in Table 3.1. Both the Range and Resolution areas received "Excellent" marks, because the system will utilize the latest piezoactors to control the x and y positions of the probe tip. The orientation of the tip should also have high resolution considering the specifications of the small motor being used. Repeatability should also be easily maintained with this simple design. Accuracy only received a "Good" grade, because of the concern with regards to performing the scan in the lateral direction. Uncertain errors and discrepancies may arrive from this new technique, because the Piezolever was not originally intended for this type of application. Also, this design is prone to cantilever errors because of its L-shape. All of these issues must be evaluated and tested prior to implementing this design. Assuming the lateral scan does not affect the speed of the scan, the

52

scan speeds will only be limited by the probe and actuators. This design should be able to quickly obtain a scan, however if only one probe is used then it may take a little longer to complete the scan, but this design does not require the convolution software algorithm that two of the final four designs need to obtain the necessary resolution. Hence, Speed received an "Excellent" grade. Maintenance is also not a significant issue for this design, because there are only four components which can quickly and easily be changed and maintained. The reason for a grade of "Good" in Maintenance is because the motor may require more maintaining than the Single Pass design which would only require a probe to be changed out just like the other designs. Wear also received a "Good" grade, because it was determined that the Piezolevers might abnormally wear when being subjected to a lateral scan and have to be frequently changed. The lowest grade of this design is in the Cost area, because the resources needed to calculate, test and implement the lateral scanning probe are very high compared to the other designs. However, Cost, Wear and Maintenance, were not the main reason for this design not being selected. The primary reason is the probes performance in the Accuracy category. This is a critical area and it was determined that there was another design that proved slightly superior than the Motor Driven Axial Rotation design.

3.5.4 Scissors

From Table 3.1, it is readily realized that the Scissors design performs exceptionally in the critical areas of Resolution, Accuracy, Speed, Range, and Repeatability. The scissors type design allows for the mechanical reduction of the displacement, so that the limiting piezostack resolution will be improved at the probe's tip. The necessary rotations about the hinge or pivoting mechanism will be less than 1° so the hinge will be built with adequate stiffness to reduce errors and ensure high resolution. The symmetric two probe design also attenuates errors, such as cantilever errors, and will increase scanning speeds by simultaneously scanning two sides at once. The piezoactuators can easily meet our Range requirements, even with the mechanical reduction mechanism. The Housing structure can be dampened in order to ensure acceptable Repeatability. As far as the five most important criteria, the Scissors design is better than any of the previous designs discussed. This design does not have the highest grade in the Cost category, which is "Good." This design is relatively cheap with three actuators and a convolution algorithm to implement, but the Single

Pass design definitely requires significantly less resources. The Scissors design will have some Wear issues to contend with as well. The stiff hinge mechanism may impose additional fatigue and wear on the device that other designs, such as the Single Pass, will not. Furthermore, Maintenance for this design was given a "Fair" grade, because each time the device needs repairs or maintenance, the system will need to be recalibrated, because of the hinge. As mentioned earlier, Cost, Wear, and Maintenance, although important enough to consider, do not influence the design choice as much as Resolution, Accuracy, Speed, Range, and Repeatability. The Scissors design excels in this area, which is why this design was chosen to be implemented in our rapid high resolution profiler.

3.6   Summary

In this chapter, several contact AFM design alternatives were examined. Two different classes of design were considered: (1) Designs that maintain the probe tip normal to the local sample surface and (2) Designs that require a convolution software algorithm to process the scanned image and the tip contour to produce the sample surface. The strengths and weaknesses of each design were cited and four designs were selected for further investigation. The Parallelogram Design, the Single Pass Design, the Motor Driven Axial Rotation Design, and the Scissors Design were all considered in the final evaluation. The criteria used in the final examination were Resolution, Accuracy, Speed, Range, Repeatability, Cost, Wear, and Maintenance. After carefully reviewing each of the final designs, the Scissors Design was chosen to be implemented.

4. System Design

4.1 Introduction

In the previous chapter, the design chosen to be evaluated is the Scissors Design. This chapter will provide a detailed description of the systems and components needed to complete this type of rapid high resolution profilometer. Both the system hardware and software will be examined in depth in order to accurately assess the applicability of this design.

4.2 System Hardware

The system hardware focuses on the probe design, including material selection, geometric dimensioning, hinge selection, piezostack and Piezolever specification review, and probe performance predictions. This section also highlights the calibration piece design which is used in the calibration of the Piezolever tip for the software image reconstruction. Finally, the general design of the framing structure, which structurally supports the instrument, and the sample positioning system, which allows the probe to move relative to the sample, are also explored.

4.2.1 Scissors Design

The Scissors Design, shown again here in Figure 4.1, is an interesting dual probe approach for conducting fast, high resolution profile scans. Figure 4.2 provides a side view of the scissors design so that a full understanding of the mechanism can be visualized. The probe operates by fully retreating Piezostacks 1 & 2 and then Piezostack 3 pushes the structure into place to perform the scan. Piezostacks 1 & 2 independently push against the preloaded torque, caused by the hinges, to position the Piezolever tips onto the surface. Once the preload of $10°$ is reached, the scan begins by incrementally activating Piezostack 3 until the Piezolever deflection is $\pm 0.005°$ of the desired preload at which time Piezostacks 1 & 2 compensate to maintain the desired tip orientation. Separately hinging the two arms along the same axis of rotation allows for independence in maintaining probe tip position while ensuring design symmetry. Once the scan is completed, the probe is moved along the length of the sample by the sliding positioning system(Figure 4.24) until the desired profile is obtained. Detailed discussions about system geometry, piezoactuator requirements, ball-in-groove sliding mechanism, Piezolever

characteristics, material composition, hinge design, and system speed performance are included in this subsection.
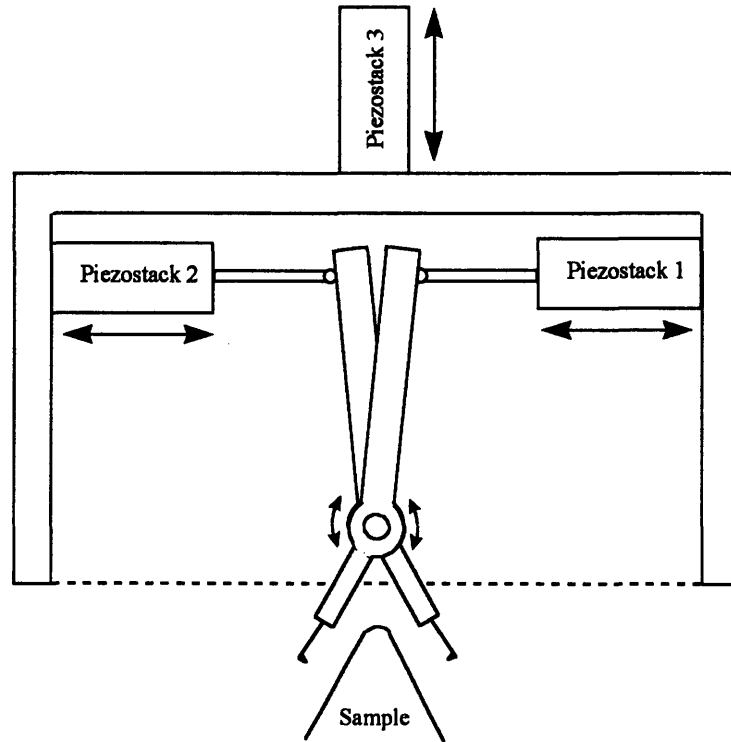
Figure 4.1 Scissors design front view.
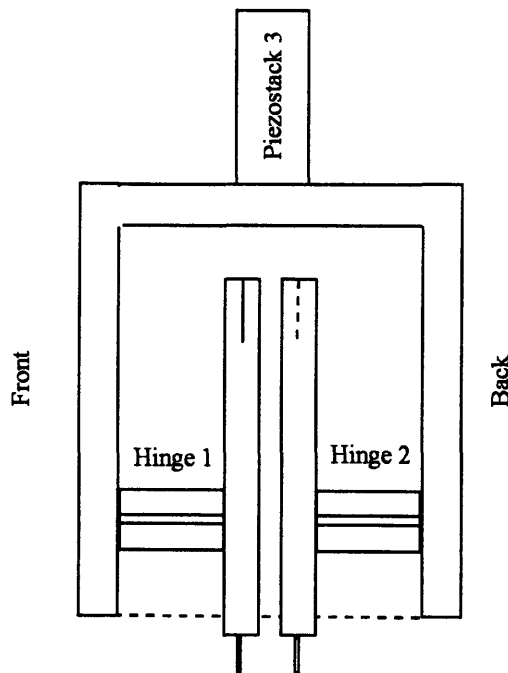
Figure 4.2 Scissors design side view.

4.2.2 Geometry

One of the obvious strengths about this design is its symmetry. Symmetry is used in precision designs to attenuate thermal and other errors while controlling forcing or loading loops. Since the application requires high speeds and very small errors, the design needs to be both lightweight and stiff at the same time. One of the largest contributors to the mass of the design is the size and specifications of the actuators. Obtaining the smallest actuators possible to perform the design will provide us with more freedom to choose the most appropriate material for the task, since that is the another large contributor to the mass of the design. Actuators and materials are discussed in more detail in subsequent subsections, however the pertinent information is that the piezoactuators chosen for our design need a mechanical reduction of 6 to 1 in order to obtain the desired resolution at the probe tip. The mechanical reduction ratio is from an optimization of the resolution of the piezoactuator in conjunction with the range of the piezoactuator. Based on a piezoactuator range of 15µm and a resolution of 30 nm, the range of the Piezolever tip is 2.5 µm and the resolution is 5 nm. If the piezoactuator requirements vary significantly, the mechanical reduction needs to be reinvestigated. From this information, the required length of the arms can be calculated. Also in order to maintain the probe tip as close to normal to the sample surface for the majority of the scan, the counter clockwise angle between the long arm, whose position is controlled by the piezoactuators, and the short arm, which has the Piezolever mounted to it, needs to be 180°. Since the mechanical reduction is 6 to 1, the portion of the arm that must be minimized is the end which contains the Piezolever. The Piezolever is 150 µm long and the chip it is mounted to is 1.6 mm wide and 3.6 mm in length, so the entire Piezolever structure is 3.750 mm in length. Next the mounting of the Piezolever chip to the scissors arm needs to be examined. The chip has tapered edges, Figure 4.3, that allow for easy alignment when installing the Piezolever. The spring loaded clip, shown in the mounting fixture, Figure 4.4, will ensure the chip is held fixed during the scanning operations.

$$500e^{-6} \text{ m}$$

36°   36°
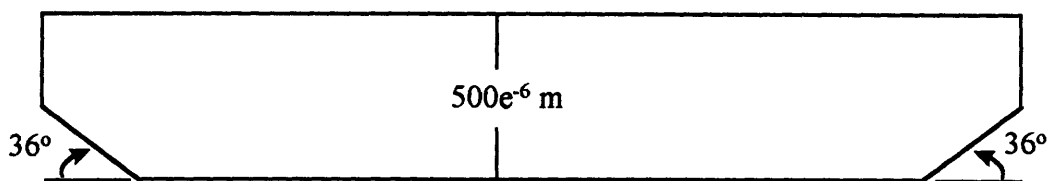
Figure 4.3 Piezolever chip back view.
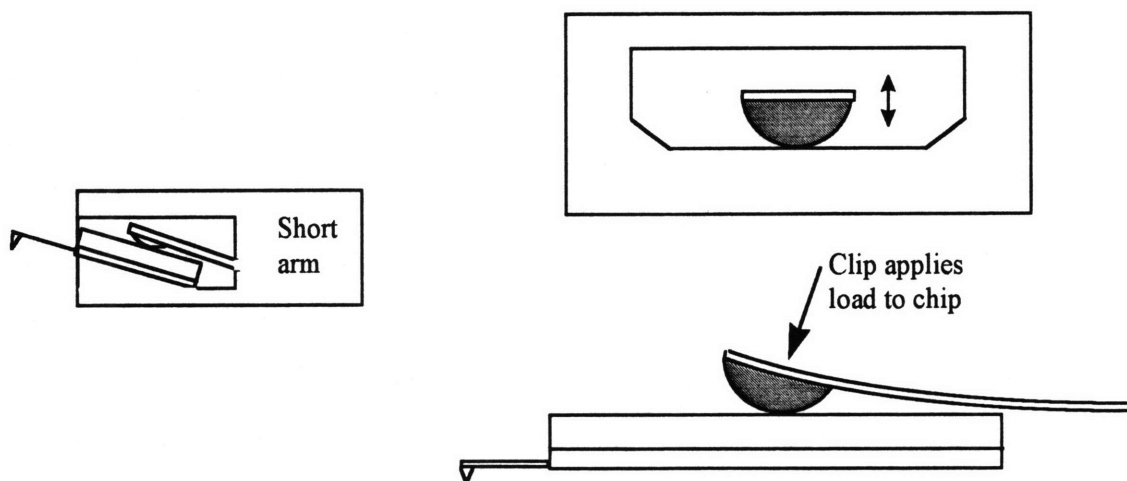
Figure 4.4 Piezolever chip mounting fixture.

The short arm, where the Piezolever is to be attached, needs some special design considerations. In order to optimize the position of the Piezolever so that the tip is oriented as close to $90°$ (relative to the local sample surface) throughout the entire scan, the short arm must be designed accordingly. Using simulations developed by Joachim Ogland[B8], the optimal tip orientation is highlighted in Figure 4.5.
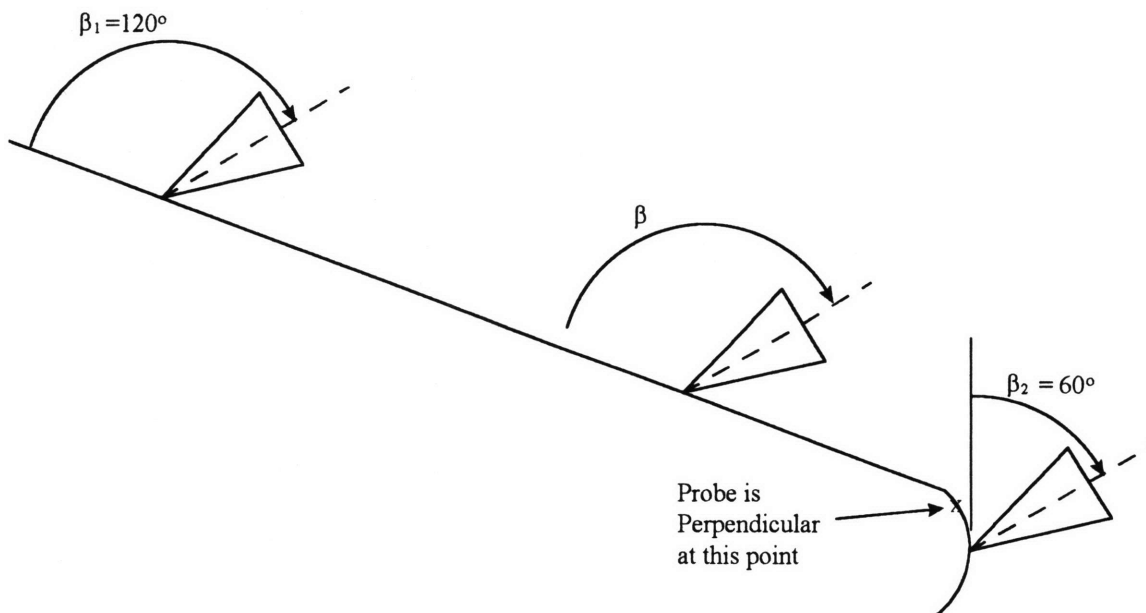
Figure 4.5 Optimal tip orientation.

Notice that the Piezolever tip is actually perpendicular close to the tip of the sample. In order to indicate the relative tip orientation to the sample, β is defined as the angle from the localized slope of the sample surface to the Piezolever tip centerline, shown in Figure 4.5. Toward the base of the sample, where the slope of the sample surface is less steep, β_1 is 120°. At the outer most point of the sample tip, β_2 is 60°. Through the entire scan the Piezolever tip centerline rotates through 60° relative to the local slope of the sample surface. This optimization directly impacts the size of the entire device, because the simulation also provides the desired dimensions of the probe. Figure 4.6 shows the configuration of the Piezolever and short arm together. As a result, the length of the distance from the axis of rotation at the hinge to the probe tip can be obtained.
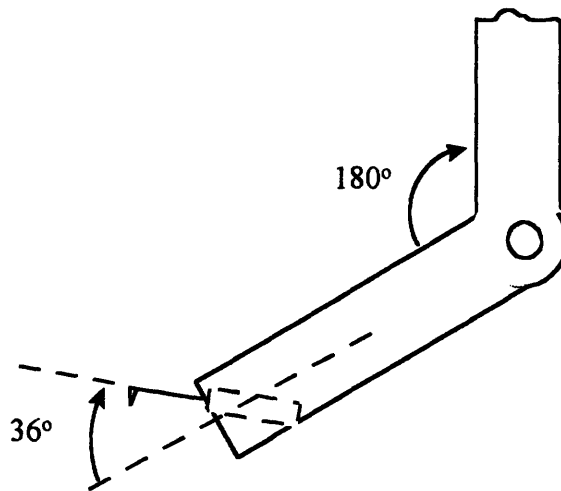
Figure 4.6 Optimal Piezolever orientation on the short arm.

Figure 4.6 further shows that the Piezolever must be oriented 36° in the clockwise direction from the short arm centerline. Also, the angle between the short arm and long arm centerlines is 180°. So from the above and the configuration shown in Figure 4.7, the shorter arm must be 5 mm in length, 3 mm in width and 3 mm in height. Since the mechanical reduction is 6 to 1, the piezoactuator must impose its displacement 30 mm away from the hinge on the long arm. Hence, the long arm will be approximately 30 mm in length. The spacing of the piezoactuators will also directly impact the size and geometry of the device and must also be considered with the system geometry. The piezoactuators must transmit a horizontal displacement to the Piezolever tip. In

order to minimize additional stresses and loads on the hinge, a sliding mechanism will be used to transmit only horizontal motions from the piezoactuators.
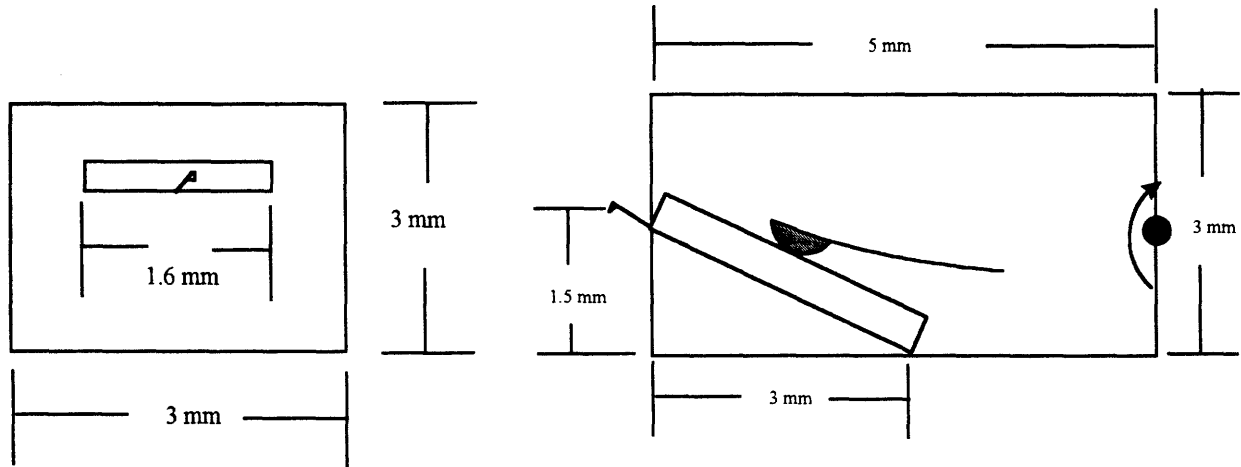
Figure 4.7 Short arm dimensions.

As the mechanism slides, the mechanical reduction ratio begins to change. In order to keep this error at a minimum, the contact point of the piezoactuator with the long arm, should be maintained as close as possible to 90° as show in Figure 4.8.
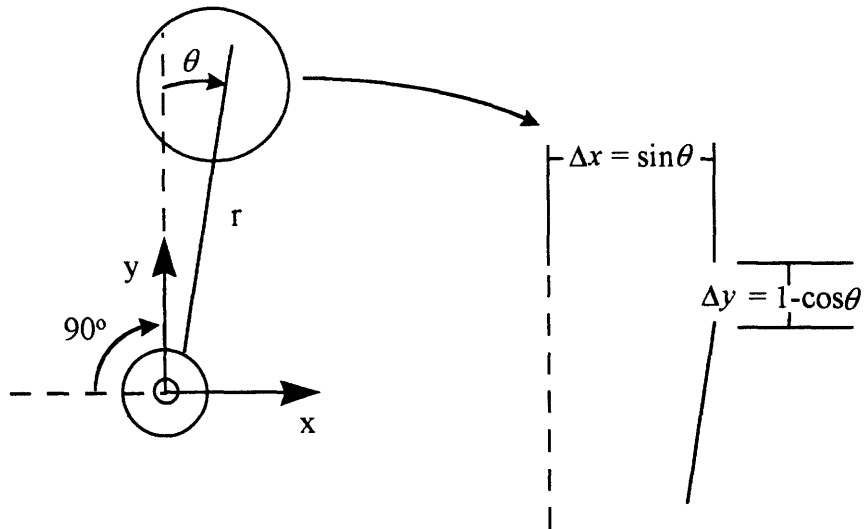
Figure 4.8 Location of piezoactuator contact point with long arm.

With the very small angle of rotation required, the equations of motion at this point become:

$$\Delta x = \sin \theta \approx \theta$$

$$\Delta y = 1 - \cos \theta \approx 1 - \left(1 - \frac{\theta^2}{2}\right) = \frac{\theta^2}{2}$$

Since the length of the long arm is 30 mm and the piezoactuator displacement will not exceed 15 μm($\pm$7.5 μm), the rotation will not exceed $\pm$250 μradians. This means that Δy will approximately range from $\pm$31 nm, which is optimal. Since the piezoactuators will be acting on the long arm in the position shown in Figure 4.8, the geometry of the housing will be impacted by the size specifications of the piezoactuators and the hinge. Examining the scenario where the tolerances are the worse case, the piezoactuator is 32.3 mm long and has a outside diameter of 12.1 mm[B3]. The space between the roof of the housing and the piezoactuator is 1 mm. The peizoactuator is 12.1 mm wide however only half of this value will be used because the length of the long arm will consider the other half. The long arm is 30 mm long, however in order to allow room for the sliding mechanism, the arm will be extended an additional 10% to 33 mm from end to the axis of rotation. Finally, the short arm is 5 mm from the axis of rotation to the beginning of the Piezolever, but the housing only needs an additional 3 mm, to support the hinge. The conservative height of the open bottom box design of the housing is 43.05 mm. This is the internal dimension of the housing, which excludes the thickness of the housing. Figure 4.9 graphically displays the dimensioning of the front view of the design showing both the height and length, which will be discussed next. The length of the housing is influenced more significantly by the length of the piezoactuators, which is 32.3 mm. Each actuator has a 1 mm attachment for the sliding mechanism which is screwed into the piezoactuator. Since two independent scissors arms are being used, the contact points can be in the same position, so only one arm thickness of 3 mm will be used. Hence the length of the housing is 69.6 mm. Finally, the width of the housing needs to be determined. The thickness of the Piezolever chip drives the thickness of a portion of the arm size. The hinge heights drive another dimension and the gap distance between scissors arms one and two also needs to be accounted for. The thickness of each arm is 3mm, and taking into consideration the size and location of each hinge, an additional 5 mm will be added for each hinge. Finally, the gap distance is approximately 10 μm so the entire width of the housing is approximately 16.01 mm. Figure 4.10 shows the dimensioning in the side view of the system which includes both the height and width. So the internal housing dimensions are 69.6 mm by 43.05 mm by 16.01 mm. Assuming the arms will be constructed with the same materials as the housing, the total volume of the housing plus the arms is $1.982e^{-4}$ m^3.
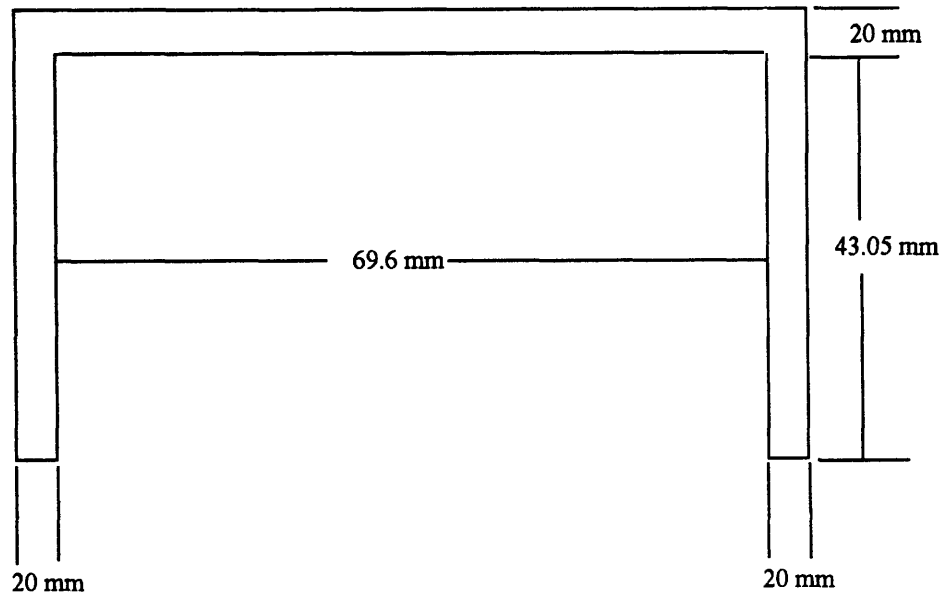
Figure 4.9 Geometry of housing front view.
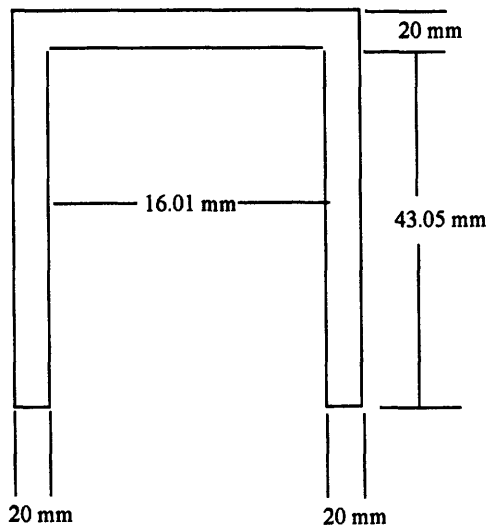
Figure 4.10 Geometry of housing side view.

4.2.3 Piezoactuators

After examining several commercially available piezoactuators, the Physik Instrumente Low Voltage Piezostack Translators best meet our requirements[B3]. In particular, the P-841.10 is a piezotranslator with piezoelectric stacks inside a metal casing which has tapped holes in the base for mounting and in the top for fixing attachments. Position sensors are integrated inside the casing and can achieve position control with a resolution of 0.2% of the nominal expansion. Table 4.1 shows detailed specifications of the piezotranslator considered.

Model	P-841.10
Nominal Expansion at +100V [μm]	15
Max. pushing force [N]	1000
Max. pulling force [N]	100
Electrical capacitance(small-signal), ±20% [nF]	1.8
Stiffness, ±10% [N/μm]	55
Resonant frequency [kHz]	18
Weight [g]	50
Total Length [mm]	32

Table 4.1 Low voltage piezostack specifications.

Since the nominal expansion is 15 μm and the sensor resolves to 0.2% of the nominal expansion, the resolution of this piezostack is 30 nm. In order to optimize the positioning capabilities of the Piezolever tip, a reasonable mechanical reduction would be needed to bring the resolution down to 5 nm. A reminder that this is not the vertical or lateral resolution of our system, but an optimization technique to ensure the system will attain the desired resolutions. Since there is a 6 to 1 mechanical reduction, the nominal range in the x-direction (motion normal to the sample centerline) of Piezolever tip has become 2.5 μm. This is well within desired parameters because the worst case profile would require the Piezolever to move 0.58 μm in the x-direction. It is interesting to note from Table 4.1 that the pushing force is ten times higher than the pulling force. This is the nature of piezoelectric material which has higher strength in compression compared to tension. This is the motivation behind the creation of the preloaded hinge and the sphere-in-groove sliding mechanism.

4.2.4 Sliding Mechanism

In the transmission of the displacement of the piezoactuator to the displacement of the scissors arm, a rotation occurs that puts undesirable stresses on the piezoactuator as well as the hinge mechanism. Since the angles are very small at this location, as discussed in subsection 4.2.2,

initially it was thought that piezoactuator could easily perform the push-pull positioning motions with a type of flexure mechanism or slider to account for the off-axial loads and displacements. However, by preloading the main hinge and setting up a sliding sphere in a groove, the piezoactuator will only need to push axially which it easily accomplishes. Figure 4.11 shows the design of the sphere in groove sliding mechanism. By applying a 2 to 3 μm film of polymeric bearing material such as polytetrafluoroethylene(PTFE) to the groove and sphere surfaces, the sliding mechanism will predictably translate the displacement of the piezoactuator to the scissors arm without applying off-axis loads to the piezoactuator[C1].
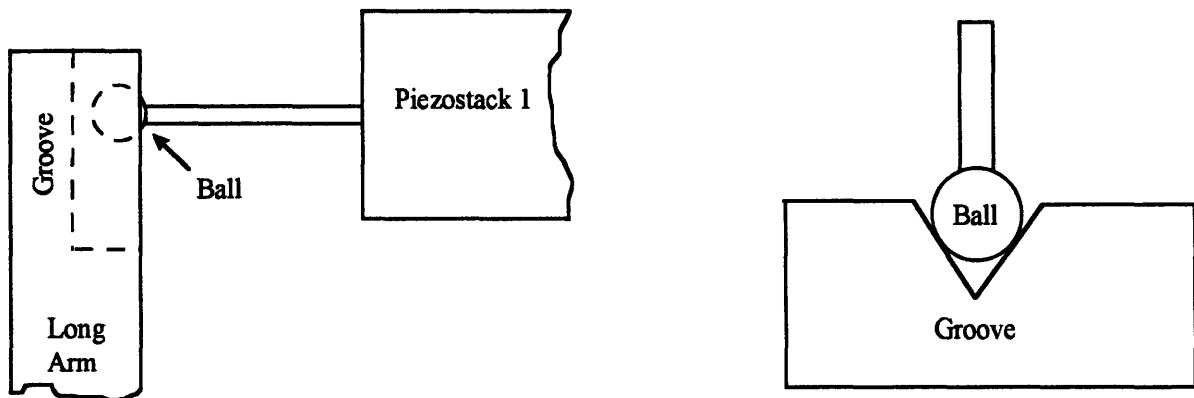
Figure 4.11 Sliding Mechanism

4.2.5 Piezolever

A self sensing contact atomic force microscope probe provides a reliable positioning system without the addition of another system. The only commercially available probes that are capable of performing this task are the Park Instrument Piezolevers[B7]. The Piezolever, Figure 4.12, is used in the Park Instruments AutoProbe, VP, SA, and XL Scanning Probe Microscopes. The Piezolever measures the stress-induced electrical resistance changes in an implanted conductive channel of the cantilever. It is closely related to a strain gage that is etched into the silicon of the cantilever. These probes are commercially available and installation is fast and easy. The chip and Piezolever are made out of silicon, and the thickness of the lever (not shown in Figure 4.12) is 10 μm. Typical electromechanical characteristics of the contact Piezolever are highlighted in Table 4.2[B7]. At this time, the Piezolevers are only purchased in groups of 25 chips and each allotment costs $1000 USD. This equates to $40 for each individual Piezolever[B7].
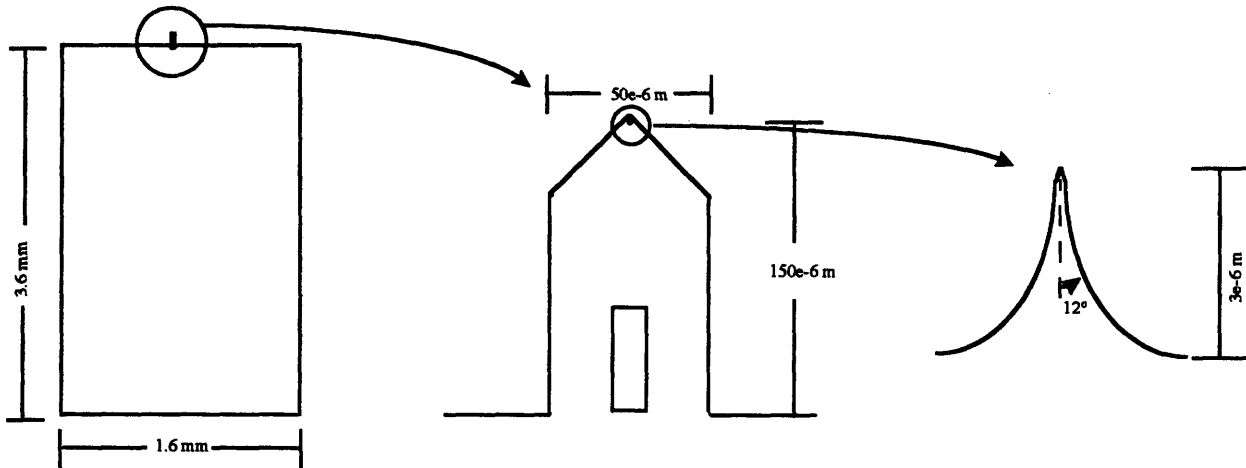
Figure 4.12 Piezolever detail.[B7]

Cantilever Type	Contact Piezolever
Force Constant	2.5 N/m
Resonant Frequency	120 kHz
Sensitivity $\Delta R/R$ per Å deflection	0.3×10^{-6}
Resistance	2 kΩ

Table 4.2 Electromechanical characteristics of the contact Piezolever.

4.2.6 Material Selection

The process of choosing the material for this application is quite critical. Subjects which are evaluated include thermal properties, strength of materials, stiffness, and density. Since the design is physically small, the need for a strong, lightweight, and well damped material is desired. The material selected also needs to be compatible with the other materials used such as the silicon used in the Piezolever, the hinge which will be made out of silicon nitride (see 4.2.7 section), and piezoactuator casing which is stainless steel. Because of the design size, thermal equilibrium may be difficult to maintain, especially if the device is handled by technicians. The thermal concerns drive the material to have a low thermal coefficient of expansion, size and mass constraints drive the system to be lightweight, and stiffness concerns push for a high modulus of elasticity. In

general, a reasonable structural material is desired, so metals and their alloys are examined. When considering a lightweight material, aluminum often is the material of choice, however there are two concerns with aluminum: thermal and damping. Aluminum's thermal expansion coefficient is relatively high and in order to compensate for aluminum's thermal limitations, the inclusion of insulating materials to isolate the heat sources and the thermal condition of the environment should be controlled. To increase damping of the system, damping material needs to be added to the aluminum surface. Aluminum has too many limitations, so steel was considered. However, steel's high density makes it very unattractive. One material that is less commonly used is molybdenum. It is slightly more expensive, however for use in this small device that will not be a significant concern. Molybdenum has a history of use in precision machines, specifically in the structures of scanning tunneling microscopes [C6]. Molybdenum has possibilities but its density is also too high. Another material, Zerodur™, a ceramic, has very good thermal properties and a reasonable density, however the material's strength is not as high as metals. Finally, titanium is a relatively strong metal that has reasonable thermal properties and low density. Titanium is not particularly well damped, but damping material can be added to the surface to quell unwanted resonances. As in most material selections, there are tradeoffs, because rarely does one material have the all the qualities that are desired. So after considering several materials, titanium provides the necessary stiffness while keeping the mechanical structure as light as possible and will be the material used to make the housing and the arms of the device.

4.2.7 Hinge Design

The hinge design is one of the crucial aspects of the scissors design. The hinge must accurately and repeatedly transmit the displacement of the piezostack to the probe tip. If a piezostack that has a range of 15 μm and resolution of 30 nm and the arm length is 30 mm and the mechanical reduction is 6 to 1, then the hinge will be required to rotate 500 μradians with a resolution higher than 1.0 μradian. In addition, the sliding mechanism, that we have chosen, requires the hinge to be preloaded such that the piezoactuators are always pushing the scissors arms. Several hinge designs which can efficiently and effectively transmit the piezoactuator displacement to the probe tip are considered in the following subsections.

4.2.7.1 Notch Hinge

In the notch hinge, two holes are drilled in close proximity to one another and the result is the hinge shown in Figure 4.13[A1]. In 1965, Paros and Weisbord discovered that if the notches are nearly semicircular and the deflections are small,

$$\theta_z = \frac{9\pi R^{\frac{1}{2}} M}{2Eht^{\frac{5}{2}}}$$

The notch hinge's center of rotation moves slightly during bending, which is one characteristic of the notch hinge. This flexure design is the foundation for other designs that are discussed below.
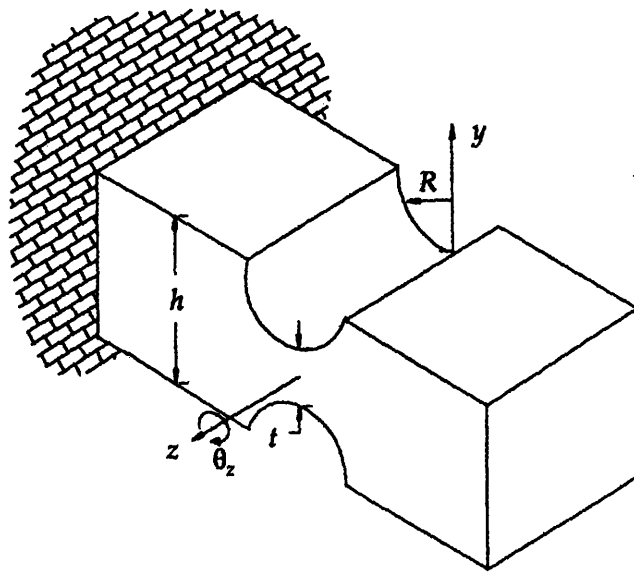
Figure 4.13 Notch hinge.

4.2.7.2 Crossed Strip & Monolithic Hinge

The crossed strip flexure, is one design that is slightly more complex, but supplies additional support. The primary advantage of this design is the resistance to axial loading is halved providing a fourfold increase in capacity to withstand buckling along the axis and a twofold increase in resistance to bending failure[C2]. Figure 4.14 shows the crossed strip hinge and Figure 4.15 shows another cross strip flexure, the monolithic hinge. The major limitation of this hinge design are the small but prevalent off-axis errors as defined by ε in Figure 4.16.

67
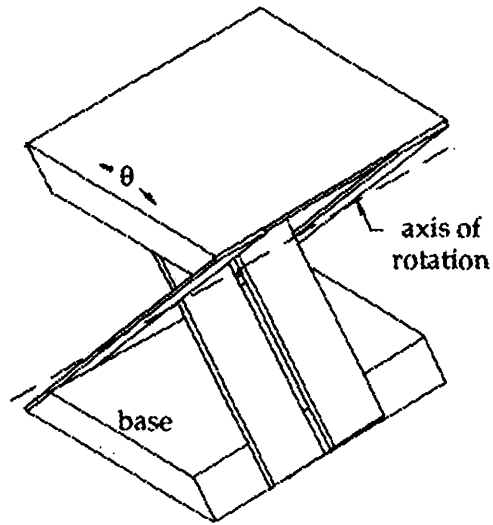
Figure 4.14 Crossed strip hinge.[A1]
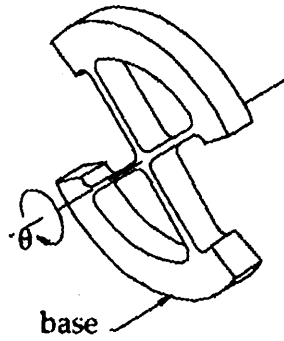
Figure 4.15 Monolithic hinge.[A1]
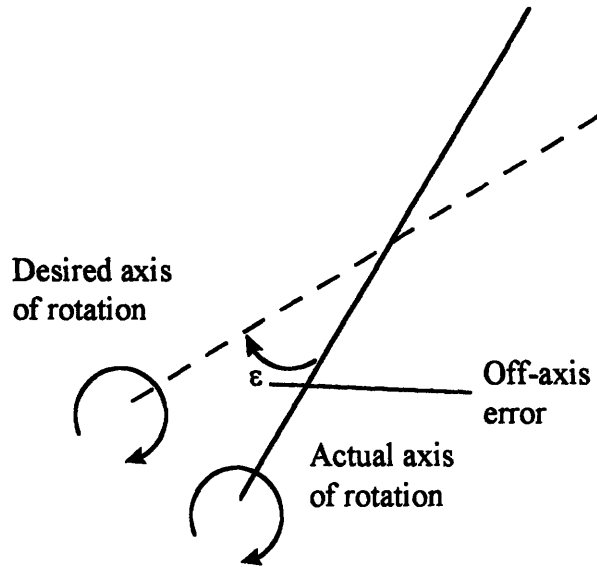
Figure 4.16 Off-axis error.

4.2.7.3 Cruciform Angle Spring Hinge

The cruciform angle spring hinge, Figure 4.17, is another hinge that has been used as an angular spring hinge. In 1955, a study investigating the twisting of beams about their longitudinal axis was conducted by Jones[C1]. This equal sided cruciform cross-sectional shape showed the best results. Typical off-axis errors for this particular hinge are 0.075% of the total angular deflection, that is 75 µradian error for an angular deflection of 0.1 radian[C1]. This hinge design will be considered for further discussion in the hinge selection subsection.
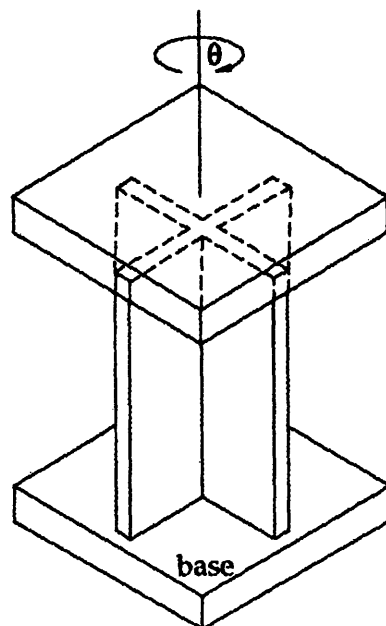
Figure 4.17 Cruciform Angle Spring Hinge.[A1]

4.2.7.4 Knife Edge Pivot

The knife edge pivot, shown in Figure 4.18, rotates about an axis much like a using a fulcrum and lever. This design has a larger range than a flexure design, however, in general, rotations greater than $45°$ are not recommended, because of the errors at the point of rotation. There are several limitations with this design including fixing the axis of rotation as the arms are moved. Preloads must be applied as well to enhance accurate rotation. Finally, as the contact surface between the knife edge and lever wears, the resolution decreases. Some designs have considered this concept with a notch hinge for precision displacements[A1].
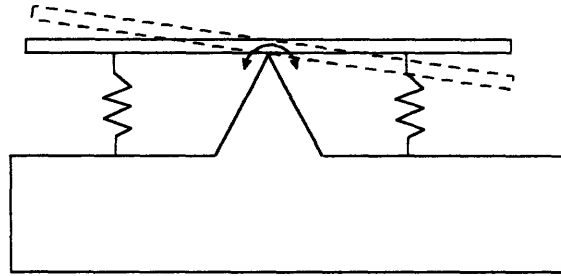
Figure 4.18 Knife edge pivot mechanism.

4.2.7.5 Kinematic Hinge

The kinematic hinge, shown in Figure 4.19, uses a sphere in groove approach modeled off of a kinematic coupling. Three spheres are placed $120°$ apart from one another along a common radius, and a v-groove, in which the three spheres slide, is cut at along the same radius. The hinge can rotate freely, however a preload is needed to ensure the mechanism continually rotates about a fix axis.
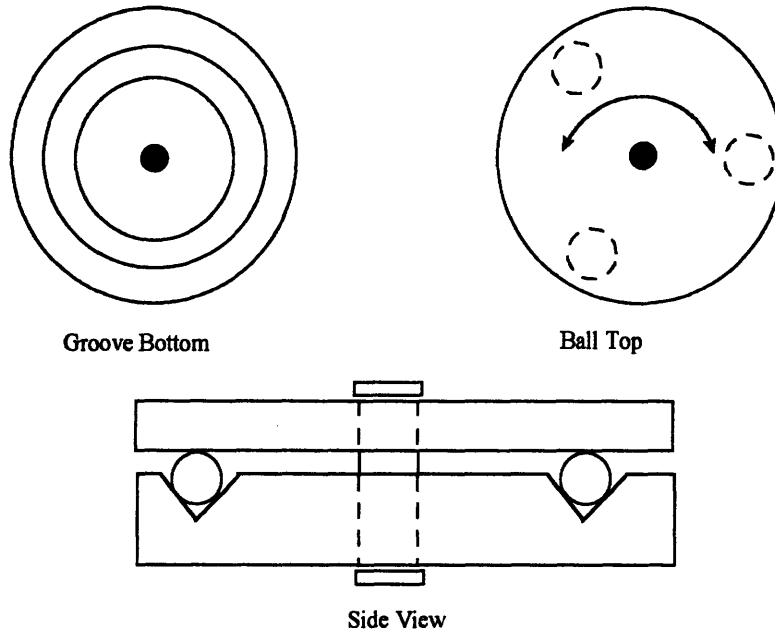
Figure 4.19 Kinematic hinge.

4.2.7.6 Pin Hinge

The pin hinge, shown in Figure 4.20, is one of the most commonly occurring hinges. A simple sliding hinge is free to rotate about its axis of rotation. Preloads and precision machining are needed for this design to meet the necessary specifications of our application. Also, since it is a sliding design lubrication is needed to reduce friction and wear.
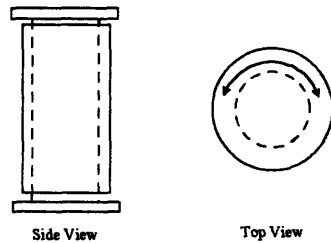
Figure 4.20 Simple pin hinge.

4.2.7.7 Hinge Selection

The hinges discussed above are reviewed in Table 4.3. The three criteria being judged are Accuracy, Resolution and Stiffness. Accuracy and Resolution pertain to the ability for the hinge mechanism to rotate about a fixed axis. Stiffness considers preloading, the ability to resist

buckling, and the ability to attenuate off-axis loads and errors. In general, the free rotation mechanisms do not provide the necessary resolution or stiffness of the flexure hinges.

Design	Accuracy	Resolution	Stiffness
Flexure	o	+	+
Cross Strip Flexure	+	+	*
Cruciform Angle Spring	*	*	*
Knife edge Pivot	+	+	o/+(preloaded)
Kinematic	+	+	o/+(preloaded)
Pin	x	o	o/+(preloaded)

* - Excellent + - Good o - Fair x - Poor

Table 4.3 Hinge Selection

From Table 4.3 and the above discussion, the best design is the Cruciform Angle Spring. For our application, this design would demonstrate a resolution of 0.3 μrad. With this design, the hinges can be specifically manufactured to optimize stiffness and precision rotation. Since we have chosen a flexure type hinge, the material's most critical feature is that it must operate well within the linear elastic region, because local yielding will adversely affect the repeatability and accuracy of the device. As a result, the ratio of yield strength to the Modulus of Elasticity, E, should be high to control deflection. However, to increase stiffness a reasonably high E is desired. With material selection a balance is sometimes difficult to achieve, however, silicon nitride is reasonably low density has the necessary mechanical properties while possessing good thermal constraints. Hence silicon nitride will be used to build the high precision hinges[A1]. Silicon nitride has a density of 3310 kg/m^3, an E of 350 GPa, and a thermal coefficient of expansion of 3.1 μm/m/°C. With this material, a cruciform hinge that is 5 mm in height and 3 mm in width and length has an angular stiffness of approximately 2000 Nm/rad and a mass of 50 mg.

4.2.8 Speed

One of the critical design requirements is the ability for the device to perform the scans as quickly as possible. The actuators specifications and the mass of the loads they drive are the critical information in determining the speed of the system. First the piezostacks, that control the position of the scissors arms will be investigated. Next, the main piezostack that drives the entire probe will be examined for speed of performance.

4.2.8.1 Piezostacks 1& 2 driving the scissors arms

Piezostacks 1 & 2 both drive the same load because the design is symmetric. Since a ball-in-groove mechanism is being utilized in the transmission of the displacement, these piezostacks will only experience pushing loads, which is the type of load piezostacks are most capable of experiencing. Since the hinge stiffness is approximately 2000 Nm/rad, the piezostacks will experience loads between 10 N and 20 N. This is well within the 1000 N push force limit discussed in Table 4.1. However, the ability of piezostacks to withstand dynamic loads is discussed in section 4.2.8.3. It is desirable for Piezostack 1 & 2 to operate 100 times faster than Piezostack 3 because nominally 100 data points, from each side, are desired for the scanned surface image.

4.2.8.2 Piezostack 3 driving the system

The third piezostack drives the entire probing system and is responsible for handling the highest loads. The primary factor determining the performance of Piezostack 3 is that this actuator is pulling the load which is more difficult for these actuators to accomplish. There are no external forces so this actuator only needs to accelerate the mass of the housing, hinges, and arms against gravity. However, if the third actuator accelerates too quickly, the piezostacks could begin to tear apart from one another. Since the mass of the system is 994 g (arms are 1.5g each, the housing is 891g, the hinges are 1 g each, and the piezostacks are 50 g each), Piezostack 3 will be driving 9.74 N. The next subsection describes the optimal attainable speed of the system.

4.2.8.3 Piezostack speeds and electronic controller limitations

Since Piezostacks 1 & 2 will be pushing loads and Piezostack 3 will be pulling loads, two tables have been set up to determine the maximum attainable frequency for a particular distance

traveled. The equations, that govern the dynamic operation of the piezostacks, were obtained from the piezostack vendor[B3]. The following equations were used to calculate the dynamic performance of the peizostacks for both pushing and pulling operations, see Table 4.4 and Table 4.6. The maximum frequency, f, achievable by the piezostacks is defined as,

$$(1) \quad f = \sqrt{\frac{2F_{dyn}}{4\pi^2 m_{eff} \Delta L}},$$

where F_{dyn} is the maximum force imposed on the actuator,

ΔL is the change in length of the piezostack,

and m_{eff} is defined as,

$$(2) \quad m_{eff} = \frac{m}{2} + M,$$

where m is the mass of the piezoactuator and M is the mass of the load [B3].

Table 4.4 shows the resulting frequency response of piezostacks with various pushing loads being expanded to different lengths. In Table 4.4, Meff is calculated using equation (2) and the Dynamic Frequency is calculated using equation (1).

Mechanical System	Mass(g)	Meff (g)	Load(N)	Max Pushing Force(N)	dL=50nm Dyn Freq (Hz)	dL=0.1 micro Dyn Freq (Hz)	dL=1 micron Dyn Freq (Hz)	dL=5 micron Dyn Freq (Hz)	dL=10 micron Dyn Freq (Hz)
Piezo Performance	5000	5025	49.245	900	13471	9526	3012	1347	953
Piezo Performance	2000	2025	19.845	900	21221	15005	4745	2122	1501
Piezo Performance	1000	1025	10.045	900	29827	21091	6670	2983	2109
Piezo Performance	500	525	5.145	900	41677	29470	9319	4168	2947
Piezo Performance	200	225	2.205	900	63662	45016	14235	6366	4502
Piezo Performance	100	125	1.225	900	85412	60395	19099	8541	6040
Piezo Performance	50	75	0.735	900	110266	77970	24656	11027	7797

Table 4.4 Piezostack speed capabilities - Pushing Load.

The intent is to move these piezostacks with 900 N of force at increments of 30 nm, however toward the tip of the sample, the distance traveled may need to be as high as 100 nm (0.1 μm). Examining the situation where the piezostack has a 19.8 N load and desires to move 0.1 μm, the resulting attainable frequency is 15 kHz. At this point, the piezostack will be able to accomplish this task with great speed, however the frequency response of the electrical system, that supplies power to the piezostacks, may limit the system performance. Appendix D shows the actual frequency response of the electrical system from Physik Instrumente [C5]. Table 4.5 highlights several points of the electrical frequency response from Appendix D. Table 4.5 further shows that the electrical amplifier will provide 1.95 μm of amplitude at 5 kHz and is the true limiting factor

of operation. So the electrical system will permit the pushing piezostacks to respond at 5 kHz which is 60 mm/s.

30W amp Frequency Response	Amplitude (m)
Amplitude at less than 700Hz:	1.50E-05
Amplitude at 1kHz:	1.46E-05
Amplitude at 2kHz:	7.50E-06
Amplitude at 3kHz:	4.50E-06
Amplitude at 4kHz:	2.70E-06
Amplitude at 5kHz:	1.95E-06

Table 4.5 Frequency Response of E-505.00 30 W Amplifier Module.

Now the performance of Piezostack 3, which will experience pulling forces, needs to be examined. Table 4.6 shows the results of the calculations of the maximum speed of the response in the pulling mode. Once again equation (1) is used to calculate the Dynamic Frequency and the Effective Mass is calculated from equation (2). The maximum pulling force experienced by Piezostack 3 is limited to 90 N. Since our system is approximately 1000 g, if a system needs to be moved at 0.1 μm increments, the piezostack could mechanically perform this operation at 6.6 kHz. However, again the electrical system limits system.

				dL = 50nm	dL=0.1 micron	dL=1 micron	dL=5 micron	dL=10 micron
Mechanical System	Mass(g)	Effective Mass	Load(N)	Max Pulling Force(N)	Dyn Freq (Hz)	Dyn Freq (Hz)	Dyn Freq (Hz)	Dyn Freq (Hz)	Dyn Freq (Hz)
Piezo Performance	2000	2025	19.845	90	6711	4745	1501	671	475
Piezo Performance	1000	1025	10.045	90	9432	6670	2109	943	667
Piezo Performance	750	775	7.595	90	10847	7670	2426	1085	767
Piezo Performance	500	525	5.145	90	13179	9319	2947	1318	932
Piezo Performance	250	275	2.695	90	18210	12876	4072	1821	1288
Piezo Performance	100	125	1.225	90	27009	19099	6040	2701	1910
Piezo Performance	50	75	0.735	90	34869	24656	7797	3487	2466

Table 4.6 Piezostack speed capabilities - Pulling Load.

So with the piezostacks, that control the position of the arms, collecting 100 data points at a conservative speed of 3 kHz, it would take the system 33 ms to perform one scan. At this rate, approximately 5 mW of power would be required. That would require Piezostack 3 to operate at 30 Hz which is well within the operating constraints and is ten times faster than most commericial scanners which operate at 3 Hz [B1 and C7]. These speeds would allow each sample to be scanned in up to thirty different locations in one second.

4.2.9 Kinematics

The Homogeneous Transformation Matrix (HTM) is used to define the geometry and motion of the device. The HTMs for the subsystems of this design are found below with the associated figures for clarity. Since the design is symmetric, only one half of the device is represented. The examination begins with the contact point of the probe tip with the sample surface and progresses through the piezolever to the short arm. Next, the long arm, with the sliding mechanism, and the piezostacks are analyzed. Finally the housing structure, Piezostack 3, and along the frame to the final reference.

Probe Tip:

$$\begin{bmatrix} x_{13} \\ y_{13} \\ 1 \end{bmatrix} = \begin{bmatrix} \cos\theta_{14} & -\sin\theta_{14} & 0 \\ \sin\theta_{14} & \cos\theta_{14} & T \\ 0 & 0 & 1 \end{bmatrix} \begin{bmatrix} x_{14} \\ y_{14} \\ 1 \end{bmatrix}$$

$\theta_{14}=0$,
$T=3 \ \mu m$
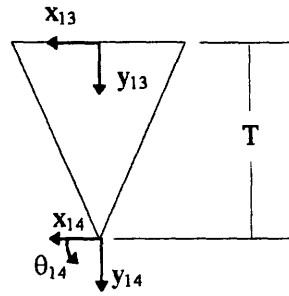
Piezolever cantilever beam:

$$\begin{bmatrix} x_{12} \\ y_{12} \\ 1 \end{bmatrix} = \begin{bmatrix} \cos\theta_{13} & -\sin\theta_{13} & \delta_{x_{1c}} \\ \sin\theta_{13} & \cos\theta_{13} & \delta_{y_{1c}} \\ 0 & 0 & 1 \end{bmatrix} \begin{bmatrix} x_{13} \\ y_{13} \\ 1 \end{bmatrix}$$

$\theta_{13} = 10°$ (nominal load)
$\delta_{x1C} = 150 \ \mu m$

$\delta_{y_{1c}} = \dfrac{2\theta_{13}\delta_{x_{1c}}}{3} = 17.45 \ \mu m$(nominal load)
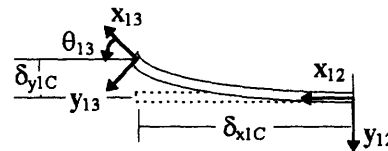
Short Arm - from the hinge to the Piezolever:

$$\begin{bmatrix} x_{1H} \\ y_{1H} \\ 1 \end{bmatrix} = \begin{bmatrix} \cos\theta_{12} & -\sin\theta_{12} & b\cos\theta_{12} \\ \sin\theta_{12} & \cos\theta_{12} & b\sin\theta_{12} \\ 0 & 0 & 1 \end{bmatrix} \begin{bmatrix} x_{12} \\ y_{12} \\ 1 \end{bmatrix}$$

$\theta_{12} = 270°$
$b = 5 \ mm$

76
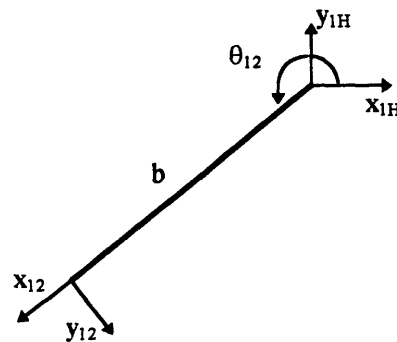
Arm - from the hinge to the piezoactuator (includes Sliding Mechanism):

$$
\begin{bmatrix} x_{1H} \\ y_{1H} \\ 1 \end{bmatrix} = \begin{bmatrix} \cos\theta_{11} & -\sin\theta_{11} & x_g \\ \sin\theta_{11} & \cos\theta_{11} & y_g \\ 0 & 0 & 1 \end{bmatrix} \begin{bmatrix} x_{11} \\ y_{11} \\ 1 \end{bmatrix}
$$
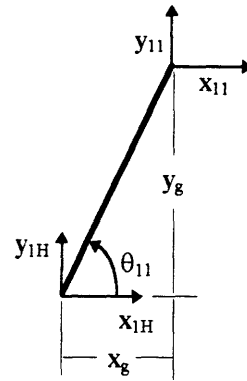
x_g will be known from the piezostack motion, y_g is a constant determined in the designing of the device, for our application it is 30 mm, and

$$
\theta_{11} = \arctan\left(\frac{y_g}{x_g}\right).
$$

Piezoactuator 1:

$$
\begin{bmatrix} x_1 \\ y_1 \\ 1 \end{bmatrix} = \begin{bmatrix} \cos\theta_1 & -\sin\theta_1 & -x_{P1} \\ \sin\theta_1 & \cos\theta_1 & 0 \\ 0 & 0 & 1 \end{bmatrix} \begin{bmatrix} x_{11} \\ y_{11} \\ 1 \end{bmatrix}
$$

$\theta_1 = 0$

x_{P1} depends on the motion of the piezostack, but is 33.3 mm, when the piezostack is not expanded.
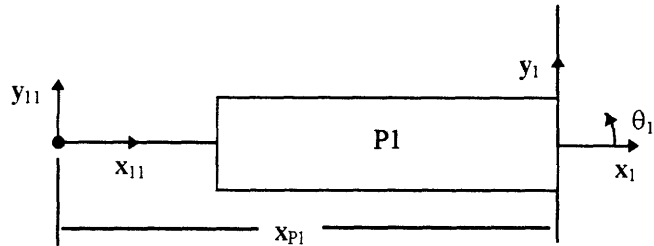
Housing - from Piezoactuator 1 to Piezoacutator 3:

$$
\begin{bmatrix} x_3 \\ y_3 \\ 1 \end{bmatrix} = \begin{bmatrix} \cos\theta_3 & -\sin\theta_3 & x_R \\ \sin\theta_3 & \cos\theta_3 & -y_R \\ 0 & 0 & 1 \end{bmatrix} \begin{bmatrix} x_1 \\ y_1 \\ 1 \end{bmatrix}
$$

$\theta_3 = 0$

$x_R = 34.8$ mm;

$y_R = 27.05$ mm;
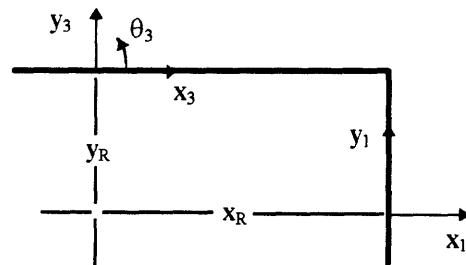
Piezoactuator 3:

$$\begin{bmatrix} x_0 \\ y_0 \\ 1 \end{bmatrix} = \begin{bmatrix} \cos\theta_0 & -\sin\theta_0 & 0 \\ \sin\theta_0 & \cos\theta_0 & -y_{p3} \\ 0 & 0 & 1 \end{bmatrix} \begin{bmatrix} x_3 \\ y_3 \\ 1 \end{bmatrix}$$

$\theta_0 = 0$

y_{p3} depends on the motion of the piezostack, but is 33.3 mm, when the piezostack is not expanded.
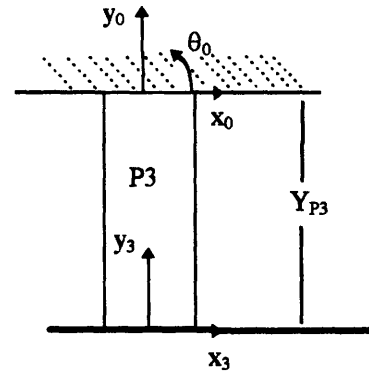
Frame - from Piezostack 3 to fix

reference on the base:

$$\begin{bmatrix} x_b \\ y_b \\ 1 \end{bmatrix} = \begin{bmatrix} \cos\theta_b & -\sin\theta_b & 0 \\ \sin\theta_b & \cos\theta_b & y_{bo} \\ 0 & 0 & 1 \end{bmatrix} \begin{bmatrix} x_0 \\ y_0 \\ 1 \end{bmatrix}$$

$\theta_b = 0$

$y_{bo} = 65.66$ mm;
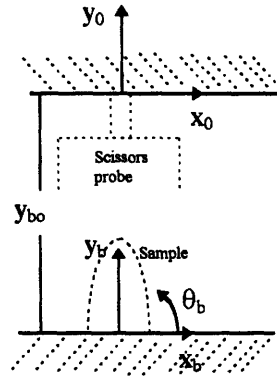
These HTMs define the system and are utilized in the simulations conducted in Chapter 5.

4.2.10 Sample Positioning System

Another interesting system to be discussed is the sample positioning system. The sampling positioning system is a separate entity from the Scissors Device, however it positions the samples in such a way that the scans are repeatable and can be accurately performed. This system needs to position the sample tip within ±0.5 μm of the desired location. Initially, the sample will be placed on an orientation piece which will align the sample. There are several options to secure the sample to the fine stage including magnetic clamps and possibly the use of sample features. The orientation piece is mounted on a fine stage carriage which is mounted on a coarse stage, Figure

4.21. The fine stage position is controlled by a voice coil and the coarse stage is on a carriage of a ballscrew mechanism.
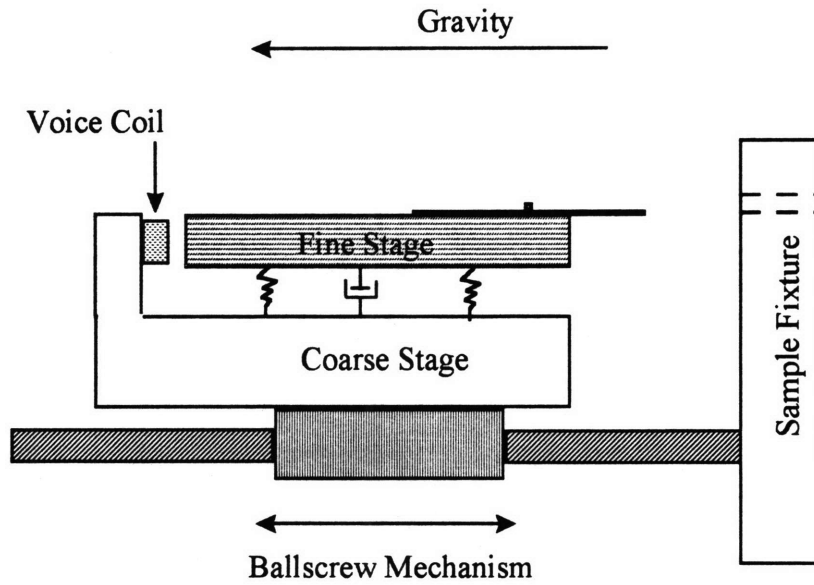
Figure 4.21 Sample positioning stage.

After a sample is placed on the orientation stage, the coarse stage traverses the distance to the sample fixture. The fine stage then delicately moves the sample into the sample fixture, Figure 4.22. The voice coil force is monitored to ensure that the sample is not damaged during the insertion of the sample into the fixture. The interior structure of the sample fixture closely matches the contour of the nominal sample shape. The opening which exposes the sample tip is constructed for a 2 μm width. This distance is nominally 5.027 μm from the sample tip. When the scan has been performed, the stage retreats and the process begins again.
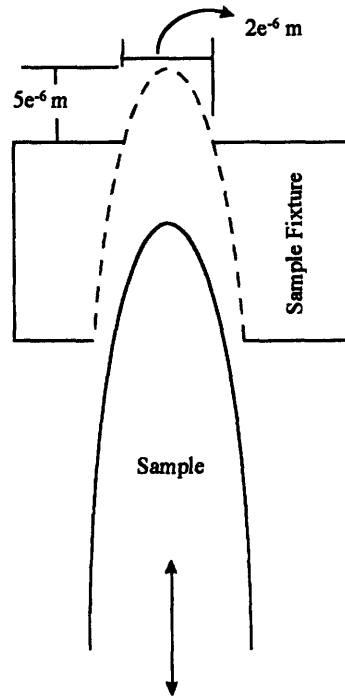
Figure 4.22 Sample fixture.

4.2.11 Frame Design

The frame on which the device is fixed is another area which needs investigation. The frame needs to be structurally sound to support the scissors probe and to easily handle sample positioning. The frame will be mounted on a vibration isolation table which is useful for damping out ambient disturbances common to any industrial setting. The frame will be an overhang design as shown in Figure 4.23. The frame will be made out of steel and the structure will be thick enough to easily withstand the loads of the probe. Piezostack 3 will be attached to a ballscrew carriage that will be used to move the scissors device along the length of the sample, Figure 4.24. The ballscrew mechanism is able to attain resolution less than 0.2 μm with a range of several centimeters[C1]. This ideal for our application as the sample is approximately 3.7 cm in length.
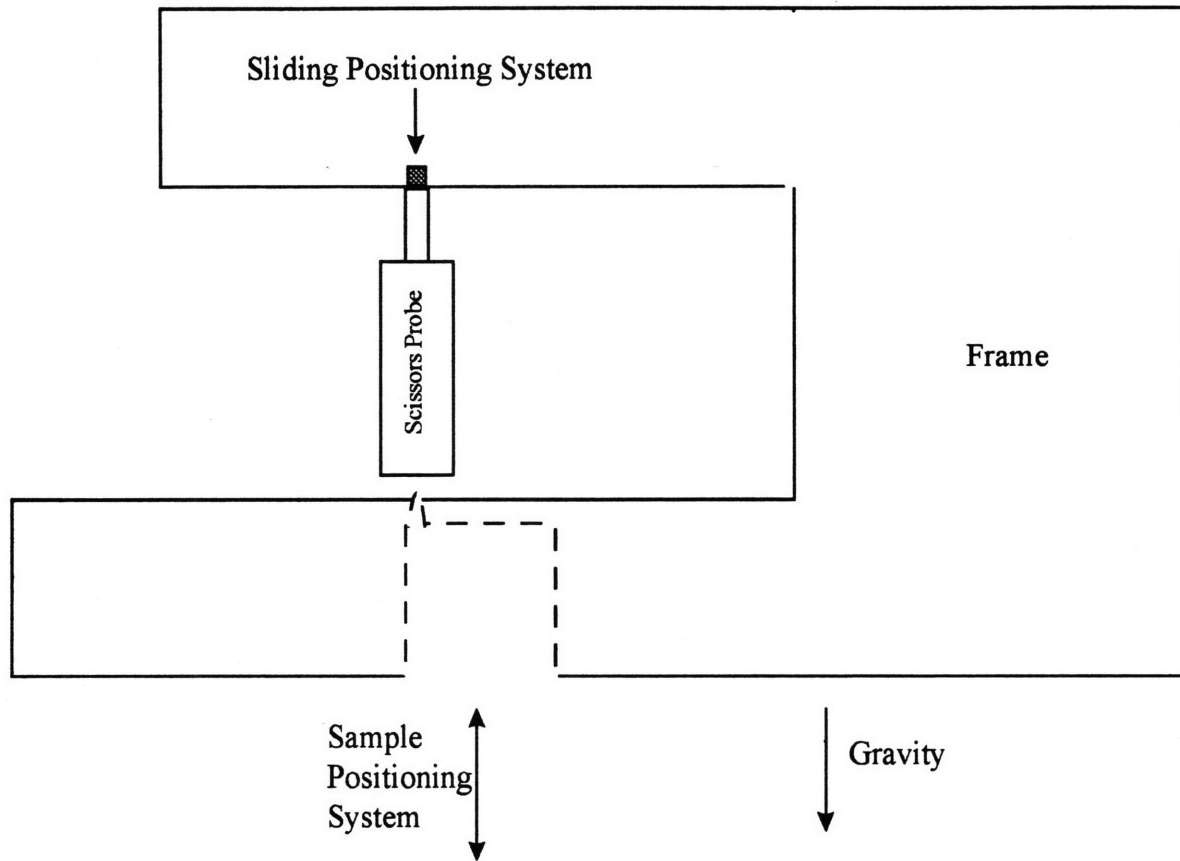
Figure 4.23 Frame Design.
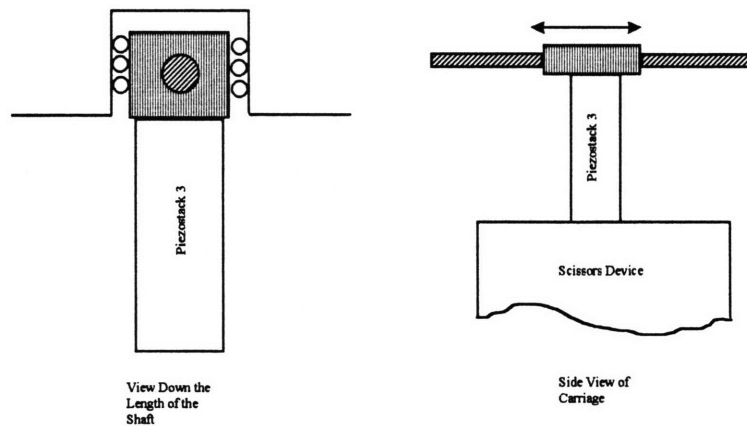
Figure 4.24 Sliding Positioning System.

4.2.12 Calibration Piece

The calibration operation is needed to obtain the contour of the Piezolever tip. This shape is then used in the reconstruction of the sample surface. Steps of known dimensions are a commonly used for calibrating commercial AFMs and could be utilized in our application. Edges, parabolas

81

or spheres can also be used. In reality, any object can be used as long as the exact dimensions of the profile are known. The advantage of a step is that minimal additional computation is needed. The other structures can be used, however the profile of the geometric surface must be subtracted away from the scanned image. With the step, the scanned image actually is the tip contour. Figure 4.25(a) clearly shows the scanning process of a step. The left edge of the step profiles the right edge of the probe tip and the right edge of the step profiles the left edge of the probe tip. Figure 4.25(b) superimposes the scanned profile image and the actual tip surface. The results are very accurate. The software used for this simulation is Matlab™ and this scan increments one nanometer at a time and calculates the minimum distance from the probe tip to the sample surface.

(a)

(b)
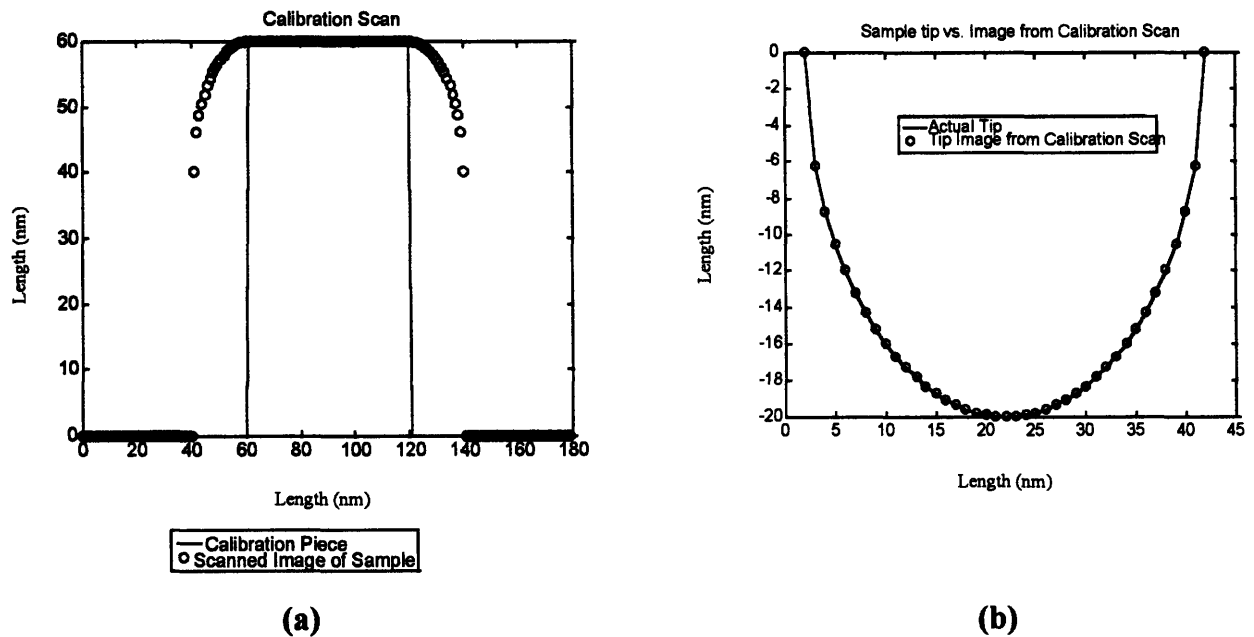
Figure 4.25 Calibration of tip shape using step.

The material composing the calibration piece should be sufficiently hard to ensure that many scans will not wear or damage the calibration piece. Silicon is sufficiently hard and easily etched into a precision calibration piece. An SEM is then used to confirm the exact dimensions of the calibration piece.

The results of the tip calibration are used along with the scanned sample image to reconstruct the actual sample surface. This is digitally accomplished through an algorithm highlighted in the next subsection.

4.3 Software

One source of errors in AFM imaging is the convolution of the sample surface with the tip contour which is why the reconstruction of the sample surface image is one of the most powerful tools in this design.   By utilizing the image of the Piezolever tip obtained from the calibration scan along with the sample surface image obtained from the primary scan, an algorithm is used to recreate the actual sample surface with fantastic results.   The technique utilized for the reconstruction of the scanned image is highlighted in a paper by David Keller[B6].   The major premise of the reconstruction is that the contour of the tip is known and that the tip is always in contact with the sample surface. Our design also loads the probe to ensure that it is continuously in contact with the sample surface. The tip shape can be obtained by scanning a known surface such as the step calibration piece used in our application. Figure 4.26 shows the rounded edges that result from a finite tip interacting with a surface. The true surface can be reconstructed from the scanned image if the point of contact between the tip and sample can be calculated from the scanned image and tip contour.   Hence, the transformation involves finding both the lateral distance between the true contact point and the apparent contact point, Δx, and the vertical distance between the true contact pint and the apparent contact point, Δs (see Figure 4.26)[B6]. At the contact point, both the tip and the sample surface have the same tangent, so the slope of the tip surface equals the slope of the true surface. Keller further proved that the scanned image also has the same slope of both the tip surface and true surface[B6]. Keller's equations below are the foundation for the reconstruction algorithm found in the simulations discussed Chapter 5. Reference Figure 4.26 for definition of variables.

Since the slope of the tip at Δx equals the slope of the image at x',

$$\frac{dt(\Delta x)}{d\,\Delta x} = \frac{di(x')}{dx},$$

Δx can be found as function of x', and the next equation

$$x' = \Delta x(x') - x,$$

is used to find x' as a function of x, which leads to

$$s(x) = i(x') + \Delta s(x'),$$

where

$$\Delta s(x') = t\left[\Delta x(x')\right].$$

One interesting and useful characteristic of the reconstruction algorithm is the fact that the algorithm does not provide false information. In other words, if the probe tip is not in contact with a particular region of the sample surface, no information about that area will impact the reconstructed image. Figure 4.27 shows "holes" in regions II and IV, and this phenomena was observed in the simulations performing using this reconstruction technique. Since most AFM tips are approximately parabolic, a parabolic tip was used in this reconstruction.

The simulations of this reconstruction algorithm will allow for both parabolic and spherical tip contours, however the true tip image will be obtained from the calibration operation. From these simulations, several tip contours will be examined as well as the performance of these tips scanning multiple surfaces.

4.4   Summary

This chapter highlighted many of the detailed design specifications for our system. The hardware section discussed the details of the scissors design including the actuators, the scissors arms, the hinge design, the material selection, the housing structure, and the system geometry. The hardware review continued with the frame, the calibration piece design, and sample positioning system were also reviewed. The homogenous transformation matrices, which define the system, were also highlighted in the hardware portion of this chapter. Finally, the theory of the software reconstruction algorithm was discussed in detail. This algorithm is the foundation for the simulations performed and evaluated in the next Chapter.

tip surface
$t(\Delta x)$

true
surface
$s(x)$

true point of contact

apparent point of contact

Δs

image
surface
$i(x')$

$\leftarrow \Delta x \rightarrow$

x'   x
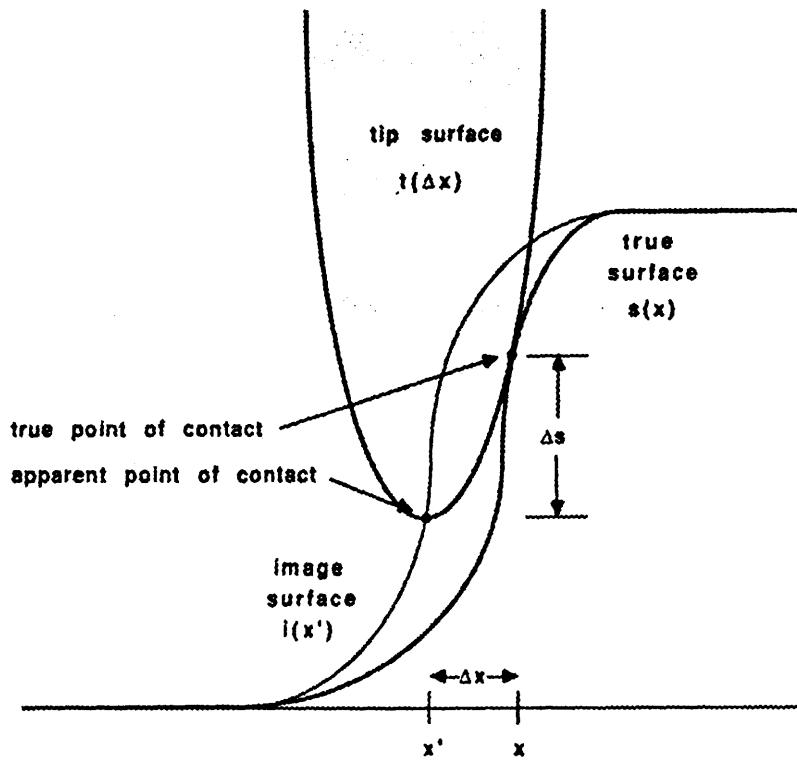
Figure 4.26 STM tip in contact with a sample surface.[B6]
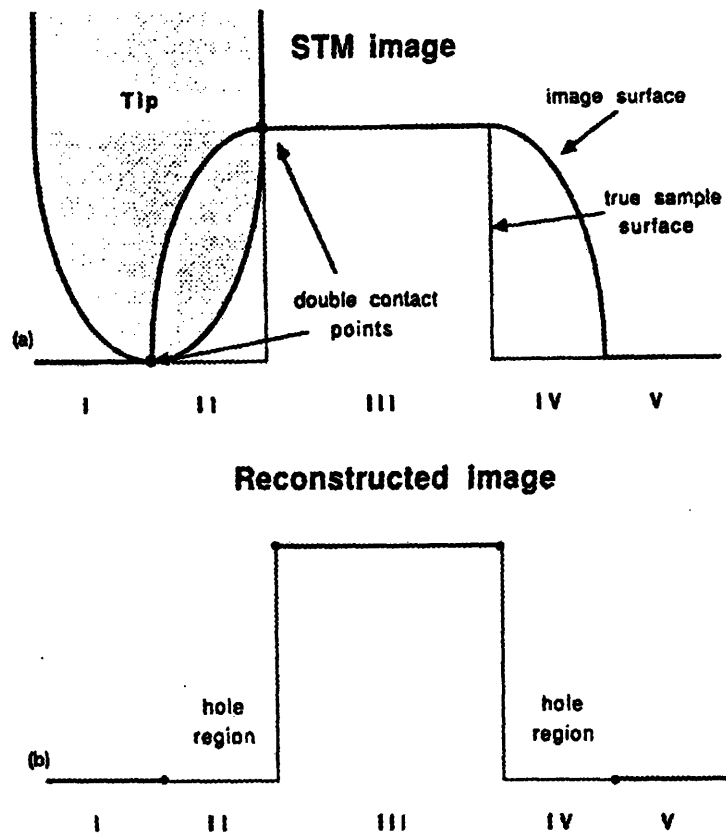
Figure 4.27 Scanned and reconstructed images, notice the "holes."[B6]

5. System Simulations

5.1 Introduction

In the previous chapter, the detailed information about the scissors design hardware and software was examined. This chapter utilizes the hardware homogeneous transform matrices (HTMs) and software reconstruction theory to implement realistic simulations of the system. To ensure the probe hardware and the HTMs are correct, simulations were performed on the hardware portion of the system. Also, the calibration simulation for each individual tip is also performed. Next, the reconstruction algorithm is highlighted. Several different surfaces are scanned and the resulting reconstructed images are discussed. The reconstruction program used to implement these simulations is based on an algorithm developed by Bernardo Aumond[D1]. Enhancements to the original algorithm include the use of multiple samples and various tips. Appendix F contains all of the code used in the following simulations.

5.2 Probe Tip Creation

Several different probe tips were created for use in the scanning of the samples. The probe tip radius size, shape, and orientation are all different variables that will be investigated. A spherical tip will be the first contour to be examined. Next, the parabolic tip, which is the typical contact AFM probe tip contour, will be explored. The third scenario considers a parabolic tip that is angled at various slopes from the vertical axis.

Circular Tip   Parabolic Tip   Angled Parabolic Tip
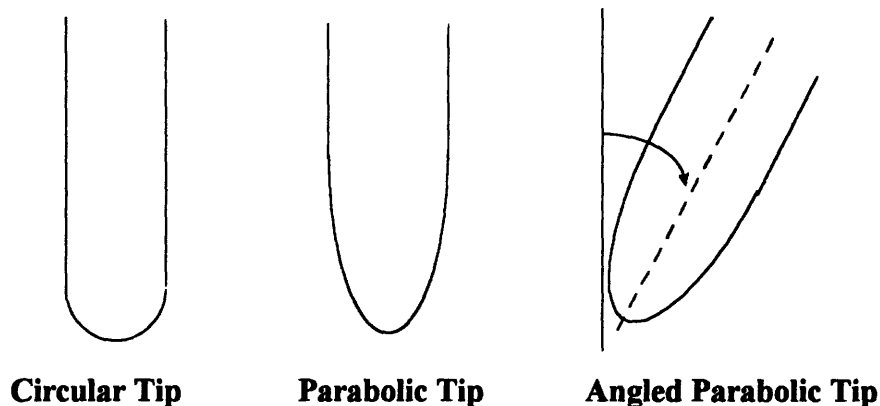
Figure 5.1 Different Tips Considered.

5.2.1 Circular Tip

The circular tip is primarily used for calibration purposes. Few contact AFM probes are spherical in shape, however the contour is still interesting to study. The input option that is controllable for this tip is the tip radius. One interesting program consideration for this and other tip configurations is that the probe tip is only a diameter wide. So when interacting with the sample surface, the sample only experiences the circular profile, because the probe sides are infinitely long with an infinite slope. Figure 5.1 shows a circular probe tip.

5.2.2 Parabolic Tip

The parabolic tip is the more common contact AFM probe tip contour. Most tips have this type of shape and even the Piezolever, used for our design, is parabolic with a 20 to 30 nm tip radius. The ability to manipulate the radius size for different simulations with this tip has been included in the algorithm. This tip is similar to the circular tip in the position normal to the sample surface, however the sides are more realistic. Figure 5.1 also shows the parabolic tip.

5.2.3 Angled Parabolic Tip

The angled parabolic tip provides an additional degree of realism in the simulations. By selecting different angles, which the parabola may encounter the sample surface, a better understanding of system performance and resolution can be realized. Since the probe tip in our design is parabolic and will also interact with the sample surface on a skewed angle, the ability to manipulate this parameter is critical for predicting system performance. The two parameters which are controllable in the simulations are the tip radius size and the angle from the vertical, where clockwise is positive. Again, because of programming constraints, the sides of the angled parabolic tip, at some point, will go to infinity with an infinite slope. Figure 5.1 shows the angled parabolic tip.

5.3   Studied Surfaces

Several different samples were examined in order to provide an adequate representation of the type of surfaces the probe tip might encounter. The sample surfaces to be examined are: (1) a step, which will be used for the calibration portion of the scan; (2) a sinusoid, which represents the size of the features on the surface which will be able to be scanned and reconstructed; and (3)

the actual sample surface with different orientations. The size of the step and the size and spatial frequency of the sinusoid surface are all parameters that are able to be simulated by the user. The sample surface and the two extreme cases, where the sample is skewed up and skewed down, do not have parameters to be manipulated. However, the program is robust enough to even handle introduced sample data from a file into the algorithm, see Appendix F.

5.3.1 Step

The step sample surface will be used in the calibration portion of the simulations. The step height can be varied depending on the user's needs. Usually, if the tip size is large, the calibrating step should be large so that a complete picture of the tip can be obtained. Figure 5.2 shows a step with a height of 50nm.
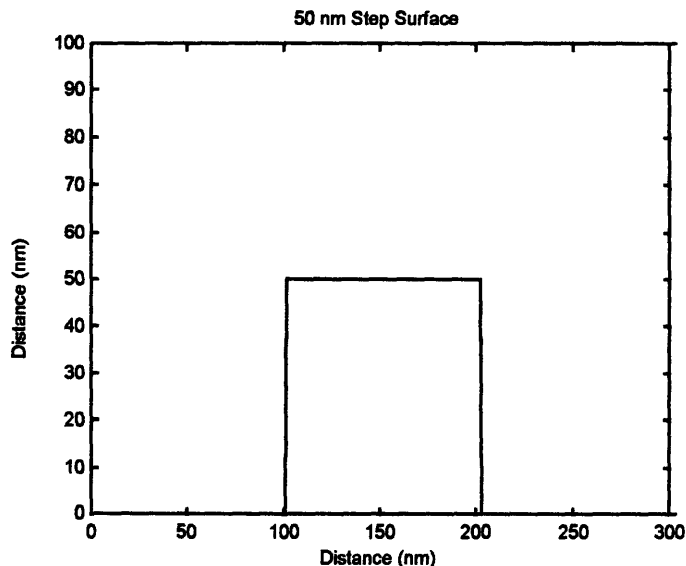
Figure 5.2 Step (height = 50 nm).

5.3.2 Sinusoids

The sinusoid sample surface is used to determine the smallest feature size a particular probe tip will be able to resolve. Since the amplitude and spatial frequencies are parameters that can be investigated, a particular surface roughness can be examined. A typical sinusoid surface is shown in Figure 5.3.
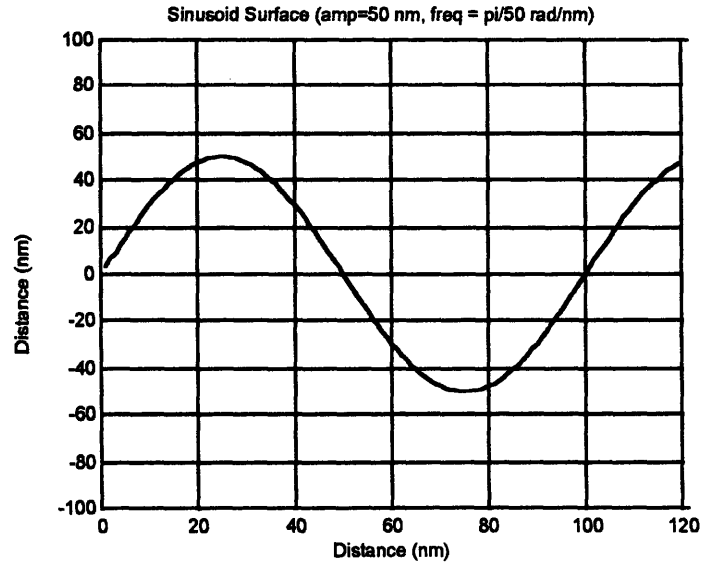
Figure 5.3 Sinusoid surface (amplitude = 50 nm, spatial frequency = pi/50 rad/nm).

5.3.3 Sample

The surface that the probe is being designed to optimally scan is called the sample. The nominal sample surface is shown in Figure 5.4. The sample construction is not always a repeatable process, which is why two worst case scenarios are considered. Figure 5.5(a) shows the sample with its tip skewed toward the left, and Figure 5.5(b) shows the sample with its tip skewed toward the right.
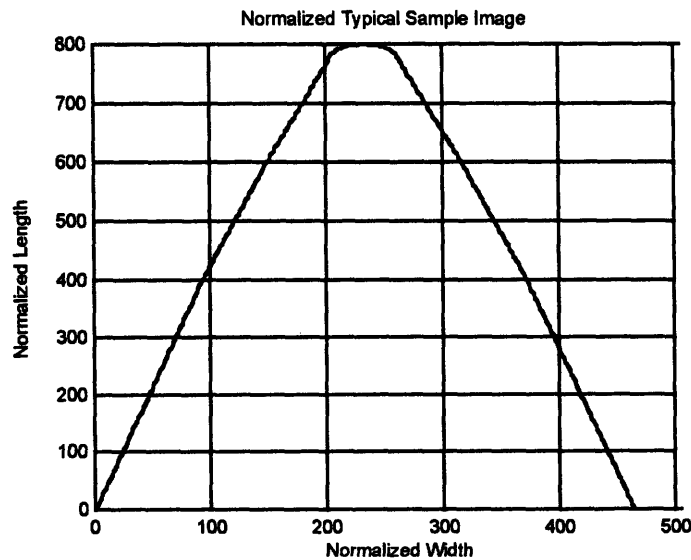
Figure 5.4 Normalized Sample Surface.
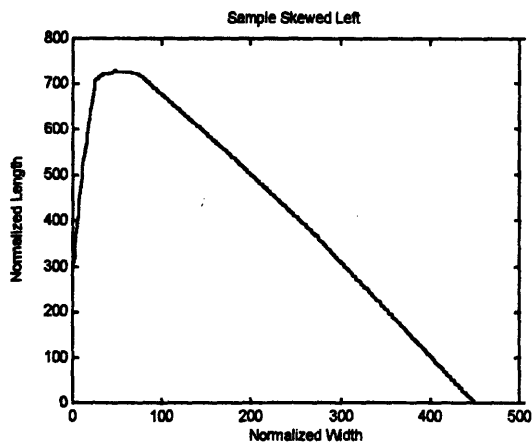
(a)

Orientation skewed left
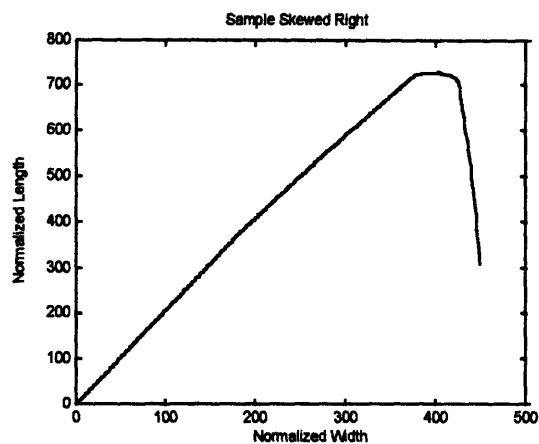
(b)

Orientation skewed right

Figure 5.5 Skewed Sample Surfaces.

5.4 Reconstruction Simulations

The reconstruction algorithm is used in all of the following simulations. However, there is one limitation of this particular program. In some of the scans, the reconstructed points are not exactly in the correct locations. This happens mostly when an edge is very sharp, such as the step. The reason for the discrepancy is that the algorithm calculates the slope of the tip at individual points and the slope of the tip does not exactly match with the slope of the scanned image because of numerical error. As a result, when the algorithm attempts to reconstruct the true surface, the points are erroneously placed. If the tip was continuously smooth, this error would not exist, so one method for improving the problem in the simulations is creating a tip with more points. The consequence of this is that the simulations will take a longer time to perform. This discrepancy will be discussed in the appropriate subsections. The first scanning scenario investigated is the calibration of the different tips. The first reconstruction scenarios to be examined are the step scans with the different tips with different parameters. Next, the scanning of the sinusoids will be investigated, again using multiple tip scenarios. Finally, the sample scans will be performed with a select number of tips.

5.4.1 Calibration

The calibration scan of the probe tips will utilize a step surface, because the scanned image requires minimal processing to obtain superb results. By superimposing the scanned image with the actual probe surface, the precision of the calibration technique can be readily observed and the results are excellent. First, the circular tip will be examined with several different radius configurations. Next, the parabolic tip will be considered. Finally, the angled parabolic tip will explore different tip orientations and size configurations. The software used for this simulation is Matlab™ and this scan increments one nanometer at a time and calculates the minimum distance from the probe tip to the sample surface.

5.4.1.1 Circular Tip Calibration Scans

The circular tip scans were quite successful. Circular tips with radii of 20 nm, 50 nm, and 100 nm were all examined in the following scans. The calibration piece used was a 50 nm high step. Figure 5.6, Figure 5.7, and Figure 5.8 show the calibration scans and results for the different tip sizes. The actual tip and step surfaces are represented by the solid line, while the scanned image data is shown with an "o" character. The scanned images perfectly match the tip surface, hence using a step to calibrate circular tip is effective.
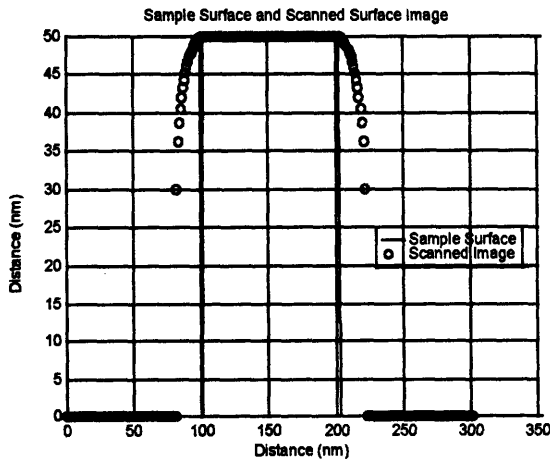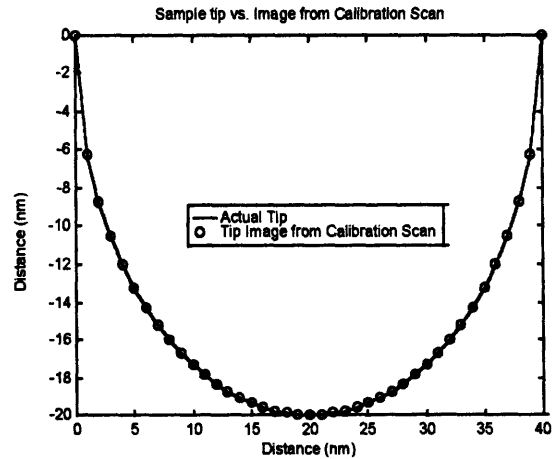
Calibration Scan   Actual Tip vs. Scanned Tip Image

Figure 5.6 Circular Tip Calibration (radius = 20 nm)
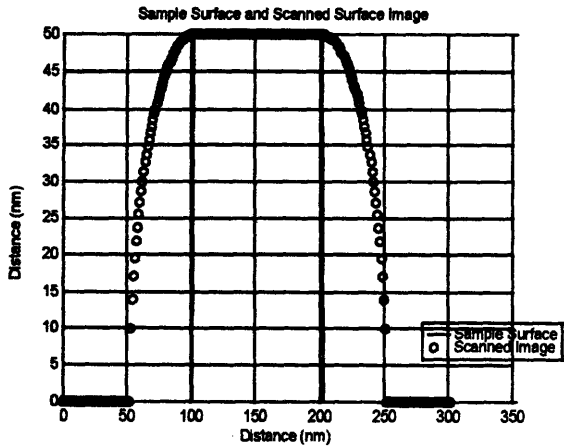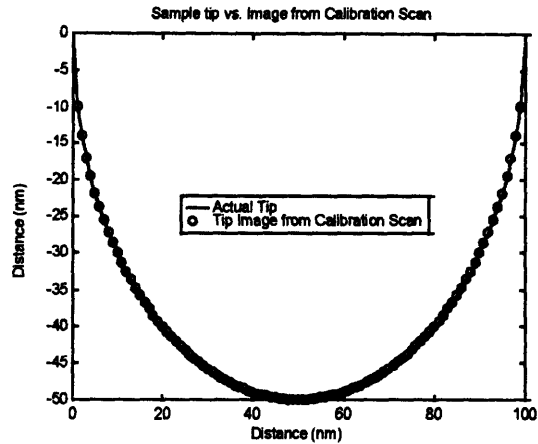
Calibration Scan   Actual Tip vs. Scanned Tip Image

Figure 5.7 Circular Tip Calibration (radius = 50 nm)
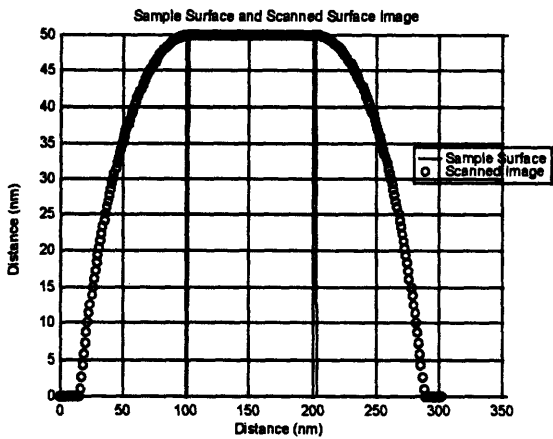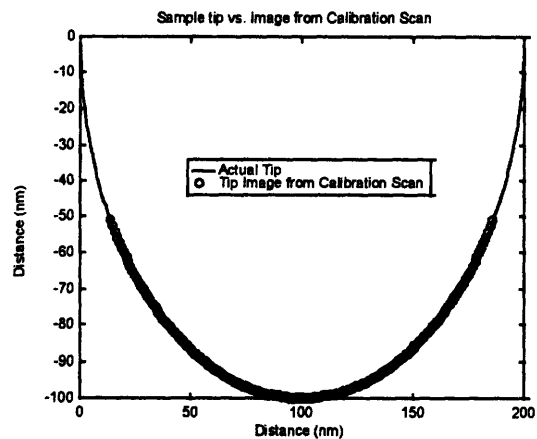
Calibration Scan   Actual Tip vs. Scanned Tip Image

Figure 5.8 Circular Tip Calibration (radius = 100 nm)

5.4.1.2 Parabolic Tip Calibration

The parabolic tip scans also revealed excellent results. Tip radii of approximately 20 nm and 100 nm were both examined. The calibration piece used was the same 50 nm high step. Figure 5.9 and Figure 5.10 show the calibration scans and results for the different tip sizes. Again, the actual sample and tip surfaces are represented by a solid line, while the scanned image is denoted with an "o" character. These scanned images compare excellently with the actual tip surface, hence using a step to calibrate parabolic tips is a success.

93
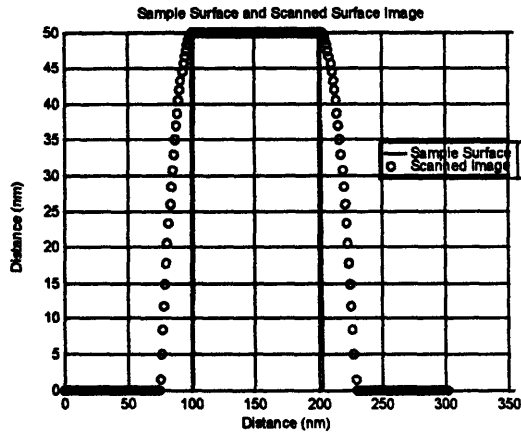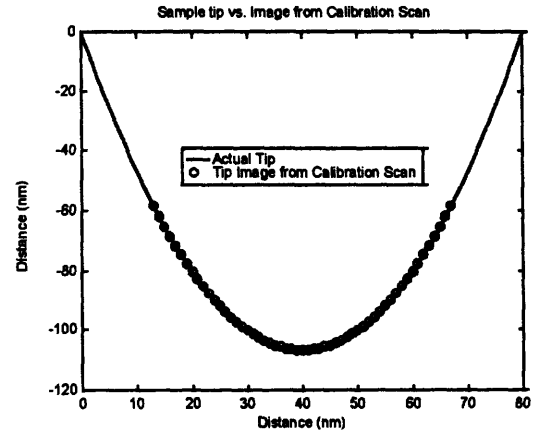
Calibration Scan

Actual Tip vs. Scanned Tip Image

Figure 5.9 Parabolic Tip Calibration (radius ≅ 20 nm)
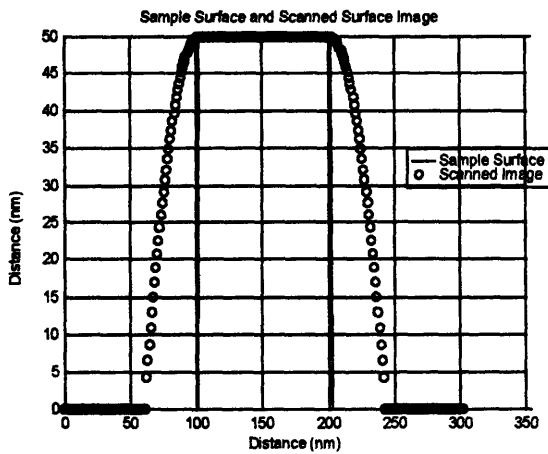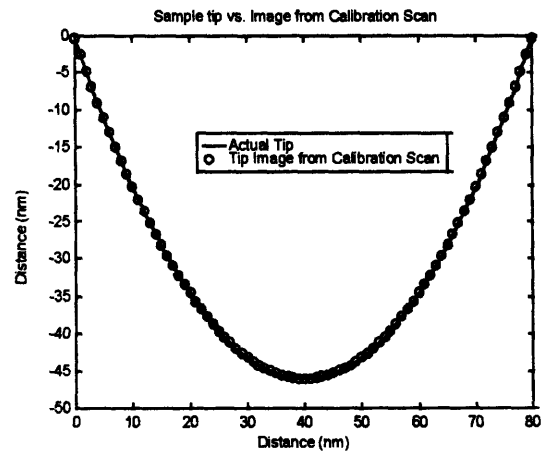
Calibration Scan

Actual Tip vs. Scanned Tip Image

Figure 5.10 Parabolic Tip Calibration (radius ≅ 100 nm)

5.4.1.3 Angled Parabolic Tip Calibration

The angled parabolic tip scans also revealed outstanding results. The scenarios for this probe tip examined two different tip radii of approximately 30 nm and 90 nm. For each different radius, three different angles were considered, 30°, 60°, and -45°. The angles are from the vertical with positive in the clockwise direction. Again, the calibration piece used for the scan is a 50 nm tall step. Figure 5.11, Figure 5.12, and Figure 5.13 show the calibration scans of the tip with a radius of 30 nm oriented along the three different angles previously mentioned. Figure 5.14, Figure 5.15, and Figure 5.16 show the calibration of the angled tip with a radius of 90 nm at the

predetermined angles. Again, the actual sample and tip surfaces are represented by a solid line, while the scanned image is denoted with an "o" character. Once again, the scanned images perfectly match the tip surface, hence the step calibration of an angled parabolic tip proves to be a viable solution.
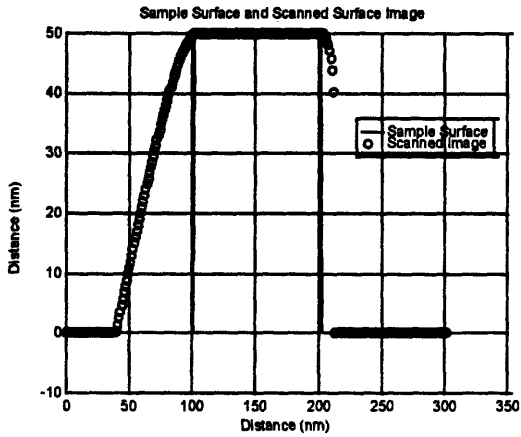
Calibration Scan
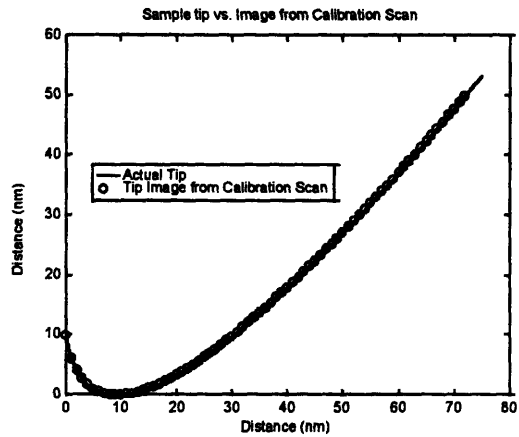
Actual Tip vs. Scanned Tip Image

Figure 5.11 Angled Parabolic Tip Calibration ($\angle 30°$ w/radius $\cong$ 30 nm)
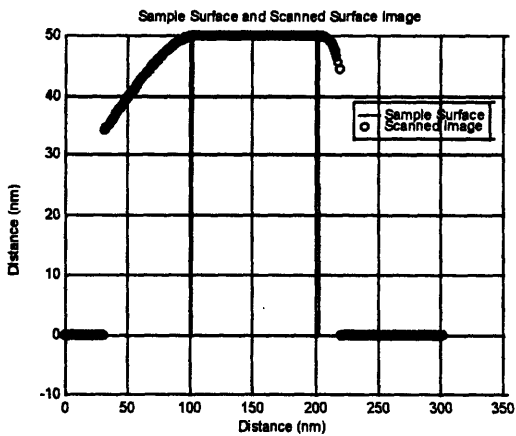
Calibration Scan
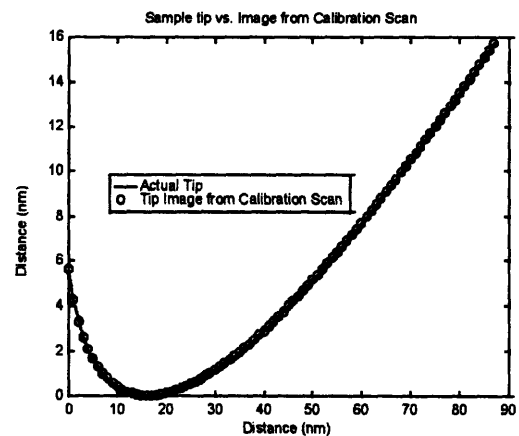
Actual Tip vs. Scanned Tip Image

Figure 5.12 Angled Parabolic Tip Calibration ($\angle 60°$ w/radius $\cong$ 30 nm)
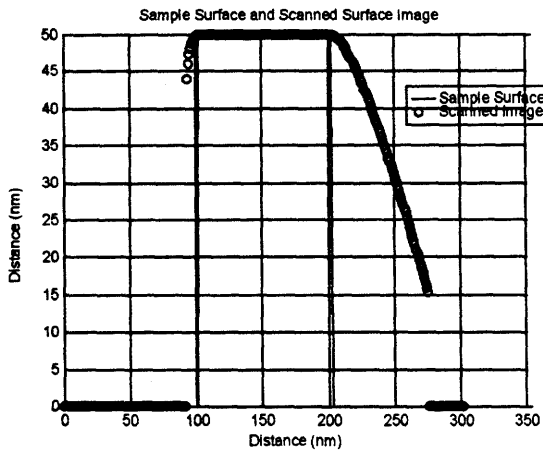
Calibration Scan
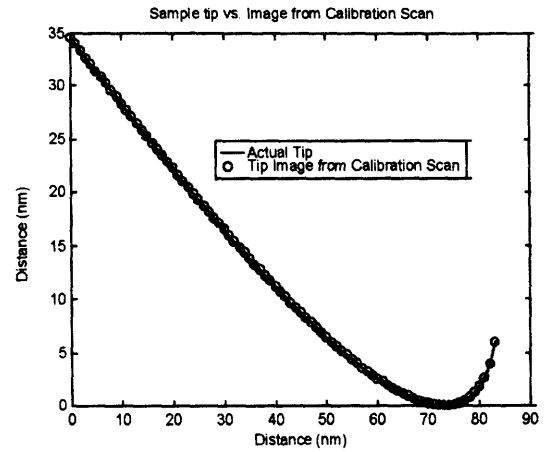
Actual Tip vs. Scanned Tip Image

Figure 5.13 Angled Parabolic Tip Calibration ($\angle$-45° w/radius $\cong$ 30 nm)
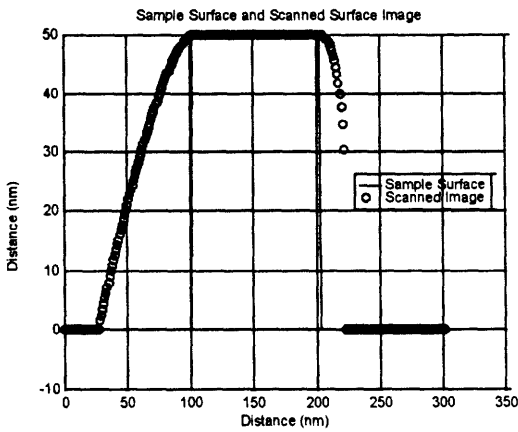
Calibration Scan
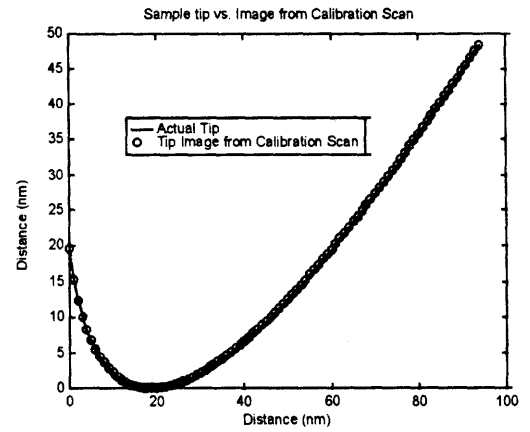
Actual Tip vs. Scanned Tip Image

Figure 5.14 Angled Parabolic Tip Calibration ($\angle$30° w/radius $\cong$ 90 nm)
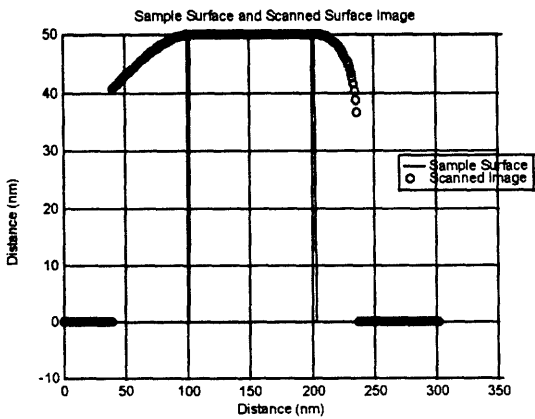
Calibration Scan
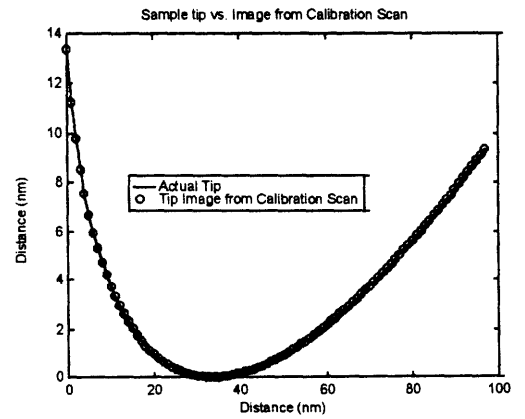
Actual Tip vs. Scanned Tip Image

Figure 5.15 Angled Parabolic Tip Calibration ($\angle 60°$ w/radius $\cong$ 90 nm)

Sample Surface and Scanned Surface Image

Distance (nm)

Distance (nm)

— Sample Surface
o Scanned Image

Sample tip vs. Image from Calibration Scan

Distance (nm)

Distance (nm)

— Actual Tip
o Tip Image from Calibration Scan

Calibration Scan

Actual Tip vs. Scanned Tip Image
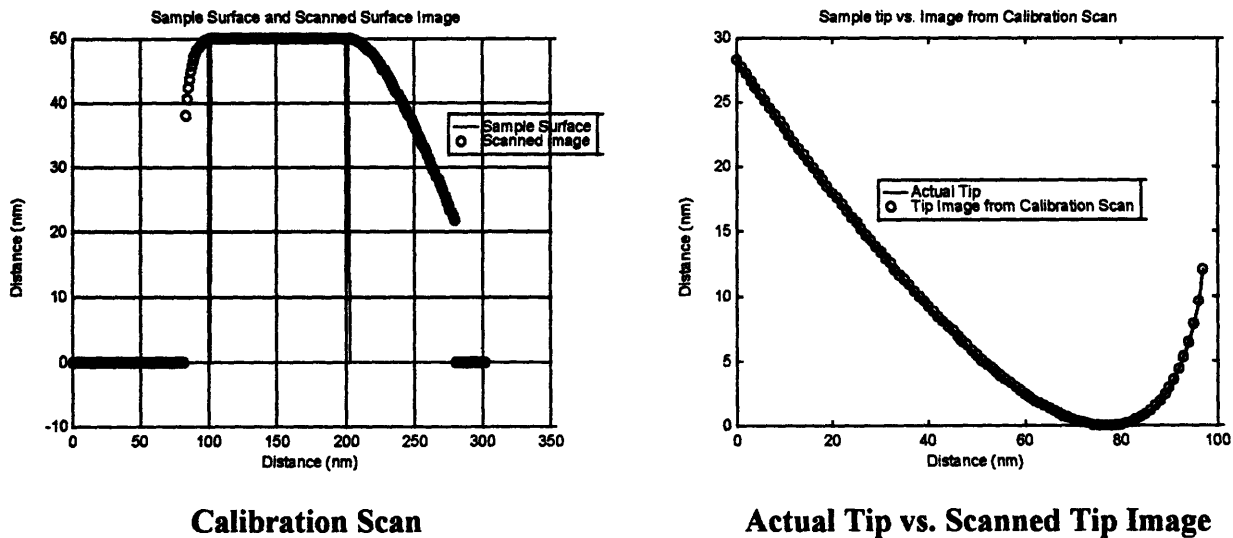
Figure 5.16 Angled Parabolic Tip Calibration ($\angle$-45° w/radius $\cong$ 90 nm)

5.4.2 Step Scans

The scanning of the step surface with the different tip sizes and orientations needs to be contemplated. In section 5.4.1, the step was used for calibrating the tip surface, now the calibrated image will be used to reconstruct the actual step surface. As discussed earlier, the numerical errors encountered in the reconstruction will be realized in this application. Also observed in these simulations are "holes," where the tip is not in contact with the surface. This phenomena was discussed in the software discussions of the previous chapter. The first tips to be examined will be the circular tips. Next the parabolic tip will be used in the reconstruction of the step. Finally, the angled parabolic tip's many configurations will be examined as possible reconstruction options.

5.4.2.1 Circular Tip Step Reconstruction

Utilizing circular tips in the reconstruction of a step also proved to be an feasible technique. The step reconstruction scans performed with circular tips were a success. Circular tips with radii of 20 nm and 100 nm were both examined in the following scans. The steps investigated were 50 nm and 100nm in height. Figure 5.17 shows the reconstruction performance of the two different radii on the step that is 50 nm high. Next, Figure 5.18 demonstrates the reconstruction ability of

the two tips on a 100 nm step. The actual step surface is represented by the solid line, while the scanned image is shown with an "o" character, and the reconstructed image is represented by an "x" character. Without the numerical error and if the "hole" regions were not considered, the reconstructed surfaces perfectly match the actual step surfaces. One method to decrease the size of the regions with "holes" is to use a smaller tip. From the figures below, the reconstructed images that used a tip with radius of 20 nm have a smaller region that cannot be observed. In summary, the reconstruction of the step using a circular tip is an effective technique and resolution increases as the probe tip size decreases.
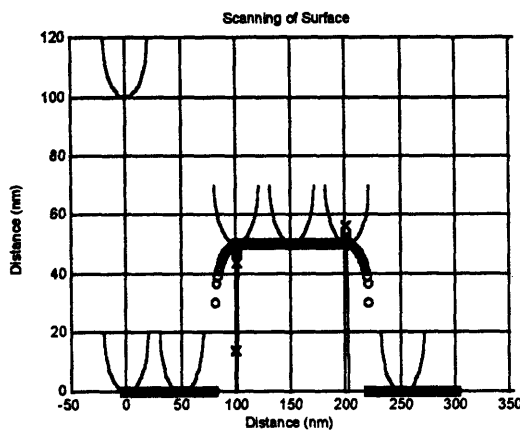
Step Scan · Surface vs. Reconstructed Image
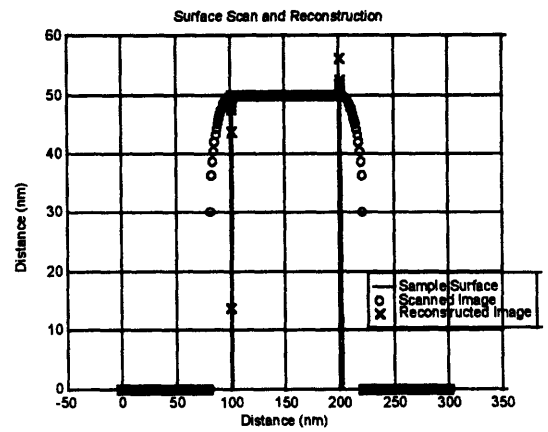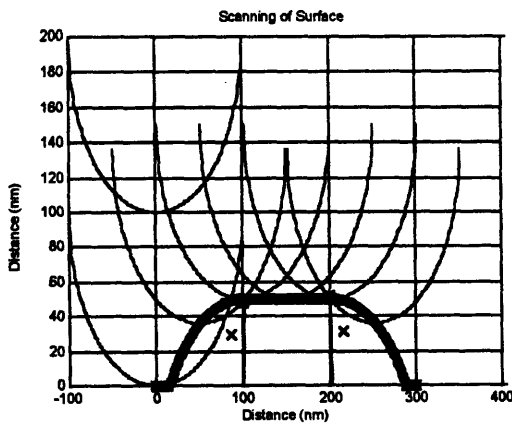
(a) Tip Radius = 20 nm
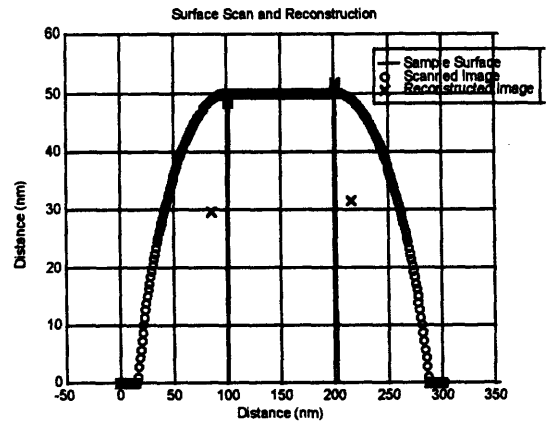
Step Scan · Surface vs. Reconstructed Image

(b) Tip Radius = 100 nm

Figure 5.17 Circular Tip Step Reconstruction (step height = 50 nm)
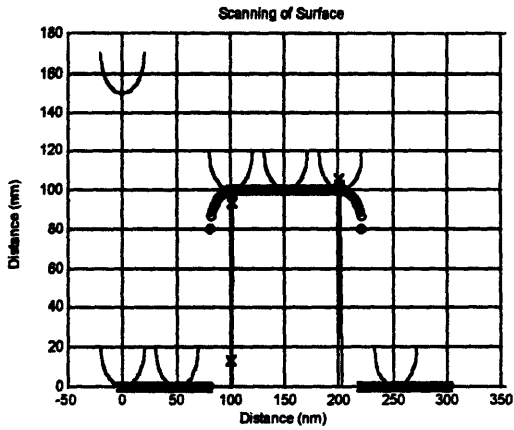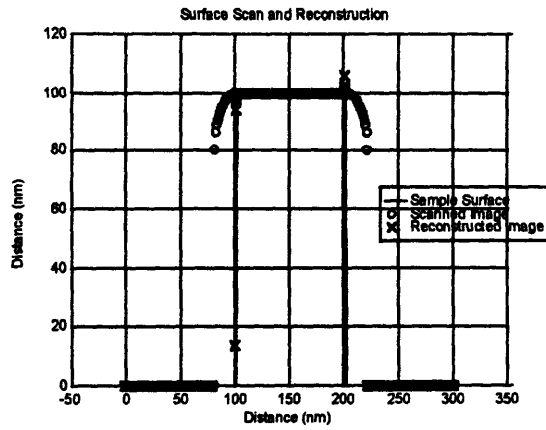
Step Scan   **Surface vs. Reconstructed Image**

(a) Tip Radius = 20 nm
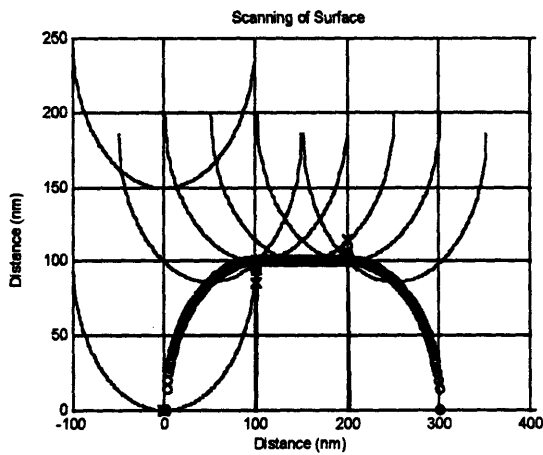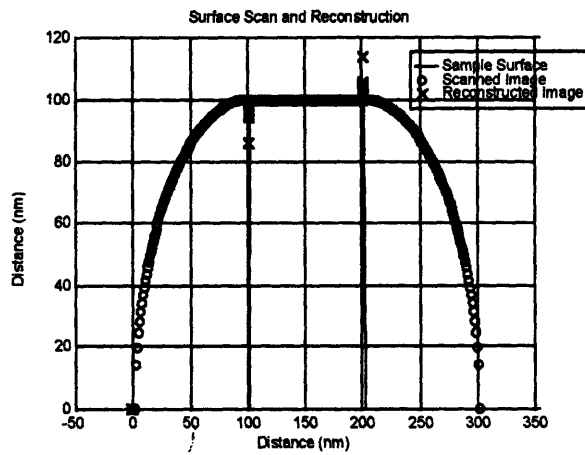
Step Scan   **Surface vs. Reconstructed Image**

(b) Tip Radius = 100 nm

Figure 5.18 Circular Tip Step Reconstruction (step height = 100 nm)

5.4.2.2 Parabolic Tip Step Reconstruction

Using parabolic tips to reconstruct the step surface, were also a success. Tip radii of approximately 20 nm and 100 nm were both examined. Again, the step heights examined were 50 nm and 100 nm. Figure 5.19 examines the reconstruction performance of different tip sizes on the step with a height of 50 nm. Figure 5.20 shows the reconstruction of the 100 nm step with the different tip radii. The step surface is represented by the solid line; the scanned image is represented by the "o" character; and the reconstructed image is depicted with the "x" character. Even though the numerical errors and "hole" regions were once again noticeable features, the

99

reconstruction image reveals accurate information about the sample surface. As stated before, as the tip size decreases, the "hole" region is diminishes. Using a parabolic tip to reconstruct a step provides excellent results.
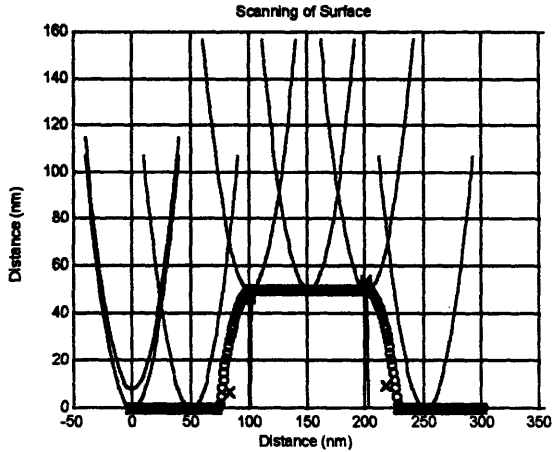
Step Scan   **Surface vs. Reconstructed Image**
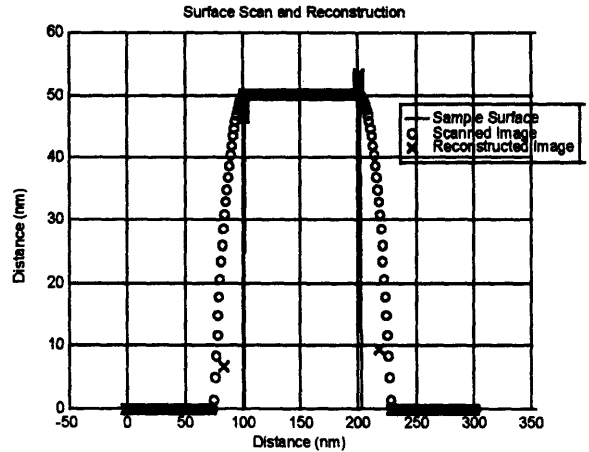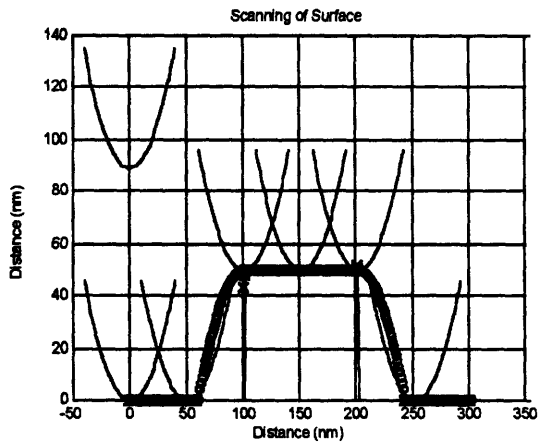
(a) Tip Radius ≅ 20 nm
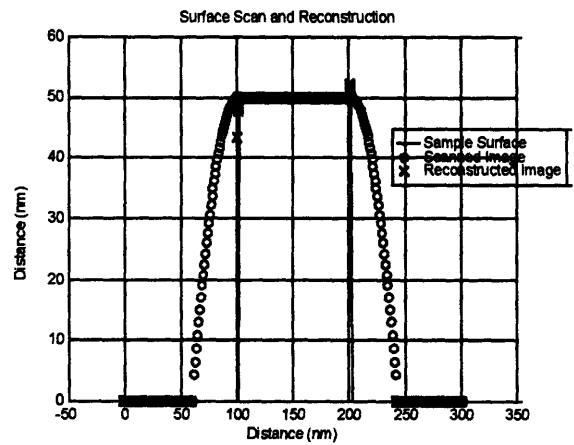
Step Scan   **Surface vs. Reconstructed Image**

(b) Tip Radius ≅ 100 nm

Figure 5.19 Parabolic Tip Step Reconstruction (step height =50 nm)
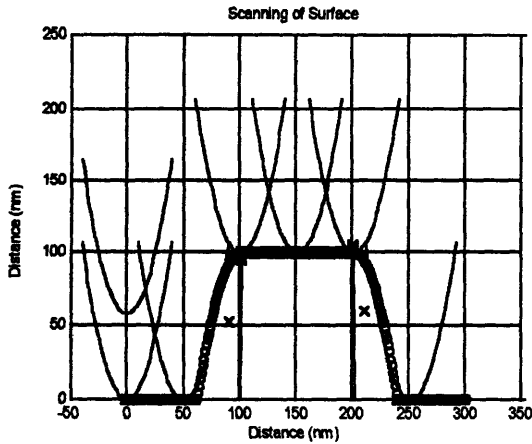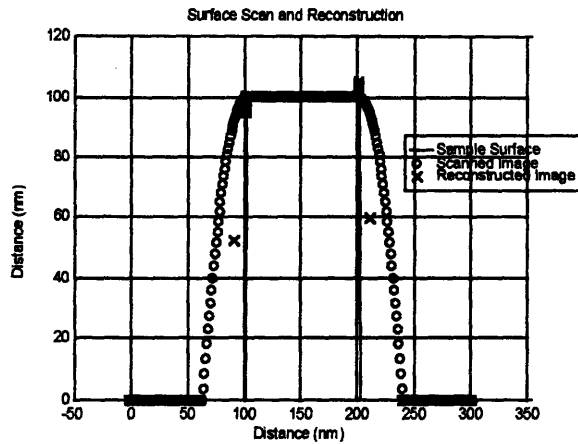
Step Scan   **Surface vs. Reconstructed Image**

(a) Tip Radius $\cong$ 20 nm
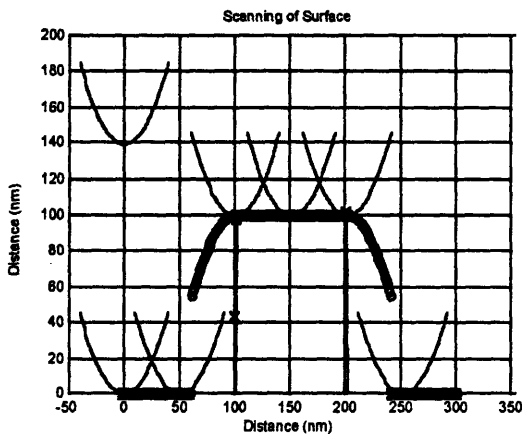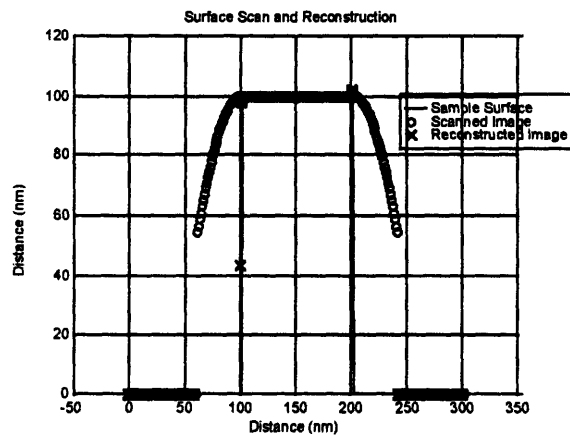
Step Scan   **Surface vs. Reconstructed Image**

(b) Tip Radius $\cong$ 100 nm

Figure 5.20 Parabolic Tip Step Reconstruction (step height = 100 nm)

5.4.2.3 Angled Parabolic Tip Step Reconstruction

The use of angled parabolic tips to reconstruct the step surface also revealed quality results. The scenarios for this probe tip examined two different tip radii of approximately 30 nm and 90 nm. For each different radius, three different angles were considered, $30°$, $60°$, and $-45°$. The angles are from the vertical with positive in the clockwise direction. The reconstruction of steps with heights of 50 nm are performed with multiple tip configurations. The reconstruction of a 100 nm step is performed with a probe tip of approximately 30 nm with angles of $60°$ and $-45°$. Figure 5.21, Figure 5.22, and Figure 5.23 highlight the reconstruction of a 50 nm step using a tip with a

101

30 nm radius oriented at the angles of 30°, 60°, and -45°. Figure 5.24, Figure 5.25, and Figure 5.26 show the reconstruction of a 50 nm step using a tip with a radius of 90 nm oriented along the three different angles mentioned previously. Figure 5.27 and Figure 5.28 reconstruct a 100 nm step using a tip with radius of 30 nm and an orientation of 60° and -45°. The step surface is represented by the solid line; the scanned image is represented by the "o" character; and the reconstructed image is depicted with the "x" character. Once again the numerical errors are present in the reconstruction simulations, however this reconstruction method does provide an accurate representation of the sample surface. The region where the "holes" occur are appropriate because the tip is not in contact with that portion of the surface. Finally, the reconstruction of the step using an angled parabolic tip proves to be a reliable high resolution solution.
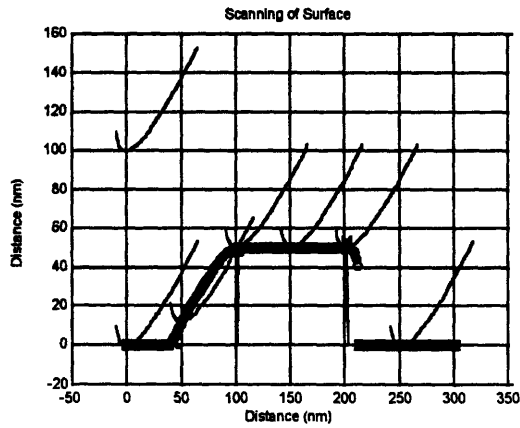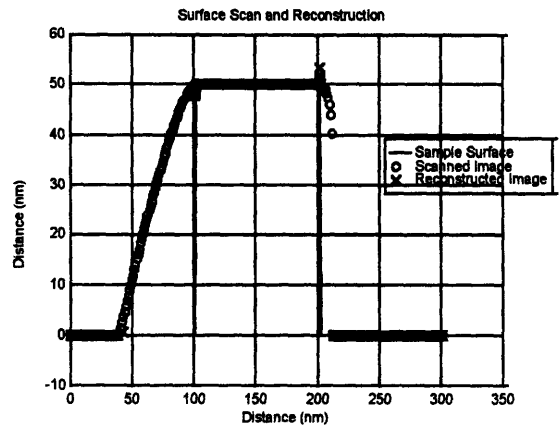
Step Scan   Tip vs. Processed Image

Figure 5.21 Angled Parabolic Step Reconstruction (∠30° w/radius ≅ 30 nm)

Step Scan   Tip vs. Processed Image

102
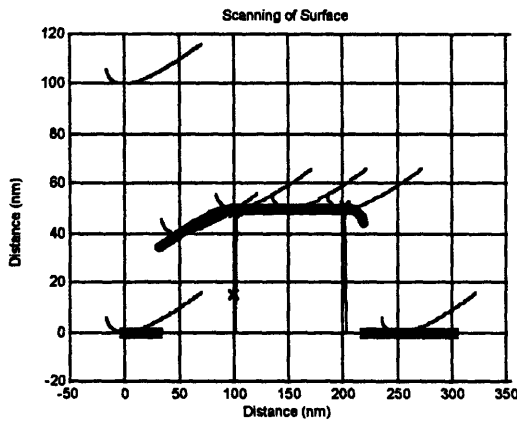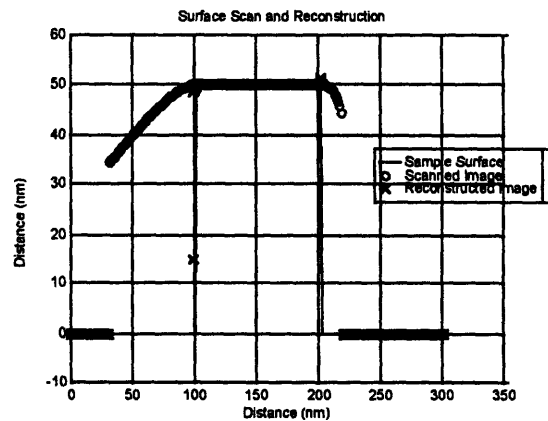
Figure 5.22 Angled Parabolic Step Reconstruction ($\angle 60°$ w/radius $\cong$ 30 nm)
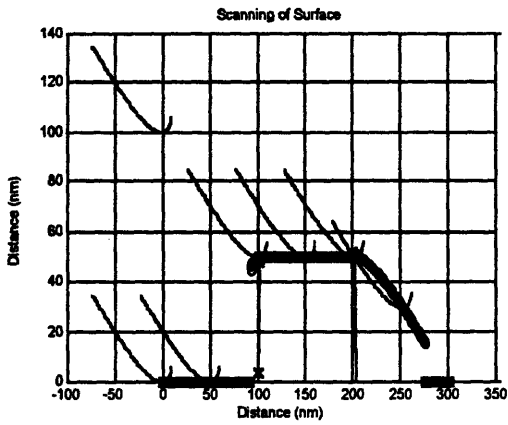
Step Scan
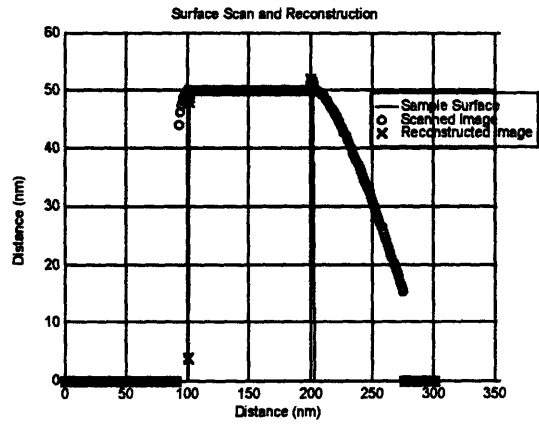
Tip vs. Processed Image

Figure 5.23 Angled Parabolic Step Reconstruction ($\angle$-45° w/radius $\cong$ 30 nm)
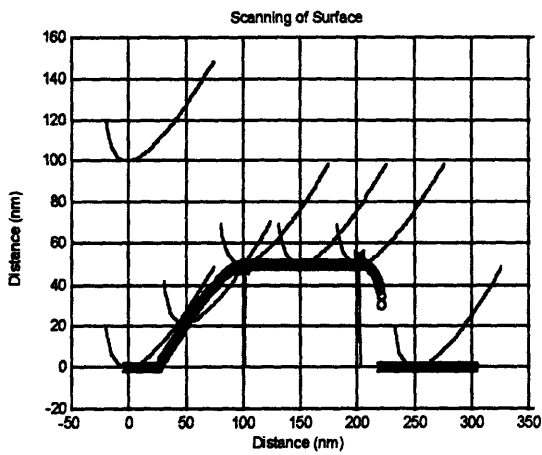
Step Scan
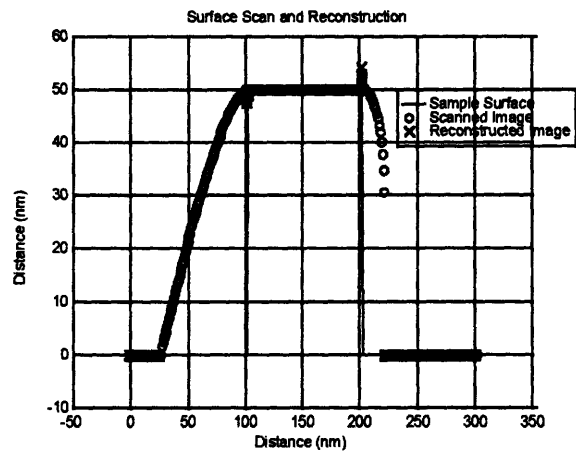
Tip vs. Processed Image

Figure 5.24 Angled Parabolic Step Reconstruction ($\angle$30° w/radius $\cong$ 90 nm)
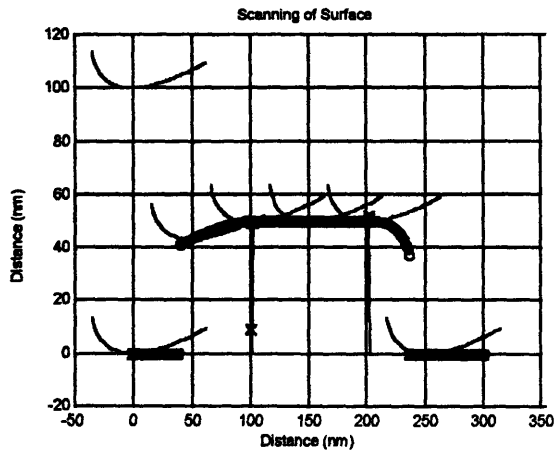
Step Scan
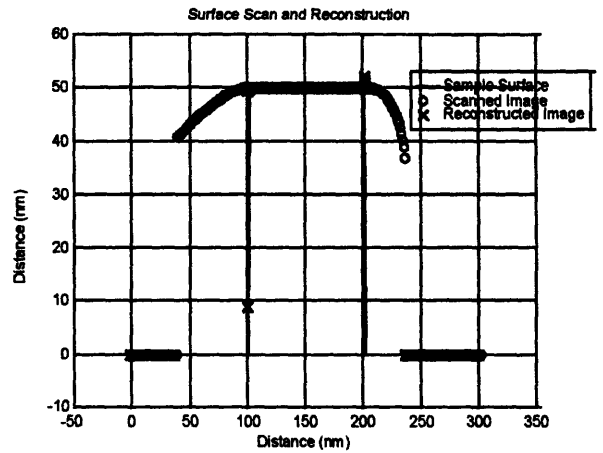
Tip vs. Processed Image

Figure 5.25 Angled Parabolic Step Reconstruction ($\angle 60^\circ$ w/radius $\cong$ 90 nm)
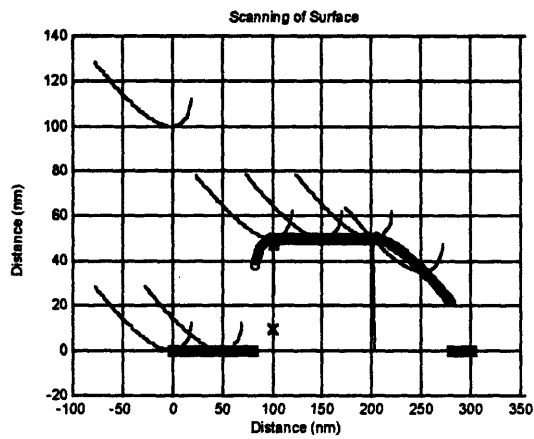
Step Scan
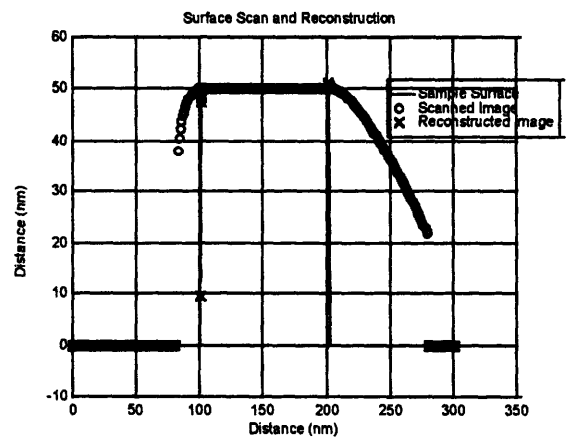
Tip vs. Processed Image

Figure 5.26 Angled Parabolic Step Reconstruction ($\angle$-45° w/radius $\cong$ 90 nm)

Step Scan

Tip vs. Processed Image

104
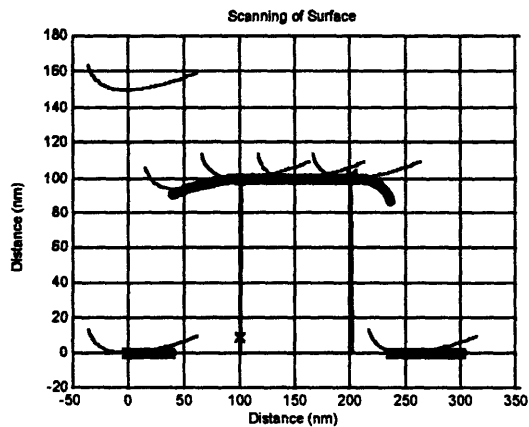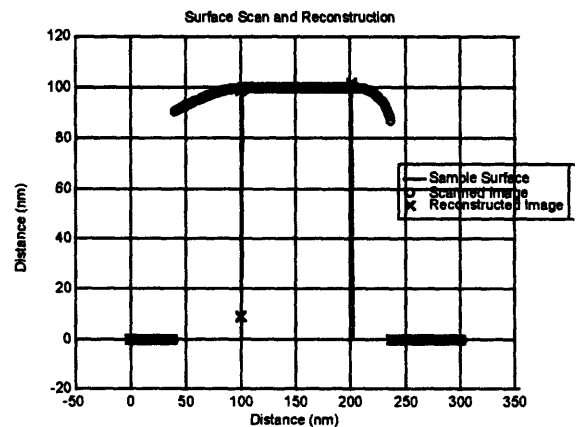
Figure 5.27 Angled Parabolic Step Reconstruction - 100 nm ($\angle 60°$ w/radius $\cong$ 30 nm)

Step Scan   Tip vs. Processed Image
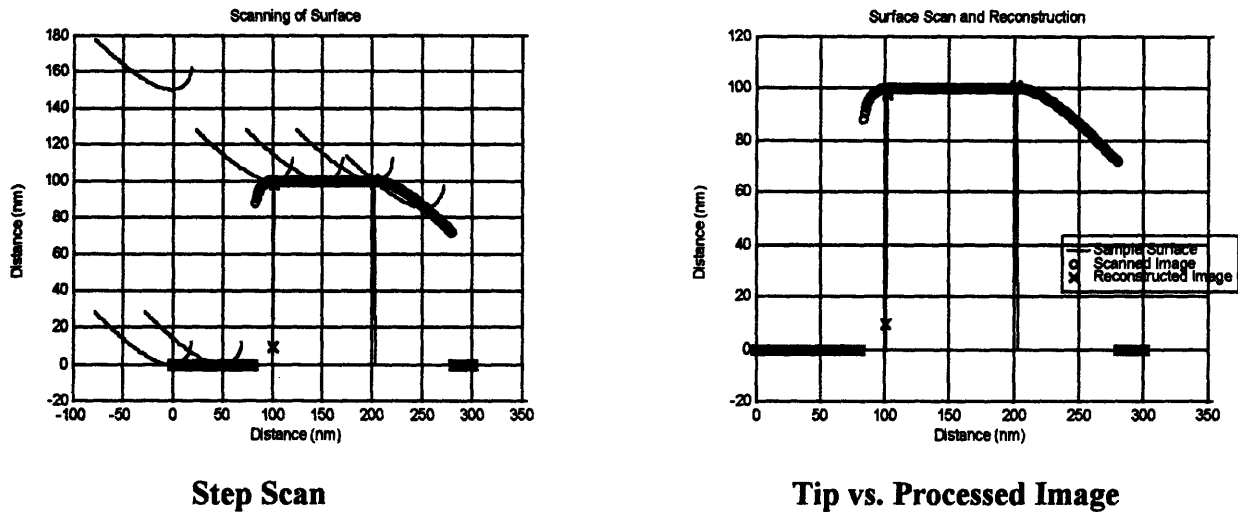
Figure 5.28 Angled Parabolic Step Reconstruction - 100 nm ($\angle$-45° w/radius $\cong$ 30 nm)

5.4.3 Sinusoid Scans

The next sample surface investigated is the sinusoidal surface. The sinusoid surface is a good representation of surface imperfections and these simulations will assist in defining the expected resolution of the system. The step scans revealed that the probe tip with the smallest radius reveals the best results. Since probe tips with a radius of 20 nm are commercially available, all of the remaining scans will be simulated with tips of this size. Again, the three tips examined are the circular tip, parabolic tip, and angled parabolic tip.

5.4.3.1 Circular Tip Sinusoid Surface Reconstruction

The sinusoid surface reconstruction scans performed with circular tips were a success. Circular tips with a radius of 20 nm were examined on surfaces with a 50 nm amplitude. Three different surface spatial frequencies of pi/20, pi/50, and pi/100 rad/nm are considered in Figure 5.29. The actual surface is represented by the solid line, while the scanned image is shown with an "o" character, and the reconstructed image is represented by an "x" character. The figures reveal that the reconstruction of the sinusoid surface with a circular tip demonstrates accurate results and if higher resolution is desired, then the probe tip size should be decreased. The 20 nm tip can only reconstruct the peaks of the high spatial frequency roughness. For surfaces with a spatial

frequency of pi/50 rad/nm, the reconstruction is almost entirely complete. Vertical and lateral resolution for the small circular tip is subnanometer for spatial frequencies less than pi/100 rad/nm
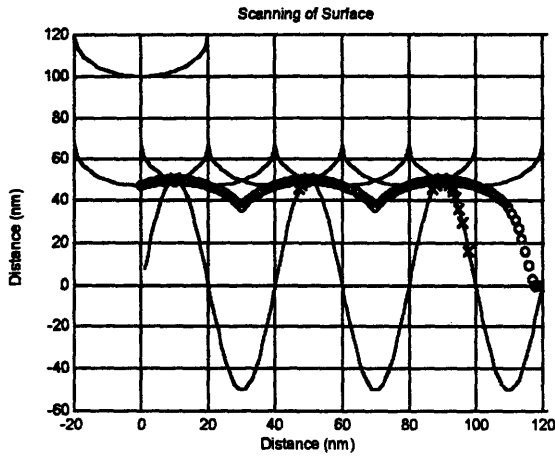
Sinusoid Surface Scan   Surface vs. Reconstructed Image
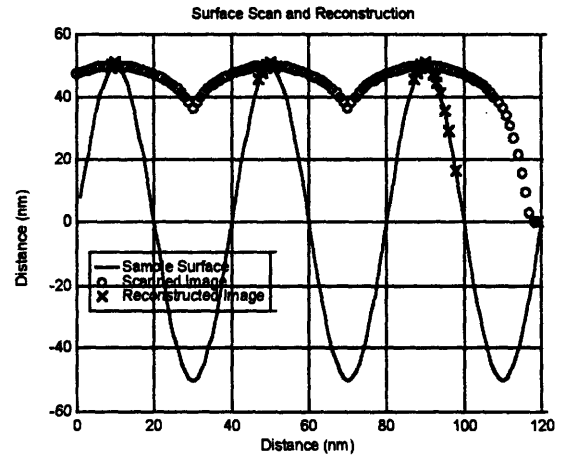
(a) Spatial Frequency = pi/20 rad/nm
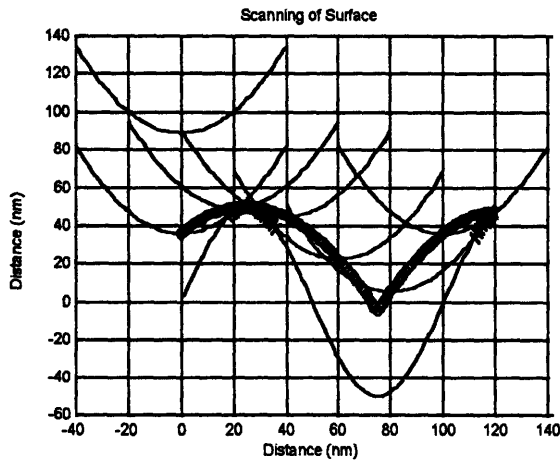
Sinusoid Surface Scan   Surface vs. Reconstructed Image
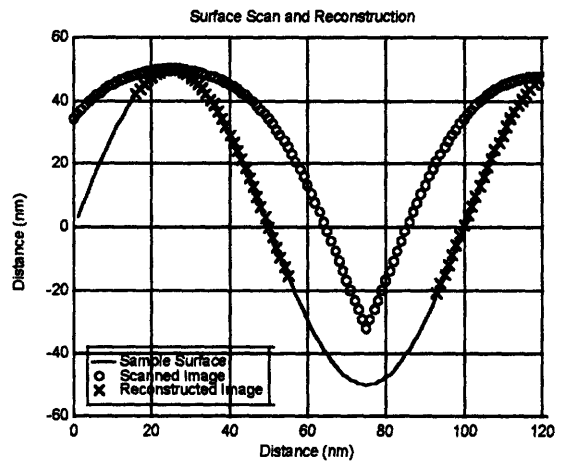
(b) Spatial Frequency = pi/50 rad/nm
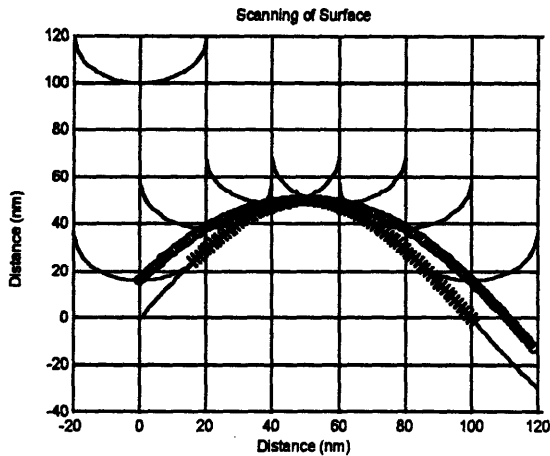
Sinusoid Surface Scan   **Surface vs. Reconstructed Image**
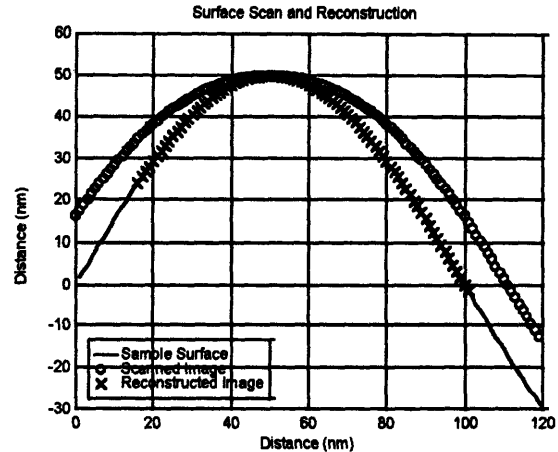
(c) Spatial Frequency = pi/100 rad/nm

Figure 5.29 Circular Tip Sinusoid Surface Reconstruction

5.4.3.2 Parabolic Tip Sinusoid Surface Reconstruction

The reconstruction simulations of the sinusoidal surfaces using parabolic tips also divulged accurate results. The probe tip radius of 20 nm was examined. Again, the simulations will consider a sinusoid surface with a 50 nm amplitude and spatial frequencies of pi/20, pi/50 and pi/100 rad/nm. Figure 5.30 examines the reconstruction performance of the sinusoid surface with the different spatial frequencies. The actual surface is represented by the solid line; the scanned image is represented by the "o" character; and the reconstructed image is depicted with the "x" character. The reconstruction image reveals accurate information about the sample surface. The parabolic tip scan resolutions are similar to the circular tip with subnanometer resolution for spatial frequencies less than pi/100 rad/nm.
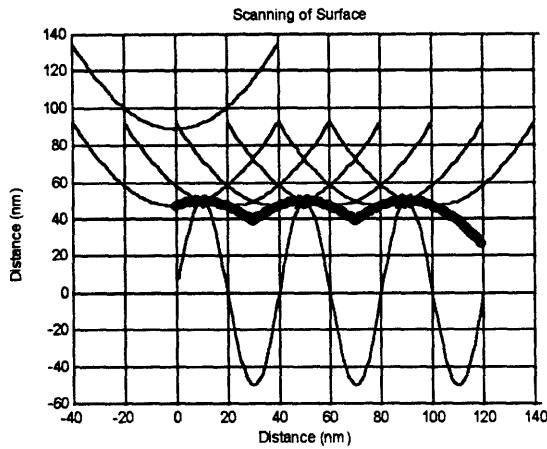
107

Sinusoid Surface Scan   **Surface vs. Reconstructed Image**

(a) Spatial Frequency = pi/20 ra/nm
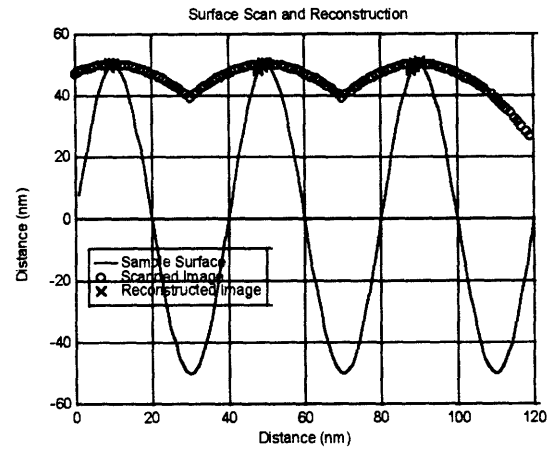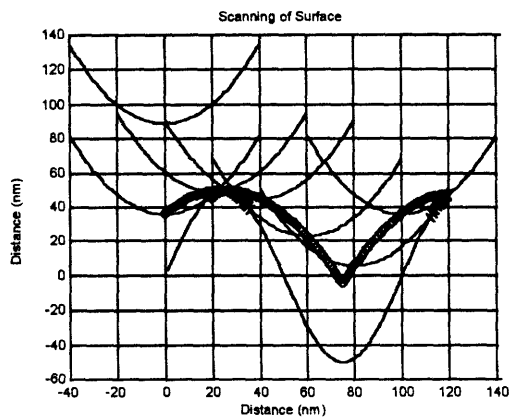
Sinusoid Surface Scan   **Surface vs. Reconstructed Image**

(b) Spatial Frequency = pi/50 ra/nm
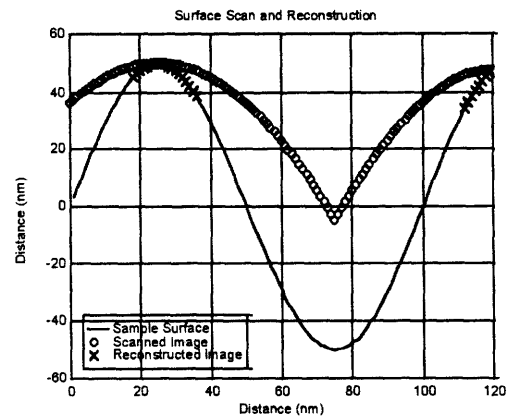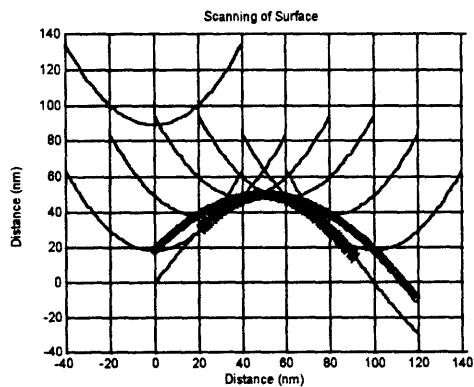
Sinusoid Surface Scan   **Surface vs. Reconstructed Image**

(c) Spatial Frequency = pi/100 rad/nm
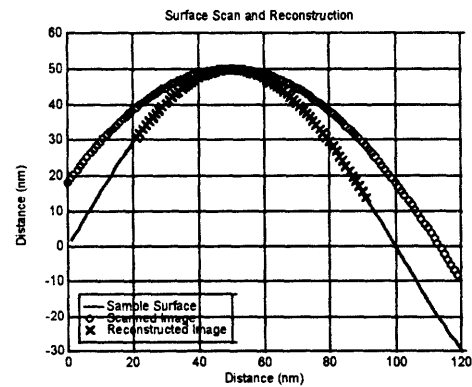
Figure 5.30 Parabolic Tip Sinusoid Surface Reconstruction.

108

5.4.3.3 Angled Parabolic Tip Sinusoid Surface Reconstruction

The use of angled parabolic tips to reconstruct the sinusoid surface also revealed quality results. The scenarios for this probe tip examined a tip with a 20 nm radius that was angled at $30°$ and $-45°$. The angles are from the vertical with positive in the clockwise direction. The reconstruction of sinusoid surfaces with a height of 50 nm and spatial frequencies of pi/20, pi/50 and pi/100 rad/nm are performed with the different tip configurations. Figure 5.31 and Figure 5.32 reconstruct the sinusoid surfaces using a tip with radius of 20 nm and an orientation of $30°$ and $-45°$. The surface is represented by the solid line; the scanned image is represented by the "o" character; and the reconstructed image is depicted with the "x" character. The angled parabola also has interesting interactions with the sinusoidal surface. Resolution on one surface slope will often be higher than another slope simply because of the angle of approach. However, in general, the resolution for the angled parabolic tip is subnanometer for spatial frequencies less than pi/100 rad/nm.
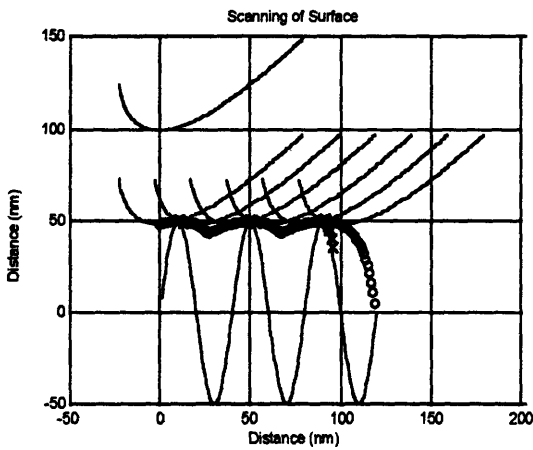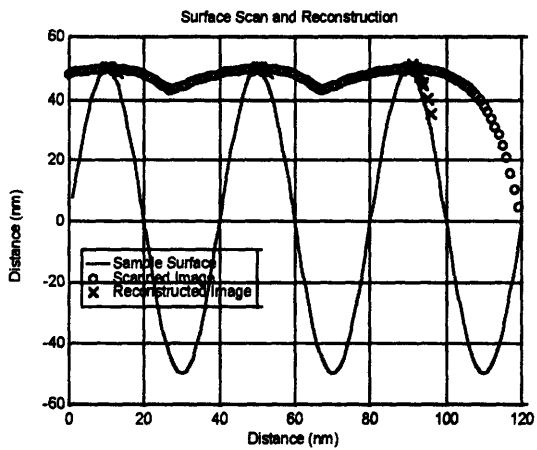
Sinusoid Surface Scan   Surface vs. Reconstructed Image

(a) Spatial Frequency = pi/20 ra/nm
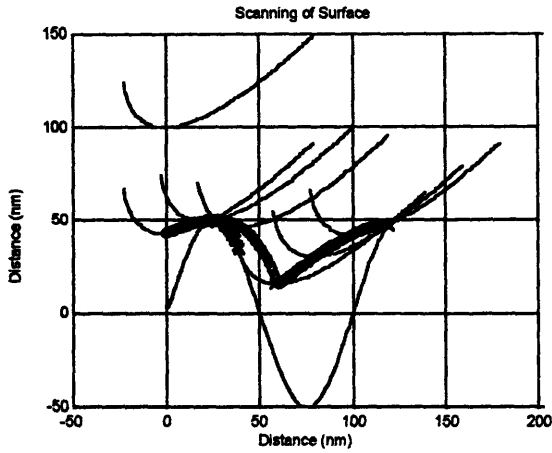
Sinusoid Surface Scan   Surface vs. Reconstructed Image
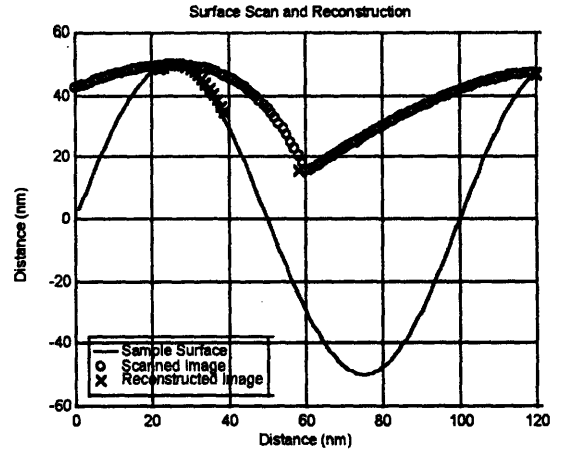
(b) Spatial Frequency = pi/50 ra/nm
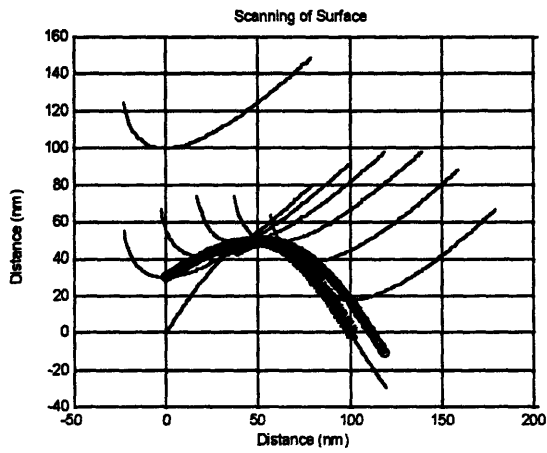
Sinusoid Surface Scan   Surface vs. Reconstructed Image
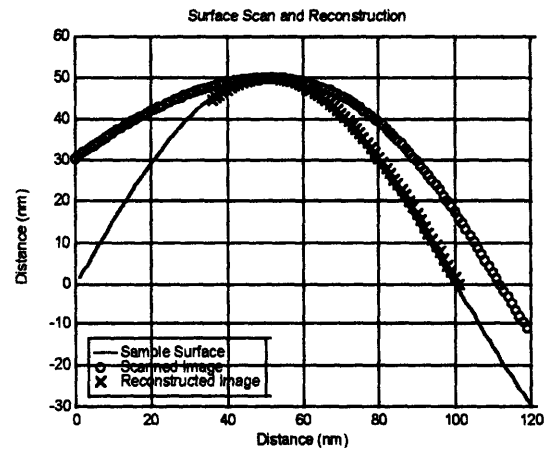
(c) Spatial Frequency = pi/100 rad/nm

Figure 5.31 Angled Parabolic Tip Sinusoid Surface Reconstruction(∠30°).
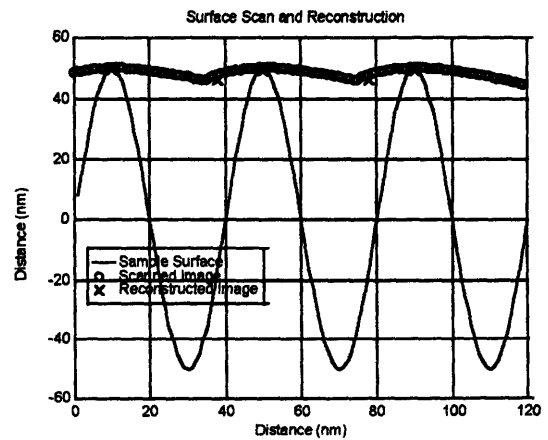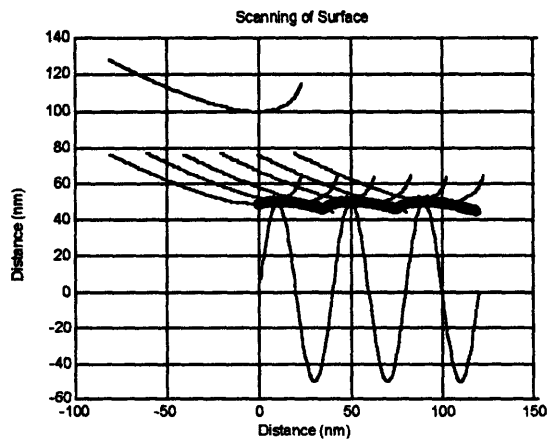
Sinusoid Surface Scan   **Surface vs. Reconstructed Image**
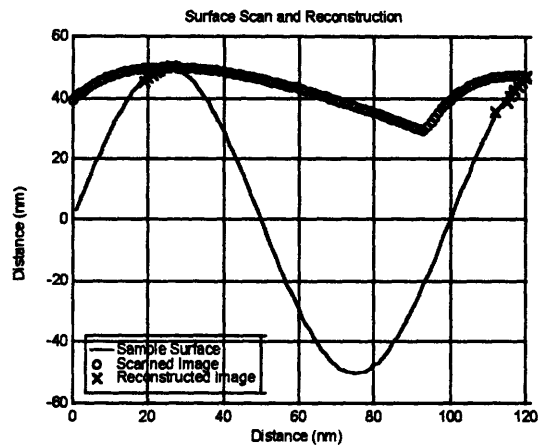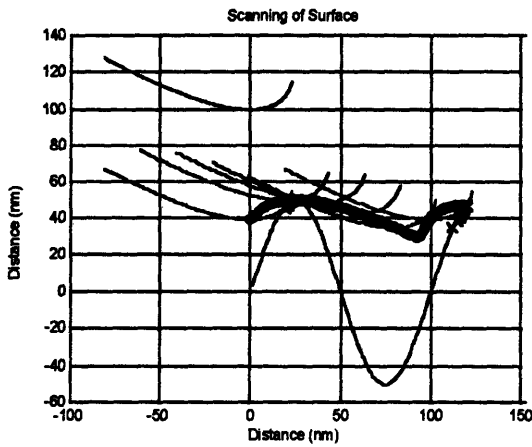
(a) Spatial Frequency = pi/20 ra/nm

Sinusoid Surface Scan   **Surface vs. Reconstructed Image**

(b) Spatial Frequency = pi/50 ra/nm
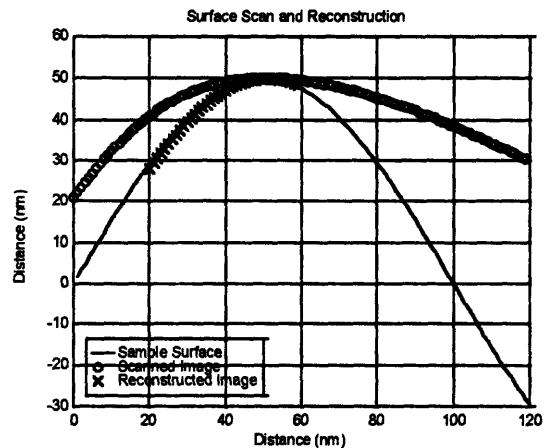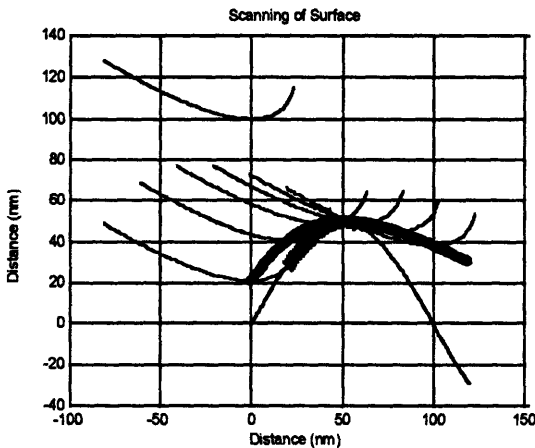
Sinusoid Surface Scan   **Surface vs. Reconstructed Image**

(c) Spatial Frequency = pi/100 rad/nm

Figure 5.32 Angled Parabolic Tip Sinusoid Surface Reconstruction($\angle$-45°).

5.4.4 Sample Scans

Finally, the surface of our application specific samples is investigated. From the scans performed on the step and sinusoidal surfaces, a great deal has been learned. The smaller the tip radius the better the reconstruction. Also, if the contour slope is continuous, the reconstruction has less numerical error. These simulations will only consider parabolic tips and specifically at the desired orientation of ±60°, depending on the side of the sample being scanned, which was defined in

111

Chapter 4 as the optimal angle. Three configurations of the sample: (1) normal, (2) skewed left, and (3) skewed right are all considered. The actual surface is represented by the solid line, while the scanned image is shown with an "o" character, and the reconstructed image is represented by an "x" character. The figures reveal that the reconstruction of the sample surface in any configuration with an angled parabolic tip is a success. Since the nominal and askew contours do not have discontinuous slopes, the predicted resolution of the reconstructed image is less than one nanometer. Also, the figures only examine one probe for the scans. Since the Scissors Design uses two probes and it is symmetric, only the single probe scan needs to be examined. Since both the skewed cases are investigated, all possibility of probe to surface interaction is being considered.
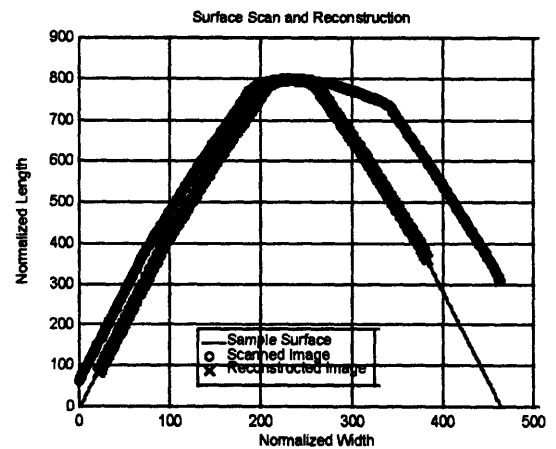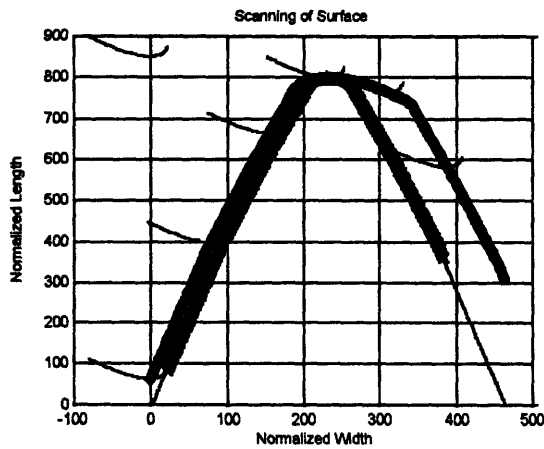
(a) Nominal Sample
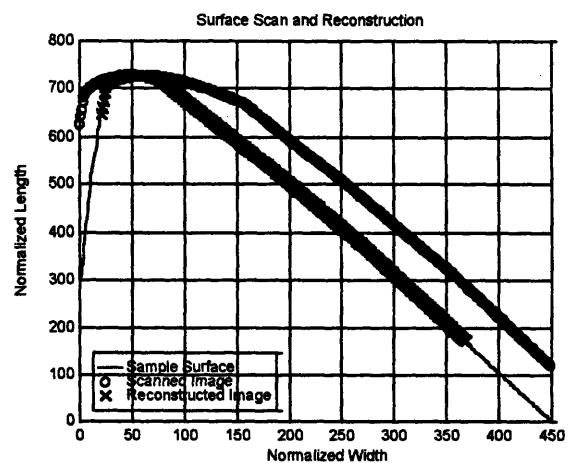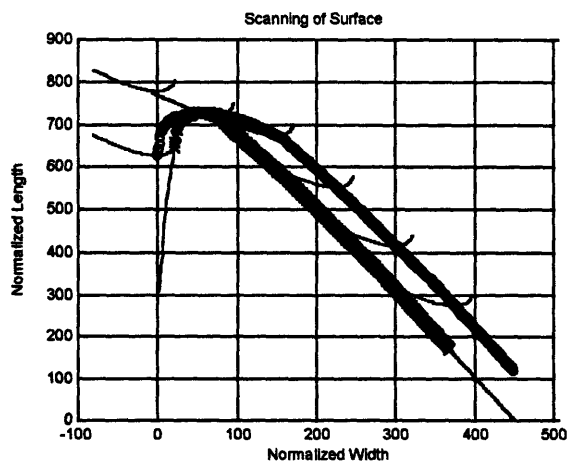
(b) Sample Skewed Left
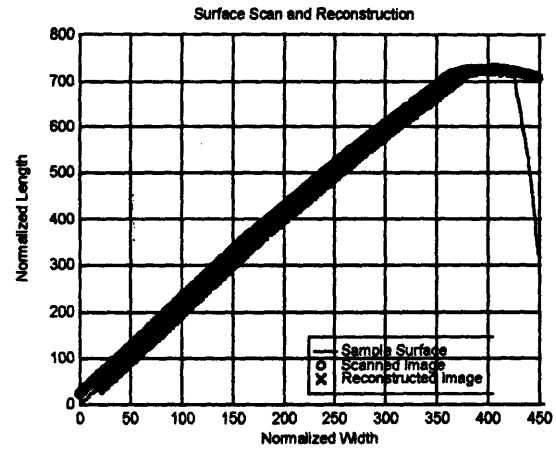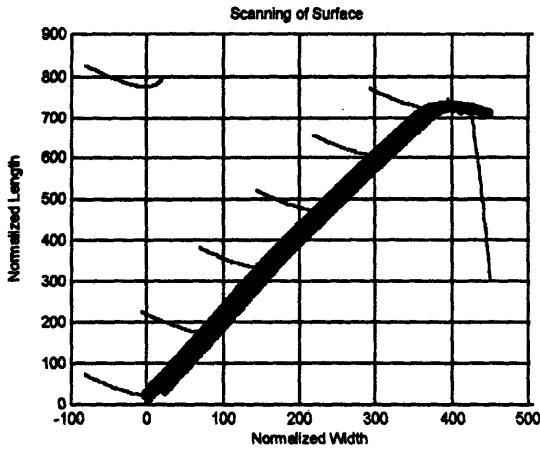
(c) Sample Skewed Right

Figure 5.33 Angled Parabolic Tip Sample Surface Reconstruction.

For comparison purposes and possible areas of further study, Figure 5.34 examines a probe tip that is parallel to the sample centerline. This type of scan is similar to the "Single Pass" design considered in the Chapter 3: Design Alternatives. The results are promising and should be examined for possible further study.
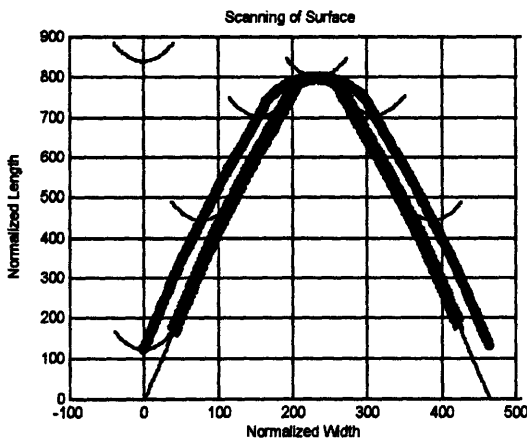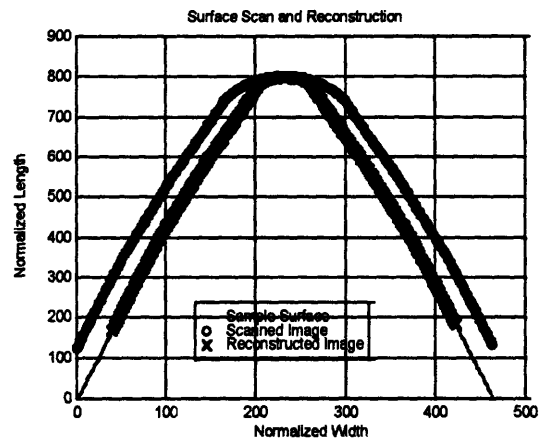
Sample Surface Scan   **Surface vs. Reconstructed Image**

Figure 5.34 Parabolic Tip Sample Surface Reconstruction

5.5 Probe mechanics simulation

Using the HTMs to predict the performance of the Scissors Design also provided excellent results. Different scans were simulated by applying various piezostack specifications, in particular, the resolution requirement. From the HTMs, the predicted probe tip contact point was

determined. To ensure the HTMs, were functioning accurately, a test was performed between the displacement of the sliding mechanism contact point on the long arm. Figure 5.35 shows the motion of the origin of the coordinate system indicated by X11 and Y11. X11 was varied ±7.5 μm, which corresponds to the piezostack range of 15 μm, while Y11 remained constant, because of the sliding mechanism effect. Figure 5.36 shows the resulting motion of the end of the short arm. The motion pertains to the movement of the X12 and Y12 coordinate system origin with respect to the hinge. X12 moves ±1.25 μm which corresponds to mechanical reduction of six to one, while Y12 motions, which are scaled by the length of the short arm, are extremely small.
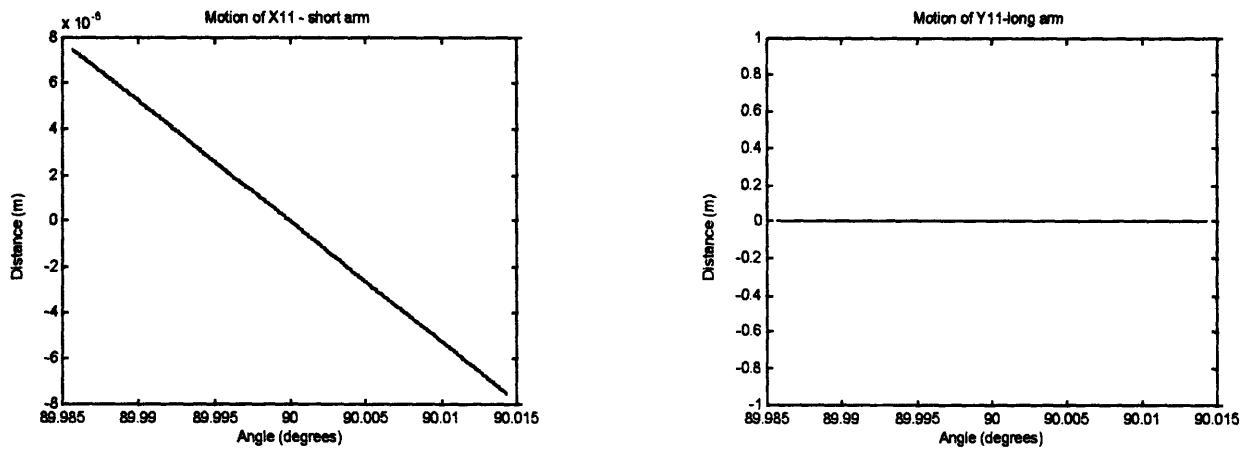
Figure 5.35 Motion of the sliding mechanism contact point (X11,Y11).
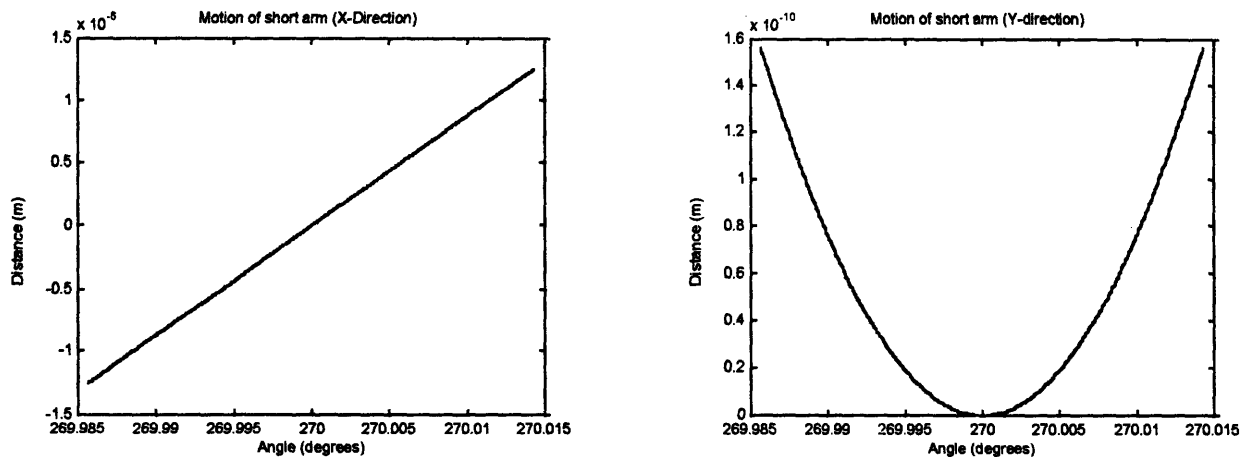
Figure 5.36 Motion of the end of the short arm (X12, Y12).

The simulations of the HTM performance on the nominal sample explore piezostacks with a range of 15 μm and a resolution of both 30 nm and 10 nm, see Figure 5.37 and Figure 5.38. For the skewed samples, the piezostack resolution was 30 nm, Figure 5.39. These three figures compare

the simulated scan results with the actual sample surface. The sample surface is indicated by the solid line and the "+" character is used to represent the contact points of the probe tip with the sample surface as predicted by the HTMs. From the figures, the Scissor Design with the probe in continuous contact will position the probe tip within 30 nm and from the reconstruction results it is predicted that the vertical resolution will be less than 1 nm and the lateral resolution will be less than 10 nm.
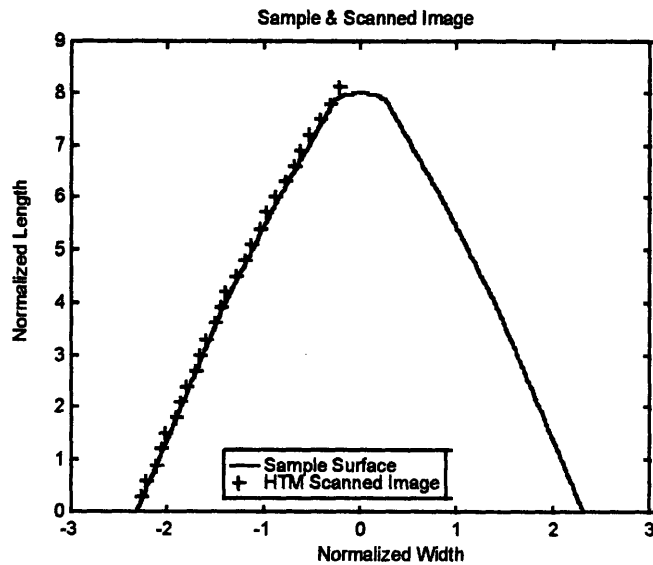
Figure 5.37 HTM scan with piezostack resolution of 30 nm.
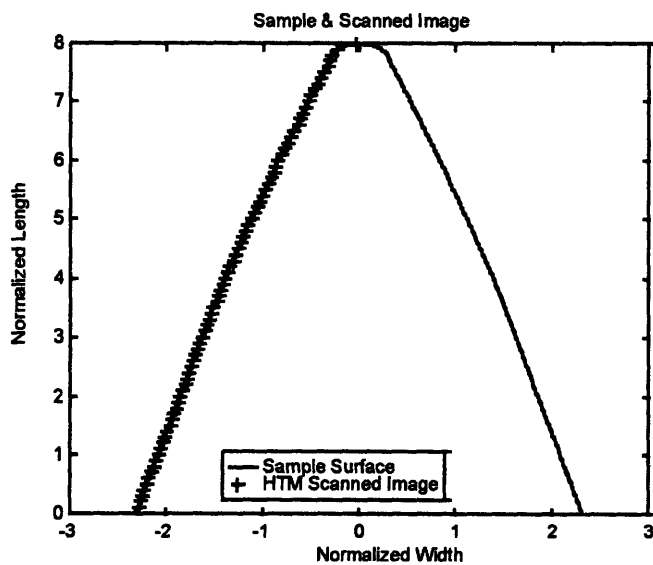
Figure 5.38 HTM scan with piezostack resolution of 10 nm.

115
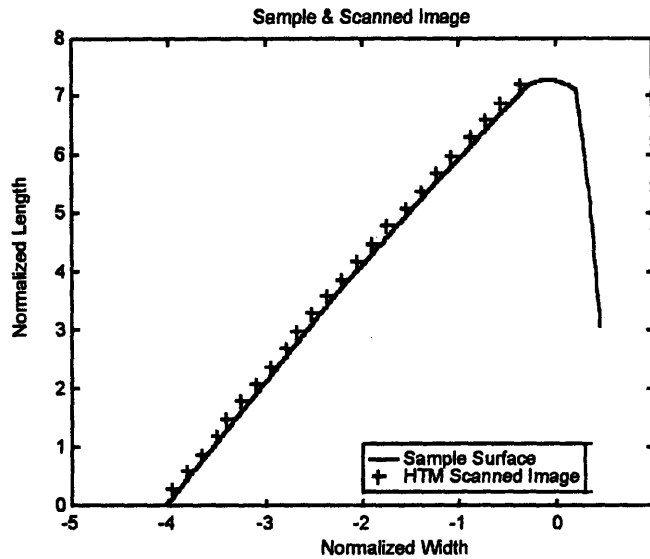
Sample skewed right

Figure 5.39 HTM scan with peizostack resolution of 30 nm.

5.6   *Summary*

This chapter explored the simulations of the design developed to predict the performance of our system. Different probe tip styles, sizes, and orientations were scanned across different sample sizes and contours to determine the most realistic and successful reconstruction. Next, the dynamics of the system were examined. Finally, a simulation for a system scan using different piezostack specifications and sample configurations. The conclusions and recommendations of our findings are highlighted in the next chapter.

6. Conclusions and Recommendations

6.1   Discussion

This chapter highlights the predicted performance of the profilometer and provides recommendations for future work.

Using a contact AFM probe in the Scissor Design configuration proves to be an effective method for measuring the profile of a dual sided sample. Simulations of this design show that it is capable of meeting the required specifications. In particular, the vertical resolution is predicted to be <1.0 nm and the lateral resolution is estimated to be <10 nm. The reconstruction algorithm provides a powerful tool in meeting these resolution requirements. Also, the scans are expected to be performed at 30 Hz which is ten times faster than most commercial AFMs and three times faster than the specification. The simulations provide strong evidence that this design is adequate to perform the profile scan, however the implementation of this design is an area of study that must be executed.

6.2   Areas of Further Study

Even though the simulations predict this design to perform with excellent results, there remains a significant amount of study in the transition from design to prototype. The following substantial activities need to be examined:

1) *Implement the Scissors Design*: testing the performance of the hinge and the proving the accuracy of the mechanical reduction, machining and calibrating the sliding mechanism;

2) *Implement the sample positioning system*: building the structure to be compatible with the actuators and sensors to ensure optimal performance;

3) *Test the reconstruction algorithm*: verify the effectiveness of reconstruction algorithm on a real system;

4) *Controller design*: once the system is in place a controller needs to be implemented to ensure zero steady state error with reasonable robustness and speed.

5) *Putting the system together*: putting the entire system together will undoubtedly reveal unexpected anomalies that will require a significant amount of investigating.

7. Appendices

7.1   Appendix A.   Code and equations of Parallelogram

Parallelogram

```
%
%          Proto-type simulation #1
%
%


clear
clg
clf

% Input Parameters (nm is the standard unit)


i=0;
j=0;
k=0;

count=0;

% Checking Max Values

for A=10000:5000:500000
   i=i+1;
   count=count+1;
for L2=1000:5000:500000
   j=j+1;

% Max Theta positive

postheta(i,j)=acos(A/(A+L2));
posdeltay(i,j)=sqrt(A^2 + (A+L2)^2);

if postheta(i,j)>=80*pi/180
   posflag=1;
else
   posflag=0;
end

% Max Theta negative

negtheta(i,j)=acos((A-L2)/A);
negdeltay(i,j)=sqrt(A^2 +(A-L2)^2);

if negtheta(i,j)>=80*pi/180
   negflag=1;
else
   negflag=0;
end

   temppos=posdeltay(i,j);
   tempneg=negdeltay(i,j);
```

```
if temppos>=tempneg
    maxdeltay=temppos;
else
    maxdeltay=tempneg;
end




if negflag==posflag & negflag==1 & maxdeltay<200000


    k=k+1;
    goodi(count,k)=i;
    goodj(count,k)=j;
    goodA(count,k)=A;
    goodL2(count,k)=L2;
    gooddy(count,k)=maxdeltay;

%    gooddy(count,k)=posdeltay(i,j);
%    neggooddy(count,k)=negdeltay(i,j);

end

end
j=0;
k=0;

end

zz=size(goodA,1);
for z=1:zz
 figure(z)
 plot(goodA(z,:),goodL2(z,:),'r+')
 title('Designs can throw 80 degrees and 200nm')
 xlabel('Distance between Piezostacks(nm)')
 ylabel('Length of bar between hinges(nm)')
end
```

Driver
X_1 TOP

$y_1 f$ x

Angular w/F_2
X_2 Top

(x_{2f}, y_{2f})

(x_{2f}, y_{2f})

$y_2 f$ (x_{2f}, y_{2f})

(x_2, y_2)
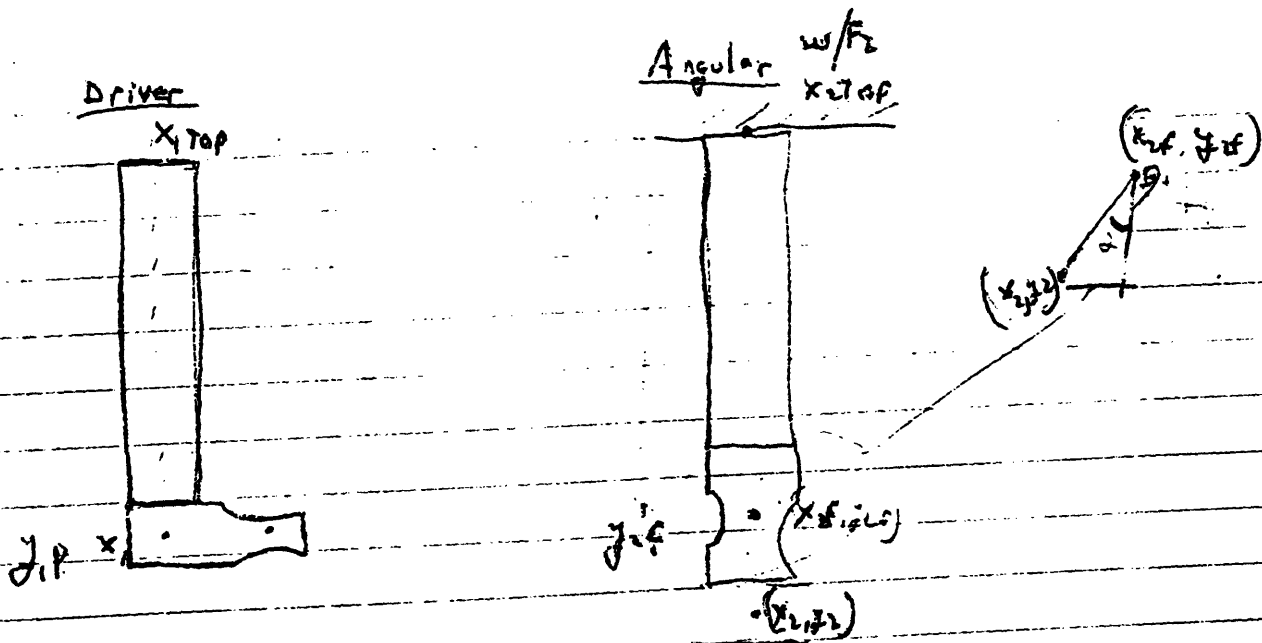
$x_1 = X_1$ Top $\Rightarrow$ fixed

$y_1 \Rightarrow$ Fixed

$x_{2f} = X_2$ Top $\Rightarrow$ fixed $F_2 = \sqrt{(x_2 \cdot x_1) + (x_2 - x_1)}$
$\Rightarrow$ fixed

$y_{2f} \Rightarrow$ fixed

$x_2 = x_{2f} + F_2 \sin\alpha$
$y_2 = y_{2f} - F_2 \cos\alpha$

Base w/ F_1

$-F_1-$ B (x_2, y_2)

(x_{1f}, y_{1f})
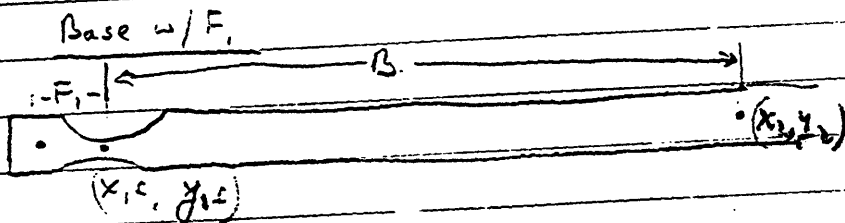
$X_{1f} = X_1 + F_1$

$y_1 f = y_1$

$X_2 = X_1 f + B \cos\theta$
$y_2 = y_1 f + B \sin\theta$
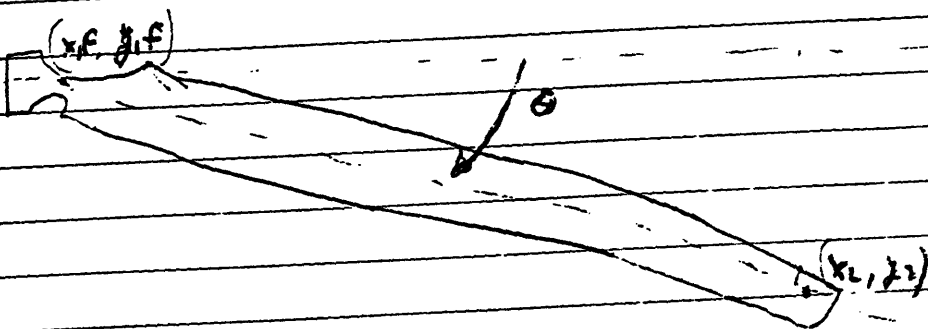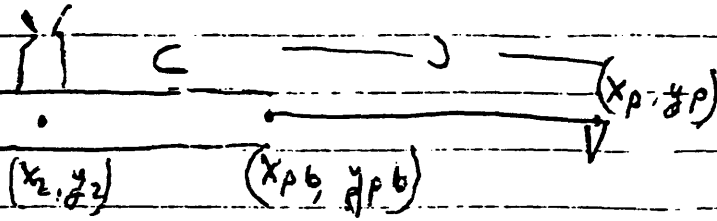
(x_f, y_f) θ

(x_2, y_2)

Probe t Case

(x_p, y_p)

(x_2, y_2) (x_{pb}, y_{pb})

$x_{pb} = x_2 + c$

$y_{pb} = y_2$

Probe

(x_p, y_p)

$\phi = \tan^{-1} \frac{y_2}{D}$ $\phi \propto i$

$$y = \frac{F}{6EI}(2L^3 - 3L^2 x - x^3)$$

122
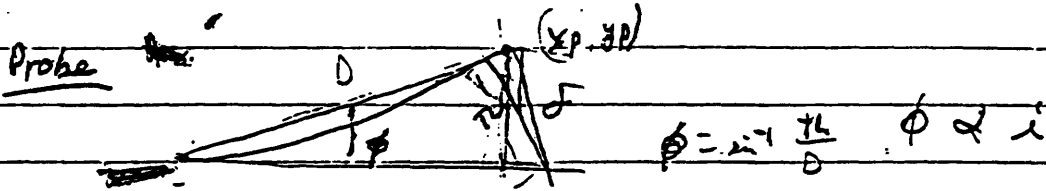
02/10/97 MON 11:21 FAX 408 747 1601   PARK SCIENTIFIC   ☑001

⚏ Park Scientific Instruments

FACSIMILE TRANSMITTAL

Please Deliver To: *Larry Barrett*
(Name)

Gillette
(Company)

Carbon Copy: _____

Fax Number: 617-258-9274

Phone Number: _____

Date Sent: 2-10-97

Sent By: *Tanya Johnson, sales*
(Name, Department)

Number of pages: *2 pages*
(Including Cover Page)

Message: *re: Our piezolevers*

Signed:_____

1171 Borregas Avenue   Phone: 408-747-1600
Sunnyvale CA 94089-1306   Fax: 408-747-1601

Piezolevers™ - Self-Sensing Cantilevers

Piezolevers operate by measuring stress-induced electrical resistance changes in an implanted conductive channel in the flexure springs of the cantilever. Piezolevers are for use in AutoProbe VP, SA, and XL Scanning Probe Microscope systems.

Chip	Cantilever	Tip
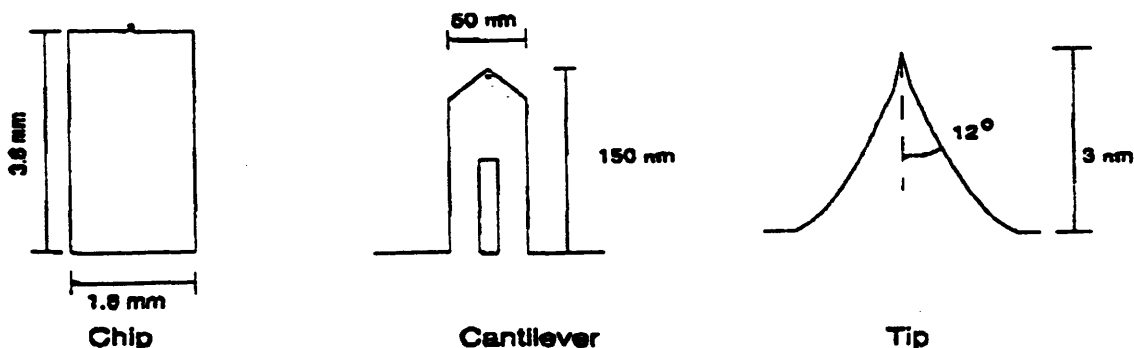
Typical Electro-Mechanical Characteristics

Cantilever type	Contact	Non-contact
Force Constant	2.5 N/m	20 N/m
Resonant Frequency	120 kHz	240 kHz
Sensitivity $\Delta R/R$ per Å deflection	0.3×10^{-6}	0.6×10^{-6}
Resistance	2 kΩ	2 kΩ

Specifications subject to change.

Ordering Information

Piezolevers		AutoProbe VP		AutoProbe SA and XL	
Quantity		Contact	Non-contact	Contact	Noncontact
Mounted - (25 chips)		PLCT-VPMT	PLNC-VPMT	PLCT-SAMT	PLNC-SAMT

To place an order, contact:
Park Scientific Instruments
1171 Borregas Avenue Sunnyvale, CA 94089
Tel: (408) 747-1600 Fax: (408) 747-1601
E-mail: sales@park.com

Please see us on the Internet at http://www.park.com

1 800 -
776 - 1607

ᴢ[ᴤ Park Scientific Instruments

Cantilever Price List
Domestic
October 1, 1996

Microlevers		Sharpened		Unsharpened	
Quantity	Price	Gold coated*	Uncoated	Gold coated*	Uncoated
Wafer - 600	$2,450	MSCT-AUFW	MSCT-NOFW	MLCT-AUFW	MLCT-NOFW
Half wafer - 300	$1,500	MSCT-AUHW	MSCT-NOHW	MLCT-AUHW	MLCT-NOHW
Unmounted -25	$300	MSCT-AUNM	MSCT-NONM	MLCT-AUNM	MLCT-NONM
Mounted -25	$400	MSCT-AUMT	MSCT-NOMT	MLCT-AUMT	MLCT-NOMT

* Not for use with AutoProbe M5 systems

MFM Microlevers		
Quantity	Price	
Unmounted - 25	$450	MSNC-MFNM
Mounted - 25	$550	MSNC-MFMT

Ultralevers		Silicon tips		Tipless	
Quantity	Price	Contact	Non-contact	Contact	Non-contact
2 half wafers -600	$5,875	ULCT-AUFW	ULNC-AUFW		
Half wafer - 300	$3,650	ULCT-AUHW	ULNC-AUHW	ULCT-NTHW	ULNC-NTHW
Unmounted - 25	$725	ULCT-AUNM	ULNC-AUNM	ULCT-NTNM	ULNC-NTNM
Mounted - 25	$850	ULCT-AUMT	ULNC-AUMT		

MFM Ultralevers		
Quantity	Price	
Unmounted - 25	$875	ULNC-MFNM
Mounted - 25	$1,000	ULNC-MFMT

FIB Tips		
Quantity	Price	
Unmounted - 5	$500	ULNC-FBBO

Piezolevers		AutoProbe VP		AutoProbe SA/XL	
Quantity	Price	Contact	Non-contact	Contact	Non-contact
Mounted - 25	$1,000	PLCT-VPMT	PLNC-VPMT	PLCT-SAMT	PLNC-SAMT

Price are subject to change without notice.

1171 Borregas Avenue   Tel: (408) 747-1600
Sunnyvale, CA 94089   Fax: (408) 747-1601

LVPZ Translators

P-840.xx, P-841.xx LVPZ Translators

- Expansion up to 90 μm
- Standard and Sensor Models
- Mechanical Preload
- For Pushing and Pulling Forces

The P-840.xx and P-841.xx series of piezotranslators are manufactured with the stacks inside a metal casing which has an M5 tapped hole in the base for mounting. The top piece has an M3 tapped hole.

A position sensor can be integrated onto the piezo stack inside the casing. With the sensor fitted it is possible to achieve position control with a linearity of 0.1 to 0.2%.

Translators with position sensors have the model number P-841.xx, those without have the number P-840.xx. Both series of piezos are mechanically preloaded.

Accessories:

P-176.20 Magnetic Adapter

To attach these piezotranslators to various positioning and adjusting mechanisms a magnetic top piece is sometimes required. The P-176.20 Magnetic Adapter has an M3 thread and can therefore be screwed directly onto the top of the P-840.xx and P-841.xx series.

Technical Data:

Operating voltage:	− 20 V to + 120 V
Mechanical preload:	100 N
Permissible temperature range:	− 20° to + 80°C
Electrical connections:	
− Operating Voltage:	Teflon coax. cable, 1 m, with LEMO-plug, Type 00S 250
− Sensor:	PVC-cable, 1 m long, with 4-pin LEMO-plug, size 0
Casing:	non-magnetic stainless steel
End piece:	non-magnetic stainless steel
Max. torque at the end piece:	35 Ncm

Option:

P-840.95 Spherical Top Piece
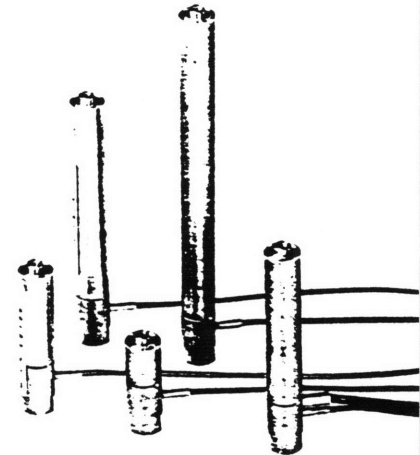
5.66
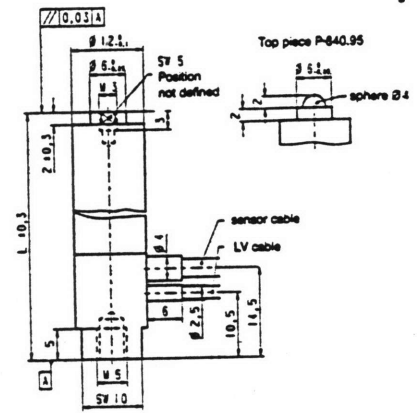
P-840/841 LVPZ Translator   5.66

Model		P-840.10 P-841.10	P-840.20 P-841.20	P-840.30 P-841.30	P-840.40 P-841.40	P-840.60 P-841.60
Nominal expansion at + 100 V, ± 10%	[μm]	15	30	45	60	90
Max. pushing force	[N]	1000	1000	1000	800	800
Max. pulling force	[N]	100	100	100	80	80
Electrical capacitance (small-signal), ± 20%	[nF]	1.8	3.6	5.4	7.2	10.8
Stiffness, ± 10%	[N/μm]	55	27	17	13	8
Resonant frequency	[kHz]	18	14	10	8.5	6
Weight[1]	[g]	31/50	39/58	47/66	60/78	73/95
Total length L	[mm]	32	50	68	86	122

[1] Weight without/with sensor

Physik Instrumente (PI) GmbH &

5.66

126

FEB-24-1997 10:21 FROM POLYTEC PI INC EAST   TO   16172589274   P.01

T (617) 623-6053
F (617) 258 - 9274

PI

Physik
Instrumente

To: Larry Barrett
Fr: Jeff North

E-505.00   LVPZT Amplifier Module

E-505.00
LVPZT
Amplifier Module,
-20 to +120 V

- **200 W Peak Power**
- **Output Voltage Range -20 to +120 V**

E-505.00 is an amplifier module for Low Voltage PZTs. It can output and sink a peak current of 2000 mA and an average current of 300 mA. E-505.00 can be operated in 2 ways:

- **Manual operation**
The output voltage can be set by a 10-turn, DC offset potentiometer in the range of 0 to 100 Volts.

- **External operation**
Output voltage is controlled by an analog signal applied to the BNC input ranging from -2 to +12 Volts. Multiplying by the gain factor of 10, an output voltage range of -20 to +120 Volts results. The DC offset potentiometer allows for a continuous variation of the input voltage range between -2 V to +12 V and -12 V to +2 V (see page 29).

For computer controlled operation, an E-515 16 bit DAC Interface/Display Module can be used (requires E-500/E-501 chassis). For frequency response with selected LVPZTs see graph below.
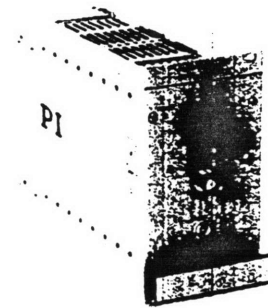
E-505.00

Please note:
E-505 00 is not a stand alone system. It requires the E-500/E-501 chassis (page 18) with integrated power supply to function as an amplifier. A 32 pin connector is used to interface with the E-500/E-501 chassis.

1.8 μF

Technical Data: E-505.00

Function:	power amplifier
Channels:	1
Maximum output power:	200 W (s. page 30)
Average output power:	30 W
Peak output current < 5 ms:	2000 mA
Average output current > 5 ms:	300 mA
Current limitation:	short-circuit proof
Voltage gain:	10 ±0.1
Polarity:	positive
Control input voltage:	-2 to +12 V
Output voltage:	-20 to 120 V
DC offset setting:	0 to 100 V with 10-turn pot.
Input impedance:	100 kΩ
Control input sockets:	BNC
PZT voltage output socket:	LEMO ERA.00.250.CTL
Dimensions:	one 14T slot wide, 3H high
Weight:	0.9 kg
Operating voltage:	requires E-530/E-531 power supply (E-500/E-501 system)

10^3
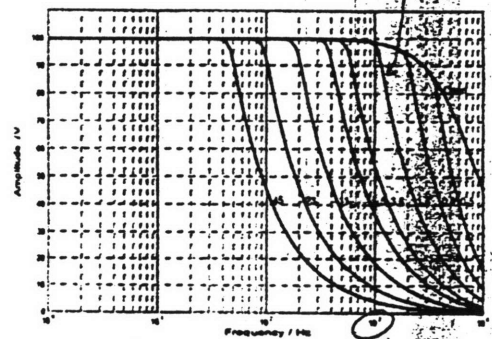
E-505, frequency response with various PZT loads. Capacitance values are in μF.

PZT Actuators

PZT Flexure MicroPositioners

PZT Actuator Drivers

Cap Displacement Sensors

PZT Control Electronics

Micro-positioners

Motor Controllers

Fiber Alignment

Honeycomb Tables

Opto-Mech Components

Index

E-662.xx LVPZT Amplifier/Position Servo Controller

- 36 W Peak Power
- Position Servo Control
- For Strain Gages & LVDT Sensors
- RS-232 Computer Interface with 12 bit D/A Converter

E-662 is a bench-top, amplifier/position servo controller with integrated RS-232 computer interface and 12 bit D/A converter for Low Voltage PZTs. The amplifier can output and sink a peak current of 360 mA and an average current of 120 mA. The position servo controller works with either strain gage sensors (E-662.SR) or LVDT sensors (E-662.LR). E-662 can be operated in 6 ways:
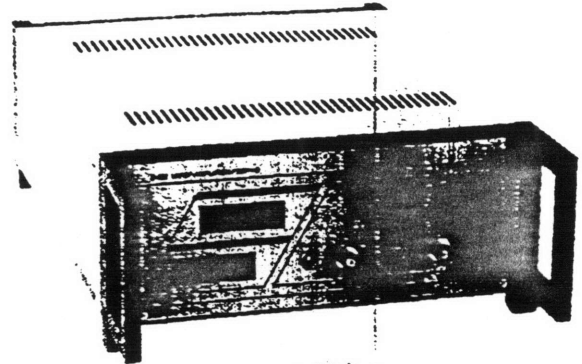
E-662

I. Open loop (amplifier mode)

Manual operation
Output voltage can be set by a 10-turn, DC offset potentiometer in the range of 0 to 100 V.

External operation
Output voltage is controlled by an analog signal applied to the BNC input ranging from -2 to +12 V. Multiplying by the gain factor of 10, an output voltage range of -20 to +120 V results. The DC offset potentiometer allows for a continuous variation of the input voltage range between -2 V to +12 V and -12 V to +2 V (see page 29).

Computer Control (toggle switch selected)
Output voltage is controlled via the RS-232 computer interface in the range of 0 to 100 V with a resolution of 12 bits. The DC offset potentiometer and BNC analog input are inactive when in computer control mode.

II. Closed loop (position control mode)

Manual operation
Displacement of the PZTs can be set by a 10-turn, DC offset potentiometer in the range of zero to nominal displacement.

External operation
Displacement of the PZT is controlled by an analog signal in the range of 0 to +10 V, applied to the BNC input. The controller is calibrated in such a way that 10 V corresponds with maximum nominal displacement and 0 V corresponds with 0 displacement. The DC offset potentiometer can be used to add an offset voltage of 0 to 10 V to the input signal.

Computer Control (toggle switch selected)
Displacement of the PZT is controlled via the RS-232 computer interface in the range of 0 to maximum nominal displacement, with a resolution of 12 bits. The DC offset potentiometer and BNC analog input are inactive when in computer control mode.

More than 40 SCPI (Standard Commands for Programmable Instruments) ASCII commands are available to program the E-662. An internal function generator provides sine, square, ramp and triangular functions up to 150 Hz. User defined functions can be stored in a table with up to 200 entries. Minimum time between two samples is 1 msec.

▶ **Important Calibration Information:**
Please read details on page 31.

Technical Data: E-662.xx

Function:	power amplifier & sensor/position servo control of PZTs
Channels:	1
Amplifier:	
Maximum output power:	36 W (see page 30)
Average output power:	12 W
Peak output current <5 ms:	360 mA
Average output current >5 ms:	120 mA
Current limitation:	short-circuit proof
Voltage gain:	10 ±0.1
Polarity:	positive
Control input voltage:	-2 to +12 V
Output voltage:	-20 to 120 V
DC offset setting:	0 to 100 V with 10-turn pot.
Input impedance:	100 kΩ
Display:	2 x 3 1/2 digit LED
Control input socket:	BNC
PZT voltage output socket:	LEMO ERA.00.250.CTL
Dimensions:	288x235x103 mm (& page 9)
Weight:	2.5 kg
Operating voltage:	90-120 / 220-240 VAC, 50-60 Hz (linear P/S)

Position Servo Control:	
Sensor Types:	strain gages (E-662.SR); LVDTs (E-662.LR)
Servo Characteristics:	P-I (analog)
Sensor socket:	LEMO ERA.0S.304.CLL
Sensor monitor output socket:	BNC
D/A Converter & Computer Interface:	
Resolution:	12 bit (à 2.5 mV input)
Computer interface:	RS-232

Amplitude / V
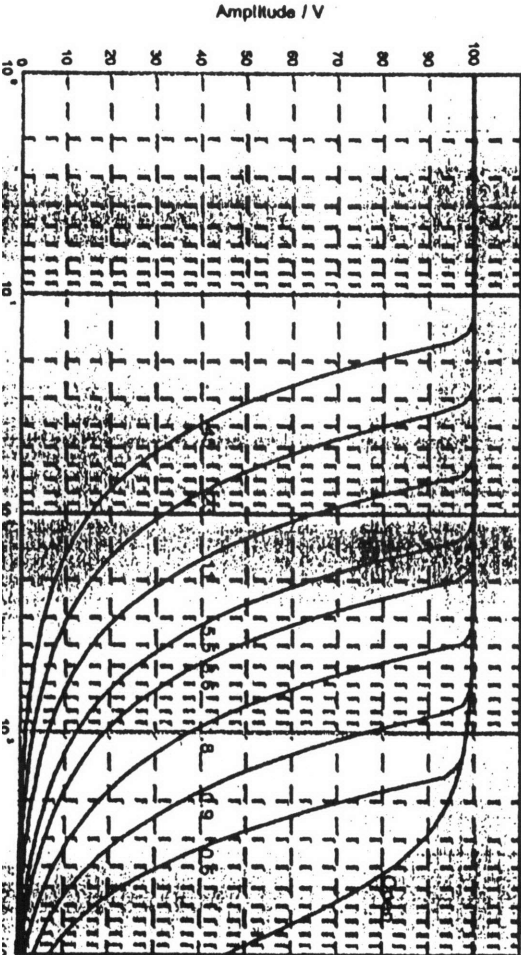
E-662, open loop frequency response with various PZT

E-500/E-501 Modular PZT Control System (HVPZT & LVPZT)

- For High Voltage and Low Voltage PZTs
- 19 and 9.5 Inch Versions
- Optional Position Servo Control Modules
- Optional Display and RS-232 & IEEE 488 Interface Module

E-500 is a modular 19" rack mount chassis for PZT amplifiers and position servo controllers. An integrated, multi-function power supply (E-530.00) provides operating voltages for all available modules. E-500 chassis are assembled to your order and tested with all ordered modules installed. A maximum of 3 amplifier/controller channels can be installed in one E-500 chassis.

E-501.00 is the 9.5" version of the E-500 chassis. Note: only one amplifier module (1 or 3 channels) and only one sensor/servo controller module (1 or 3 channels) can be installed.

Configuration example:
E-500 chassis with three optional E-507 HVPZT Amplifiers, E-509.L3 PZT Servo Controller for LVDT sensors and E-515.i3 16 bit DAC Interface/Display.

The E-500 chassis can be equipped with up to 3 amplifier/controller channels. **HVPZT and LVPZT amplifier modules can be combined.**

Technical Data: E-500/E-501

Function:	19" (E-501: 9.5") chassis for PZT electronics: amplifier modules, sensor modules, position servo control modules, display/interface modules
Channels:	1, 2, 3 (E-500); 1,3 (E-501)
Dimensions:	288x450x158 mm (E-500), 288x235x158 mm (E-501), (s. page 9)
Integrated power supply:	E-530.00 (E-500); E-531.00 (E-501)
Operating voltage:	E-500: 90-264 VAC, 50-60 Hz, primary switched P/S; E-501: 90-120 / 220-264 VAC, 50-60 Hz, linear P/S

Configuration example:
E-501 chassis with optional E-503 LVPZT Amplifier, E-509.C3 PZT Servo Controller for capacitive sensors and E-515.i3 16 bit DAC Interface/Display.

E-509.xx   Sensor/Position Servo Control Module for PZTs

- Position Servo Control
- Increases PZT Stiffness
- Eliminates Drift & Hysteresis
- For Capacitive Sensors,
  Strain Gage Sensors & LVDT Sensors

E-509 is a displacement sensor module with an integrated position servo controller for PZT positioning systems. Versions for three different sensor types are available: Strain Gage Sensors, LVDT (Linear Variable Differential Transformers) and Capacitive Sensors. One and three channel modules are available for Strain Gage Sensors and LVDT Sensors. The capacitive sensor module is available as a one, two and three channel version.

The position servo control part of the E-509 is identical for all versions: an analog P-I (Proportional Integral) controller. Proportional and integral gain can be set internally by trimmers. Sensor bandwidth and control bandwidth can also be set. If necessary a notch filter can be installed to allow operation of the piezo positioning system closer to its mechanical resonant frequency.

E-509 compensates for drift and hysteresis of PZT actuators. It also increases the stiffness of a PZT by quickly adjusting the operating voltage on the PZT as soon as a change in force or load occurs.
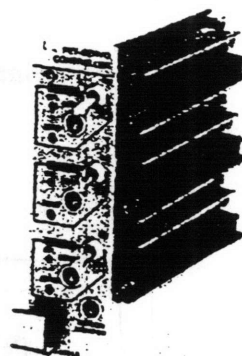
E-509.L3

Please note:
E-509 is not a stand alone system. It requires the E-500/E-501 chassis (page 18) with integrated power supply to function as a PZT servo controller. A 32 pin connector is used to interface with the E-500/E-501 chassis.

Technical Data: E-509.xx

Function:	displacement sensor electronics and position servo controller for PZTs
Channels:	1 (E-509.x1); 2 (E-509.C2), 3 (E-509.x3)
Sensor types:	strain gages: E-509.Sx; LVDTs (E-509.Lx), capacitive sensors (E-509.Cx)
Servo characteristics:	P-I (analog)
Rear connector:	32-pin connector
Sensor socket:	LEMO ERA.0S.304.CLL (E-509.Cx: LEMO EPL.00.250.NTD)
Sensor monitor output socket:	LEMO ERA.0S.303.CLL (3 channel versions) BNC (1 & 2 channel versions)
Dimensions:	one 7T slot wide, 3H high
Weight:	0.35 kg (E-509.x3); 0.25 kg (E-509.x2); 0.2 kg (E-509.x1)
Operating voltage:	requires E-530/E-531 power supply (E-500/E-501 system)

▶ **Important Calibration Information:**
Please read details on page 31.

TOTAL P.06

7.5   Appendix E. Alternative Designs (Non-AFM specific)

①

②

capacitive

③

④

5)

.X.
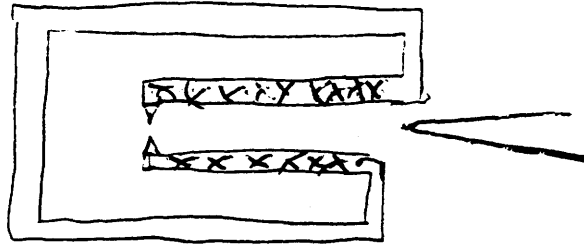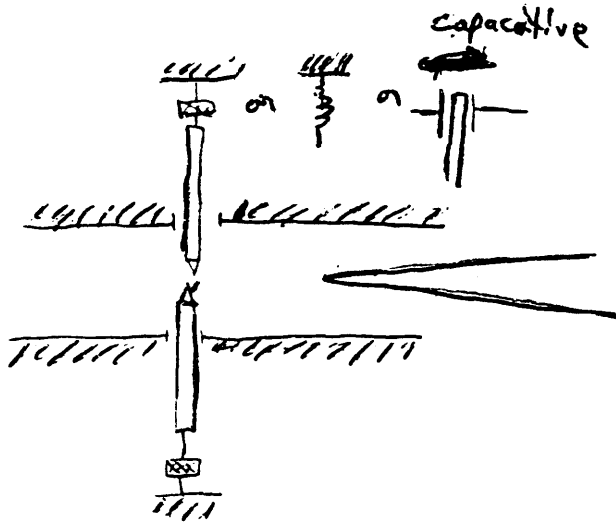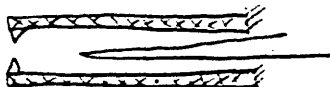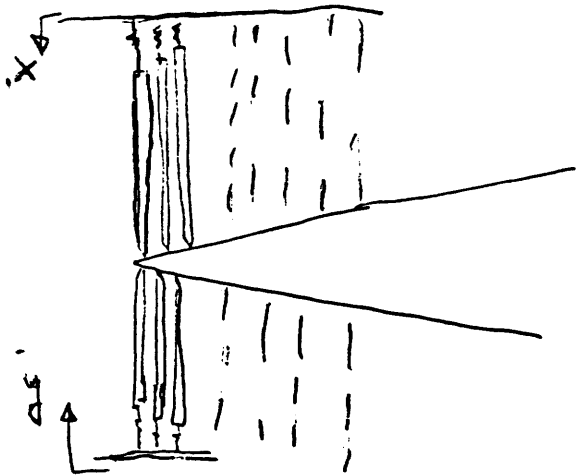
6)

EMS
reel
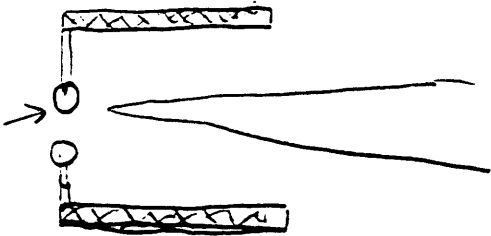
7)
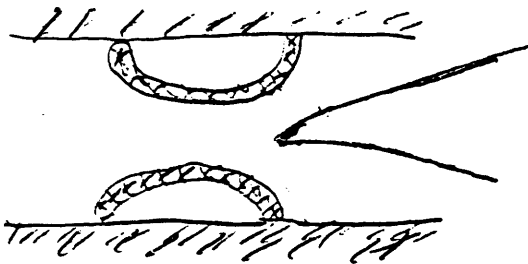
Different Designs for Double Probe
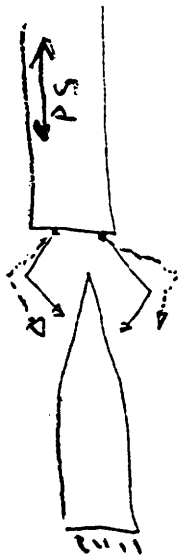
Design A
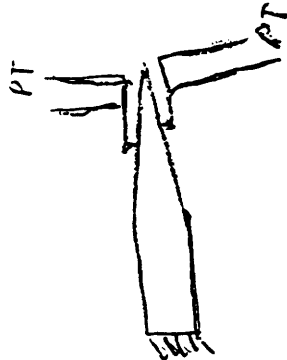
Design B
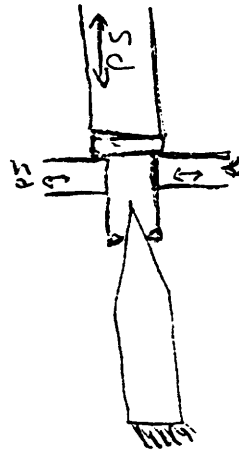
Design C

Design D
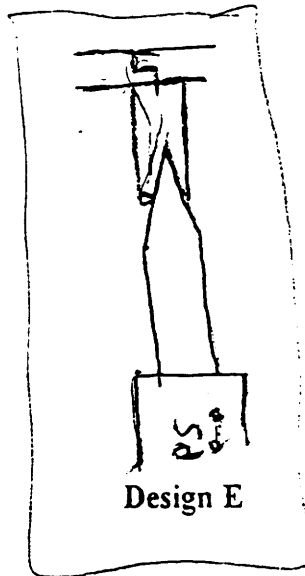
Design E
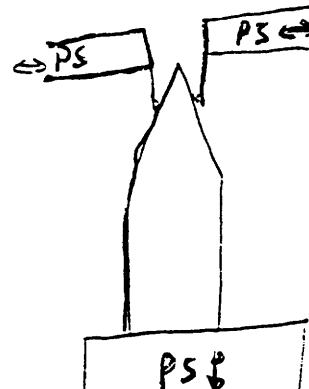
Design F
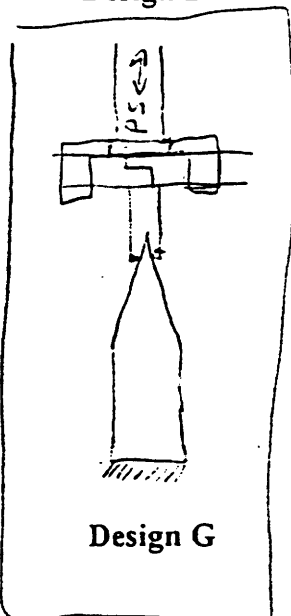
Design G
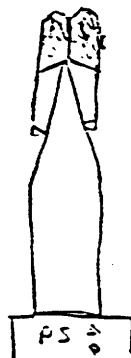
Design H
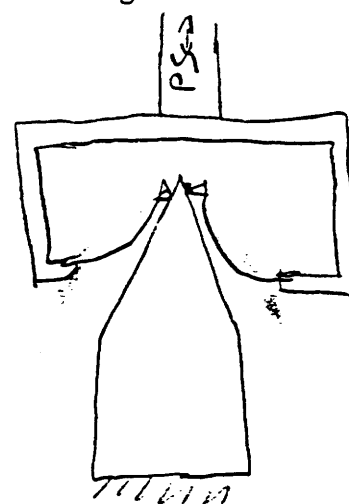
Design I

Different Designs for Double Probe

LVOT   LVDT
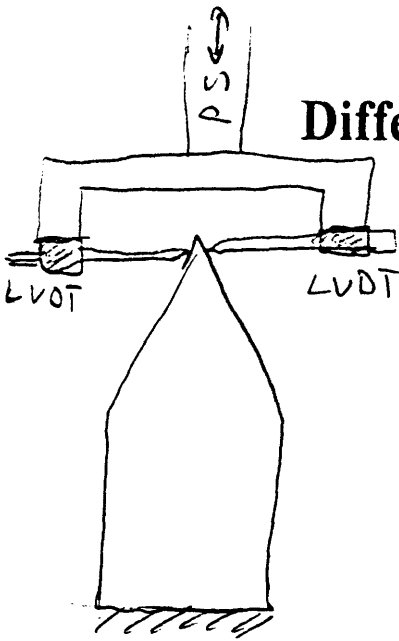
Design A J   Design B K   Design C L

Design D M   Design E N   Design F O

Design G P   Design H Q   Design I R

7.6   Appendix F. Code for Simulation Section

```
% Simulation using Homogeneous Transformation Matrix
% HTM

clg;
cla;
clear;
%close all;


%[pres,prange,a,b]=simin(1)

%scale=6;

% getting the sample

n=7;
isize=0;
iangle=0;

[sampx,sampy]=samples(n,isize,iangle);

sampx=sampx*1e-9;
sampy=sampy*1e-9;

[sv si]=max(sampy);
sampx=sampx-sampx(si);
sampyofst=-5.15e-3 - 3.9005e-8;
sampy=sampy+sampyofst;

sampx0=sampx;
sampy0=sampy;
% Sliding Mechanism & Pos11 relative to Hinge: Arm A


% Solving the Slider!

pres=30e-9;
prange=7.5e-6;
a=30e-3;
b=5e-3;

%pres=10e-5;
%prange=10e-3;

tstep=pres % x motion resolution

%redfact=.9;    % 90% of nominal expansion
redfact=1;
stop=redfact*prange % displacement range
```

```
x11=-stop:tstep:stop; % Varies the X Motion driven by Piezostack

x11offset=0;% Optimal location for transmission of piezostack displacem
ent

x11=x11+x11offset;

y11=a;


t11offset=pi/2;

x1ref=0  ;
y1ref=0  ;

hit=1;
chk1=1;
chk2=1;
for i=1:size(x11,2)
%   t11(i)=atan(y11/x11(i));
  t11(i)=atan(x11(i)/y11)+pi/2;
%   if t11(i)<0
%       t11(i)=pi/2 + (t11(i)+pi/2);
%   elseif t11(i)>0
%       t11(i)=pi/2 - (pi/2 - t11(i));
%   end

  Mh11= [cos(t11(i)) -sin(t11(i))  x11(i);
         sin(t11(i))  cos(t11(i))   y11  ;
            0            0           1  ];



 Ph1=Mh11*[x1ref;y1ref;1];
  X11(i)=Ph1(1);
  Y11(i)=Ph1(2);



% Cantilever Tip

x14=0;
y14=0;
t14=0;

Tlen=3e-6; % Piezolever Tip Length
%Tlen=1e-3;
%Tlen=0;

M1413= [cos(t14) -sin(t14)    0  ;
         sin(t14)  cos(t14)  Tlen ;
```

```
            0              0       .   1  ];

P1413=M1413*[x14;y14;1];


% Cantilever or Piezolever

theta=0; % Deflection of Piezolever in degrees

t13=1.15+theta; %36 degrees of piezolever + bending
t13=t13*pi/180;
%t13=0;
Len=150e-6;
Wid=50e-6;
thi=10e-6;

E=10e6;

pl=150e-6; % length of Piezolever

%delx=1e-3;
%delx=Len;
delx=0;

dely=0;

x13=P1413(1);
y13=P1413(2);

M1312= [cos(-t13)  -sin(-t13)   pl*cos(-t13)+delx;
         sin(-t13)   cos(-t13)   pl*sin(-t13)+dely;
            0            0            1 ];

P1312=M1312*[x13;y13;1];


%Pos12 Relative to Hinge bar b

%x12=P1312(1);
%y12=P1312(2);
x12=0;
y12=0;

t12dt11=pi;% Angle from bar a to b (CCW)

 t12=t12dt11+t11(i);
 T12(i)=t12;
 %b=a/scale;

 M12h= [cos(t12)  -sin(t12)   b*cos(t12);
```

```
                sin(t12)    cos(t12)    b*sin(t12);
                  0            0           1      ];

  P12h=M12h*[x12;y12;1];

  X14(i)=P12h(1);
  Y14(i)=P12h(2);


% Check to see if hit sample!

for jj=2:size(sampx,2)
    if X14(i)>=sampx(jj-1) & X14(i)<=sampx(jj)
        chk1=chk1+1;
      if jj<=si
        if  Y14(i)<=sampy(jj)% & Y14(i)>=sampy(jj-1)
           simagex(hit)=X14(i);
           simagey(hit)=hit*tstep+sampyofst;
           sampy=sampy-tstep;
           hit=hit+1;
        end
      elseif jj>si
        if Y14(i)<=sampy(jj-1) & Y14(i)>=sampy(jj)
         simagex(hit)=x11(i);
         simagey(hit)=hit*tstep;
         sampy=sampy-tstep;
         hit=hit+1;
        end
      end
    end
end

% P14=inv(M1413)*inv(M1312)*inv(M12h)*[x1ref;y1ref;1];
% X14(i)=P14(1);
% Y14(i)=P14(2);


end



figure(1)
plot(fliplr(180*t11/pi),X11)
title('Motion of X11 - short arm')
xlabel('Angle (degrees)')
ylabel('Distance (m)')

figure(2)
plot(180*t11/pi,Y11-a)
title('Motion of Y11-long arm')
xlabel('Angle (degrees)')
```

```
ylabel('Distance (m)')

figure(3)
plot(180*T12/pi,X14)
title('Motion of short arm (X-Direction)')
xlabel('Angle (degrees)')
ylabel('Distance (m)')

figure(4)
plot(180*T12/pi,Y14+b)%+b+pl*cos(t13))
title('Motion of short arm (Y-direction)')
xlabel('Angle (degrees)')
ylabel('Distance (m)')

%dx14=diff(X14);
%dy14=diff(Y14);

ofix=min(sampy0);
%ofix1=sampy(1);
figure(5)
plot(sampx0,sampy0-ofix, simagex, simagey-ofix,'r+')
title('Sample & HTM Scanned Image');
xlabel('Width (m)');
ylabel('Length (m)');
legend('Sample Surface', 'HTM Scanned Image');


%figure(5)
%plot(dx11,'ro')
%title('Difference of X11')

%figure(4)
%plot(dy11,'ro')
%title('Difference of Y11')
```

```
%**************************** Samples.m ************
%***     Creates the samples to be scanned
%***
%***
%***     Larry Barrett
%***     April 23, 1997
%***************************************************

%  Sample surface


function [sampx,sampy]  =samples(n,isize,iangle)

%n=6
%isize=50
%iangle=0

if n==1

% Calibration piece
if isize>100
 numpts=isize;   %Pts per surface - Height in nanometers
 idif=0;
else
 idif=101-isize;
 numpts=isize+idif;
end
 nosurf=3;
 startptx=0;
 startpty=0;
 for u=1:1:numpts
   sampx(u) = u + startptx;
   sampy(u)=  startpty;
 end

 %for u=numpts+1:1:2*numpts
 %   calx(u) = numpts+startptx;
 %   caly(u)=  u-numpts+startpty;
 %end

 for u=numpts+1:1:2*numpts
   sampx(u) = u + startptx;
   sampy(u)=  numpts+startpty-idif;

  % calx(u) = u-numpts + startptx;
  % caly(u)=  numpts+startpty;
 end

 %for u=3*numpts+1:1:4*numpts
 %   calx(u) = 2*numpts +startptx;
 %   caly(u)=  -u+4*numpts+startpty;
```

```
%end

for u=2*numpts+1:1:3*numpts
   sampx(u) = u+startptx;
   sampy(u)=  startpty;
%  calx(u) = u-2*numpts +startptx;
%  caly(u)=  startpty;
end


end


if n==2

% Sinusoid

numpts=120;
amp=isize; %50
freq=iangle % *pi/120 2.4
startptx=0;
startpty=0;
for u=1:1:numpts
   sampx(u) = u + startptx;
   sampy(u)=  amp*sin(freq*u)+startpty;
end
%for u=numpts+1:1:numpts+30
%  sampx(u)=u+startptx;
%  sampy(u)=sampy(u-1);
%end
end


if n==3

% Nominal Sample




yn=fliplr(yn);
base=[yn y];
base=base-min(yn);
height=[fliplr(x) 1 x];
```

```
xsamp=[0:stepsize:max(base)];
ysamp=interp1(base,height,xsamp);
%figure(1)
%hold
xsamp=xsamp/stepsize+1;
ysamp=ysamp/stepsize;


%plot(xsamp,ysamp,'r+');

num=size(xsamp,2);

for i=1:1:num
    sampy(i)=ysamp(i);
    sampx(i)=xsamp(i);
end


end


if n==4 | n==5

% Nominal Sample Left or Right




yn=fliplr(yn);
base=[yn y];
base=base-min(yn);
height=[fliplr(x) 1 x];

xsamp=[0:stepsize:max(base)];
ysamp=interp1(base,height,xsamp);
%figure(1)
%hold
xsamp=xsamp/stepsize+1;
ysamp=ysamp/stepsize;

stop=size(xsamp,2)/2;
for k=1:1:stop
    xsamp1(k)=xsamp(k);
    ysamp1(k)=ysamp(k);
    xsamp2(k)=xsamp(stop+k);
```

```
       ysamp2(k)=ysamp(stop+k);

       xi(k)=k;
end
if n==4
  sampx=xsamp1;
  sampy=ysamp1;
end

if n==5
  sampx=xsamp2;
  sampy=ysamp2;
end

%plot(sampx,sampy)

end

if n==6 | n==7


% Sample Skewed Left or right




yn=fliplr(yn);
base=[yn y];
base=base-min(yn);
height=[fliplr(x) 1 x];

xsamp=[0:stepsize:max(base)];
ysamp=interp1(base,height,xsamp);

xsamp=xsamp/stepsize+1;
ysamp=ysamp/stepsize;

stop=size(xsamp,2)/2;
for k=1:1:stop
    xsamp1(k)=xsamp(k);
    ysamp1(k)=ysamp(k);
    xsamp2(k)=xsamp(stop+k);
    ysamp2(k)=ysamp(stop+k);

    xi(k)=k;
```

```
end
ysamp2=ysamp2-min(ysamp2);


 rot=-12.94*pi/180; % For Long skew
%rot=12.94*pi/180;  % for Short Skew

count1=1;
 for v=1:1:stop

  Mh= [cos(rot) -sin(rot)    0 ;
        sin(rot)  cos(rot)    0  ;
           0        0        1  ];

  Ptip = Mh*[xsamp1(count1);ysamp1(count1);1];
  xsampl(count1)=Ptip(1);
  ysampl(count1)=Ptip(2);
  count1=count1+1;

end

%xsamp2=fliplr(xsamp2); % For Long skew
ysampl1=ysampl-min(ysampl);
xsampl1=xsampl-min(xsampl);

xli=min(xsampl1)+1:1:max(xsampl1);
%xi=[xi1 xi2];

yli=interp1(xsampl1,ysampl1,xli);

rot=-12.94*pi/180; % For short skew left side
% rot=12.94*pi/180;  % for Short Skew

count1=1;
 for v=1:1:stop

  Mh= [cos(rot) -sin(rot)    0 ;
        sin(rot)  cos(rot)    0  ;
           0        0        1  ];

  Ptip = Mh*[xsamp2(count1);ysamp2(count1);1];
  xsamps(count1)=Ptip(1);
  ysamps(count1)=Ptip(2);
  count1=count1+1;

end

%ysamps=fliplr(ysamps); % For short skew
ysamps1=ysamps;%-min(ysamps);
xsamps1=xsamps;%-min(xsamps);
```

```
xsi=(round(min(xsamps1)))+1:1:max(xsamps1);
%xi=[xi1 xi2];
ysi=interp1(xsamps1,ysamps1,xsi);
xsi=max(xli)+xsi-min(xsi)+1;


sampx=[xli xsi];
if n==6 % Skew right
 sampy=[yli' ysi'];
end
if n==7
 sampy=fliplr([yli' ysi']); % Skew left
end

%plot(xsampl,ysampl,'y',xsamps,ysamps,'g',sampx,sampy,'r+');
%plot(sampx,sampy,'y')

end
```

```
% Simulation Input routine
% Input


function [res,range,isize,iangle]=simin(n)

if n==1

% Choice of sample

samp=input('Type of sample desired: (1) Step, (2) Sinusoid, (3) Sample:
  ');
if samp==1
  isize=input(' Input the height of the Step  (nm):  ');

  iangle = 0;
end
if samp==2

   isize=input(' Input the amplitude of the Sine wave  (nm):  ');
   iangle=input('Input the spatial frequency of the sine wave (rad/nm):
  ');
end

if samp==3
   isize=0;
   iangle = 0;
end

res=samp;
range =0;

end


if n==2  %  Tip

tip=input('Type of tip desired: (1) Sphere, (2) Parabola, (3) Angled Pa
rabola:  ');

if tip==1
  isize=input(' Input the tip radius (nm):  ');
  iangle = 0;
end
if tip==2
  isize=input(' Input the tip radius (nm):  ');
  iangle = 0;
end

if tip==3
  isize=input(' Input the tip radius (nm):  ');
  iangle = input('Input the angle of rotation CW from the vertical (deg
```

```
rees):   ');
end


res=tip;

range=0;
end


if n==3

% Piezostack Resolution and Range

  res=input('Please enter the piezoactuator resolution: (m) ');
  range=input('Please enter the piezoactuator range: (m)  +/-');
  a=input('Please enter the length of arm A, where the piezoactuator im
poses displacement:  (m)  ');
  b=input('Please enter the length of arm B, where the Piezolever is at
tached:  (m)  ');

end
```

```
%***************************** Simul.m ************
%***      Conducts simulations of the scissor design
%***
%***
%***      Larry Barrett
%***      April 23, 1997
%**********************************************************

cla;
clg;
clear;
close all;


% Print the Tip vs. Calibration?
wf2=0;   %0 no, 1 yes!

% Select Sample Parameters

[cal,dd,isize,iangle]=simin(1);



% Sample creation

%cal=1; % Declare the type of sample desired

[calx,caly]=samples(cal,isize,iangle);

calymax=max(caly);



% Select Tip Parameters

[n,dd,isize,iangle]=simin(2);


% tip creation

%n=1;     % Declare the type of tip desired

[tipx,tipy,startx,starty,height,xi]=tip(n,calymax,isize,iangle);
tipxbeg=tipx+abs(min(tipx));
tipybeg=tipy;
tiprepx=tipx;
tiprepy=tipy;

if n==3

   [vy indy]=min(tipy);
```

```
   mx=min(tipx);
   tipx=tipx-indy-mx;
   tiprepx=tipx;
end

figure(1)
%if cal<4
 plot(calx,caly,tipx,tipy,'r')
% else
% plot(caly,calx,tipy,tipx,'r')
%end
grid
 title('Scanning of Surface')
 xlabel('Distance (nm)')
 ylabel('Distance (nm)')

hold


% Simulation

for j=1:1:size(calx,2)
    for i=1:1:size(tipx,2)
     if tipx(i)<min(calx)
        vdist(i)=tipy(i);
     elseif tipx(i)==min(calx) & min(calx)==0
        vdist(i)=tipy(i)-caly(1);
     elseif tipx(i)>max(calx)
        if cal>=3
        vdist(i)= tipy(i)-caly(max(calx))+50;
        else
        vdist(i)= tipy(i)-caly(max(calx));
        end

     %elseif tipx(i)>max(calx) & max(calx)=
     else
        vdist(i)=tipy(i) - caly(tipx(i));
     end
    end
  prof(j)=min(vdist);
   tipx=tipx+1;
end

for k=1:1:size(prof,2)
  profx(k)=k-1;
  profy(k)=-prof(k)+starty-height;
end

%figure(2)
%plot(profx(k),profy(k),'ro')
```

```
%if cal<4
plot(profx,profy,'ro')
%else
%plot(profy,profx,'ro')
%end


% Repeating the location of the tip image during the scan

fac=6; % Number of times image is to be repeated

repeat=size(calx,2)/fac;

for m=1:1:size(calx,2)/repeat
    % if cal<4
      plot(tiprepx,tiprepy-prof(1+(m-1)*repeat),'b');
    %else
    % plot(tiprepy-prof(1+(m-1)*repeat),tiprepx,'b');
    %end
    tiprepx=tiprepx+repeat;
end


% Restructing the image

% slopes of the scanned image

%spts=size(profx,2)*4; % make it odd
%dstep=tiprepx(max)-tiprepx(min);
%xssi=linspace(min(profx),max(profx),spts);
%yssi=interp1(profx,profy,xssi);
%yssi=yssi';
%for iii=1:1:size(yssi,2)-1
%    dimage(iii)=(yssi(iii+1)-yssi(iii))/(xssi(iii+1)-xssi(iii));
%end


dimage=diff(-prof+starty-height);

% slopes of the tip

%spts=size(tiprepx,2)*4 +1; % make it odd
%dstep=tiprepx(max)-tiprepx(min);
%xsi=linspace(min(tiprepx),max(tiprepx),spts);
%ysi=interp1(tiprepx,tiprepy,xsi);
%ysi=ysi';
%for ii=1:1:size(ysi,2)-1
%    dtip(ii)=(ysi(ii+1)-ysi(ii))/(xsi(ii+1)-xsi(ii));
%end

dtip=diff(tiprepy);
```

```
% dt for both of these is one because of the unity step

for i=1:1:size(dimage,2)
      for j=1:1:size(dtip,2)
              % want to find the smallest difference in slope for each p
oint
            small(j)=abs(dtip(j)-dimage(i));
        end
        [delta(i),index(i)]=min(small);

end

%lowptx=(size(tiprepx,2)+1)/2;

[val lowptx]=min(tiprepy);
%[val lowptx]=min(ysi);
for k=1:1:size(delta,2)
%     if index(k)<lowptx
%        profrecx(k)=profx(k)+xsi(index(k))-xsi(lowptx);
%        profrecy(k)=profy(k)+ysi(index(k))+ysi(lowptx);
%     else

%        profrecx(k)=profx(k)+xsi(index(k))-xsi(lowptx);

%        profrecy(k)=profy(k)+sign(dimage(k+1))*(ysi(index(k))-ysi(lowptx)
);
%
%        profrecy(k)=profy(k)+(ysi(index(k))-ysi(lowptx));

%   if profrecy(k) >max(profy)
%        profrecy(k)=profrecy(k)-max(profy);
%   end

%     end

      profrecx(k)=profx(k)+tiprepx(index(k))-tiprepx(lowptx);
      profrecy(k)=profy(k)+tiprepy(index(k))-tiprepy(lowptx);
end

%if cal<4
plot(profrecx,profrecy,'gx')
%else
%plot(profrecy,profrecx,'gx')
%end


% Printing Desired Plots
figure(2)
plot(calx,caly,'y',profx,profy,'ro', profrecx,profrecy,'gx')
 grid
```

152

```
 title('Surface Scan and Reconstruction')
 xlabel('Distance (nm)')
 ylabel('Distance (nm)')
legend('Sample Surface','Scanned Image','Reconstructed Image')


% Tip to tip profile w.r.t. Calibration Piece

cc=1;
for q=1:size(profx,2)-1
  if profy(q)~=profy(q+1)
      tipxc(cc)=cc;
      tipyc(cc)=-profy(q);
      cc=cc+1;
   end
end

% Accounting for numerical errors

tipxc=tipxc(2:size(tipxc,2));
tipyc=fliplr(tipyc(2:size(tipyc,2)));
%tipyc=fliplr(tipyc);



if wf2==1
 figure(3)
 if n==1
    if isize ==20
    aa=-2;
    end
    if isize==50
    aa=-1;
    end
    if isize==100
    aa=12;
    end

 end
 if n==2
  if isize ==25
   aa=+7;
  end
  if isize==35
   aa=-2;
  end
  if isize==15
   aa=+11;
  end
 end
 if n==3
```

```
    aa=-2;
 end

 plot(tipxbeg,tipy-starty,'y', tipxc+aa,tipyc-min(tipyc)-height,'ro')
 xlabel('Distance (nm)')
 ylabel('Distance (nm)')
 title('Sample tip vs. Image from Calibration Scan ')
 legend('Actual Tip','Tip Image from Calibration Scan')
end
```

```
%**************************** tip.m ************
%***     Defines the tip for simulations of the scissor design
%***
%***
%***     Larry Barrett
%***     April 23, 1997
%****************************************************

function [tipx,tipy,startx,starty,height,xi]=tip(n,calymax,isize,iangle
)
%clear;
%n=3;
%calymax=60;
%isize=20;
%iangle=60;

% Setting the probe above the sample

ymax=round(calymax)+50;




% Tip creation

% Spherical


if n==1

 tiprad=isize;   %20  Nanometers
% numpts=100;
 startx=0;
 starty=ymax+tiprad;

 count=1;
%   for u=-numpts:1:numpts
  for u=-tiprad:1:tiprad
%    tipx(count) = tiprad*u/numpts + startx;
%    tipy(count) = -sqrt(tiprad^2-(tiprad*u/numpts)^2)+starty;
    tipx(count) = u + startx;
    tipy(count) = -sqrt(tiprad^2-u^2)+starty;


   count=count+1;
  end

 tiprepx=tipx;
 tiprepy=tipy;
 height=tiprad;
%height=0;
```

```
% plot(tipx,tipy+tiprad,'r')
%hold
end


% Parabolic

if n==2

 tiprad=isize;   %25 Close to 20 Nanometers Tip
 numpts=40;
 startx=0;
 starty=ymax+tiprad;
%starty=280;

 count=1;
 for u=-numpts:1:numpts
   tipx(count) = u + startx;
   tipy(count) = (1/tiprad)*u^2+starty;
   count=count+1;
 end


 height=round(max(tipy))-round(min(tipy));

 tipy=tipy-height;

 tiprepx=tipx;
 tiprepy=tipy;


% plot(tipx,tipy,'g')
% hold
end


% Parabolic Angled
%n=3

if n==3
% clear;
% isize=35;
% iangle=-45;
 tiprad=isize;   %35 Close to 20 Nanometers Tip
 numpts=isize+20;  %  50;
 startx=0;
 starty=0;
%starty=280;
 rot=-iangle*pi/180; % Angling the tip 30 degrees CW from Vertical!

 count=1;
```

```
  for u=-numpts:1:numpts
    tipxrf(count) = u + startx;
    tipyrf(count) = (1/tiprad)*(tipxrf(count))^2+starty;
 %   xx(count)=u;
  % yy(count)=xx(count);
    count=count+1;
  end

 count1=1;
  for v=-numpts:1:numpts

   Mh= [cos(rot)  -sin(rot)    0 ;
         sin(rot)   cos(rot)    0  ;
            0          0        1  ];

   Ptip = Mh*[tipxrf(count1);tipyrf(count1);1];
   tipx1(count1)=Ptip(1);
   tipy1(count1)=Ptip(2);

     count1=count1+1;
  end


% plot(tipx1,tipy1,'r')
% hold

tipx2=tipx1;
tipy2=tipy1;

c=1;
if sign(iangle)==1 | sign(iangle)==0
[val,indx]=min(tipx1)
for w= -numpts:1:numpts
    if(w+numpts+1)>indx
%    if tipx(w+numpts+1)>=min(tipx1)
        tipxa(c)=tipx2(w+numpts+1);
        tipya(c)=tipy2(w+numpts+1);
        c=c+1;
      end
end
end

if sign(iangle)==-1
[val,indx]=max(tipx1)
for w=-numpts:1:numpts
    if(w+numpts+1)<indx
%    if tipx(w+numpts+1)>=min(tipx1)
        tipxa(c)=tipx2(w+numpts+1);
        tipya(c)=tipy2(w+numpts+1);
        c=c+1;
     end
```

```matlab
        end
    end



%end

tipya=tipya-min(tipya);

if sign(min(tipxa)) <=0
 aa=round(min(tipxa))+1;
else
 aa=round(min(tixa))-1;
end

bb=round(max(tipxa))-1;
cc=bb-aa;
xi=aa:1:bb;
yi=interp1(tipxa,tipya,xi);


% The Matlab software couldn't handle this operation in
% the function called so it is in the mainroutine.

%xi=xi-((size(xi,2)+1)/2+min(xi));
%[vy indy]=min(tipy);
%mx=min(xi);
%xi=xi.+indy.+min(xi);
%xi=xi';
%for z=1:size(xi,2)

%   xxi(z)=xi(z)+indy;
%end



starty=abs(round(min(yi)))+ymax;

tipx=xi;
%tipx=tipx+mx+indy;
tipy=yi+starty;
tipy=tipy';

 %height=round(max(tipy))-round(min(tipy));
  %height=abs(tipy(1)-tipy(size(tipy,2)));
  height=0;

 tiprepx=tipx;
 tiprepy=tipy;
%figure(1)
```

```
%plot(tipxa,tipya+starty,'g+',tipx,tipy,'yo')
end
```

8. References

[A1] S.T. Smith and D.G. Chetwynd, *Foundations of Ultraprecision Mechanism Design*, 1992

[A2] M. A. Paesler, P. J. Moyer, *Near-field Optics Theory, Instrumentation and Applications*

[A3] N. Taniguchi, *Nanotechnology: Integrated Processing Systems for Ultra-precision and Ultra-fine Products*, 1996

[A4]S.T. Smith and L.P. Howard, "A precision, low-force balance and its application to atomic force microscope calibration," *Review of Scientific Instruments*, Vol 65, April 1994, p. 903.

[A5] Joseph E. Griffith, David A. Grigg, "Dimensional metrology with scanning probe microscopes." *Journal of Applied Physics* 74, (9) Nov. 1993

[A6] D.G. Chetwynd and S.T. Smith, "High Precision Surface Profilometry: from Stylus to STM" in *From Instrumentation to Nanotechnology*.

[A7] T.V. Vorburger, "Methods for Characterizing Surface Topography," *Tutorials in Optics, Optical Society of America*, Washington, D.C., 1992

[A8] J.F. Song, T.V. Vorburger, J.Fu, "Stylus profiling at high resolution and low force," *Applied Optics*, Vol 30 No. 1, Jan. 1991.

[A9] R.D. Young, J. Ward, and F. Scire (1972) "The Topographiner: An instrument for measuring surface microtopography," *Rev. Sci. Instrum.*, 43(7), 999-1011.

[A10] G. Binnig, C.F. Quate, and Ch. Gerber, *Phys. Rev. Lett.* 56, 930 (1986)

[A11] M. Tortonese, R.C. Barrett and C.F. Quate, "Atomic resolution with an atomic force microscope using piezoresistive detection." *Applied Physics Letters*, 62(8), February 1993.

[A12] T.H. McWaid, T.V. Vorburger, J.Fu, J.F. Song, and E. Whitenton, "Measurements of micrometer and sub-micrometer surface features," 1994.

[A13] E. Betzig & J. K. Trauman. *Near-Field Optics: Microscopy Spectroscopy, and Surface Modification Beyond the Diffraction Limit*

[A14] Y. Martin, C.C. Williams, and H.K. Wickramsasinghe. "Atomic force microscope-force mapping and profiling on a sub 100 angstrom scale." *Journal of Applied Physics*. Vol. 61, pages 4723-4729.

[A15] H. Heinzelmann, E. Meyer, H. Rudin and H.J. Guntherodt. "Force Microscopy." In *Scanning Tunneling Microscopy and Related Methods*, 1990.

[A16] U. Hartmann, "Theory of Non-contact force microscopy," Springer Series in Surface Sciences, Vol. 29, *Scanning Tunneling Microscopy III*, page 293-359, 1993.

[A17] C.C. Williams and H.K. Wickramasinghe. "Scanning thermal profiler." *Applied Physics Letters*. Vol. 49. Pg. 1587-1589 (1986).

[A18] J.J. Saenz, N. Garcia, P. Grutter, E. Meyer, H. Heinzelmann, R. Wiesendanger, L. Rosenthaler, H.R. Hidber, and H.J. Guntherodt, *Journal of Applied Physics*, Vol. 62, pg 4293 (1987)

[A19] H. K. Wickramasinghe, American Institute of Physics Proceedings, *Scanned Probe Microscopy*, 241, page 16, 1992.

[A20] C.C. Williams, W. P. Hough, and S.A. Rishton. "Scanning capacitance microscopy on a 25nm scale." *Applied Physics Letters* Vol. 55. Pg. 203-205 (1989).

[B1] Park Scientific Instruments, 1171 Borregas Ave. Sunnyvale, CA 94089, Tel: (408) 747-1600, Fax: (408) 747-1601. Http://www.park.com.

[B2] S. Kalpakjian, *Manufacturing Processes for Engineering Materials*, 2nd Ed. Addison-Wesley, 1991.

[B3] Physik Instrumente, Products for Micropositioning, Catalogue Edition E, Polytec-Platz 5-7, 76337 Waldbronn, Tel. (07243)604-100, Fax. 604-145.

[B4] Precision Motion Controls 160 E. Virginia St. #264 San Jose, CA 95112.

[B5] Marco Tortonese, Park Scientific Instruments, 1171 Borregas Ave. Sunnyvale, CA 94089, Tel: (408) 747-1600, Fax: (408) 747-1601. Http://www.park.com

[B6] David Keller, "Reconstruction of STM and AFM images distorted by finite-size tips," *Surface Science*, **253** (1991) 353-364.

[B7] Park Scientific Instruments Piezolever Information Faxes, 1171 Borregas Ave. Sunnyvale, CA 94089, Tel: (408) 747-1600, Fax: (408) 747-1601. Http://www.park.com.

[B8] J. Ogland, *Design of a High Precision Profilometer*, Mechanical Engineering, BS Thesis (MIT, 1997)

[C1] A.H. Slocum, *Precision Machine Design*, Prentice Hall, 1992

[C2] A.P. Fein, J.R. Kirtley, and R.M. Feenstra, "Scanning tunneling microscope for low temperature, high magnetic field and spatially resolved spectroscopy, " *Rev. Sci. Instrum.* 58(10).

[C3] W.C. Young, *Roark's formulas for Stress and Strain*, 6th ed., McGraw-Hill, London, pp 679-681.

[C4] R.V. Jones, Angle-spring hinges, *J. Sci. Instrum.*, **32**, 36-338.

 [C5] Physik Instrumente, Products for Micropositioning, Faxes on LVPZ Translator Controllers, Polytec-Platz 5-7, 76337 Waldbronn, Tel. (07243)604-100, Fax. 604-145.

[C6] Digital Instruments, Inc. 520 E. Montecito St., Santa Barbara, CA 93103.

[D1] Bernardo Aumond, MIT Mechanical Engineering Mechatronics Research Laboratory.